Biotransformation and Interactions of Selenium with Mixed and Pure Culture Biofilms

A Thesis Submitted to the College of

Graduate Studies and Research

In Partial Fulfillment of the Requirements

For the Degree of Doctor of Philosophy

In the Department of Geological Sciences

University of Saskatchewan

Saskatoon

By

Soo In Yang

PERMISSION TO USE

In presenting this thesis in partial fulfilment of the requirements for a Postgraduate degree from the University of Saskatchewan, I agree that the Libraries of this University may make it freely available for inspection. I further agree that permission for copying of this thesis in any manner, in whole or in part, for scholarly purposes may be granted by the professor or professors who supervised my thesis work or, in their absence, by the Head of the Department or the Dean of the College in which my thesis work was done. It is understood that any copying or publication or use of this thesis or parts thereof for financial gain shall not be allowed without my written permission. It is also understood that due recognition shall be given to me and to the University of Saskatchewan in any scholarly use which may be made of any material in my thesis.

Requests for permission to copy or to make other use of material in this thesis in whole or part should be addressed to:

Head of the Department of Geological Sciences
University of Saskatchewan
114 Science Place
Saskatoon, Saskatchewan, Canada S7N 5E2

ABSTRACT

Biofilms have been reported to have an important role in the biogeochemical cycling of toxic elements in aquatic systems. Despite this important role, the complexity of biofilms and chemical and physical modifications that occur in conventional microscopic techniques hinder research progress. Thus, this research utilized a suite of less destructive synchrotron-based techniques to investigate selenium biotransformation in biofilms.

Natural biofilm collected from a coal mine-affected field site was examined with X-ray absorption spectroscopy (XAS), the results of which suggested the presence of methylated and elemental selenium. Biofilms generated in the laboratory using collected coal mine-affected water were investigated using confocal laser scanning microscopy (CLSM), (μ-)XAS and extended X-ray absorption fine structure (EXAFS). The results showed biotransformation of added oxyanion species (selenate, selenite, arsenate or arsenite). Micro X-ray fluorescence imaging (μ-XRF) and μ-XAS combined with CLSM revealed that selenium was highly localized in the biofilm in chemically reduced forms. Isolation and partial 16S rRNA gene sequencing suggested there were 4 principle bacterial genera responsible for these biotransformations of selenium. Further examination of multispecies biofilm and pure-culture biofilm (*Arthrobacter* sp SASK-Se22) exposed to high concentrations of selenate and selenite was carried out using synchrotron-based nano-scale scanning transmission X-ray microscopy (STXM) and nano-XRF imaging at the selenium L and K near-edges. These results demonstrated that selenium was biotransformed to nano-particulate elemental selenium and that the selenium particles were closely associated with lipid within the biofilm.

The distributions of selenate and selenite as well as elemental selenium within this complex biofilm structure were investigated using a novel combination of STXM and XRF on identical areas of biofilms. Transmission electron microscopy showed that the biogenic elemental selenium was sub-micron-sized, ranging from 50 to 700 nm in diameter, and was closely associated with microorganisms. The presence of submicron-sized elemental selenium may suggest possible applications of the biofilms in bioremediation or in the semiconductor industry where micro- to nano- sized selenium particles are in great demand.

Overall, this research demonstrated a novel application of synchrotron-based spectroscopic and imaging techniques to biofilm research, the results of which advance understanding of selenium biotransformation in multispecies and pure-culture biofilms.

ACKNOWLEDGMENTS

I would like to express my gratitude to my supervisor, Dr. Ingrid J. Pickering for her patience and thoughtful advice throughout my Ph.D. program. I appreciate Dr. Graham N. George for his advice. I also thank Drs. John R. Lawrence at Environment Canada, M. Jim Hendry, and Jim Merriam in Geological Sciences for their advice in this research.

Next, my appreciation goes to members of the Pickering/George research group for their help at the beamline. I specially thank Dr. Mercedes G. Gallegos for her great help during beamtime. I also thank Drs. James Dynes, Jian Wang, Samuel Webb, Barry Lai, Matthew Latimer, Eric Nelson, Susan Kaminskyj, and Helen Nichol for their help, advice, and sharing of their expertise with me.

I am most grateful to my parents, brother, sister, sister-in-law, nephew, and fiancée for their great encouragement throughout the program.

I would also like to express my appreciation for financial support from Natural Sciences and Engineering Research Council of Canada (NSERC) discovery grant (to Dr. Pickering) and University of Saskatchewan and invaluable training experience and funding from Canadian Institutes of Health Research-Training Grant in Health Research Using Synchrotron Techniques (CIHR-THRUST) Fellowship.

This thesis is based on synchrotron-based data collected at the Canadian Light Source (Chapters 4 and 5), the Advanced Photon Source (Chapters 4 and 5) and the Stanford Synchrotron Radiation Lightsource (Chapters 2 to 5). Complete facility acknowledgements are included in the relevant chapters.

TABLE OF CONTENTS

LIST OF TABLES

LIST OF FIGURES

LIST OF ABBREVIATIONS

APS:	Advanced Photon Source
AFM:	Atomic Force Microscopy
AHL:	*N*-Acyl Homoserine Lactone
AI	Autoinducer
ANOVA:	Analysis of Variance
As:	Arsenic
AAS:	Atomic Absorption Spectrometry
BC:	British Columbia
CCD:	Charge Coupled Device
CLS:	Canadian Light Source
CLSM:	Confocal Laser Scanning Microscopy
DOE:	Department of Energy
DMA(III):	Dimethylarsinite
DMA(V):	Dimethylarsinate
EPS:	Extracellular Polymeric Substances
ESRF:	European Synchrotron Radiation Facility
EXAFS:	Extended X-ray Absorption Fine Structure
GPx:	Glutathione Peroxidase
GM:	Goddard Marsh
KB:	Kirkpatrick-Baez
NL:	Liquid nitrogen
MMA(III):	Monomethylarsinite
MMA(V):	Monomethylarsonate
MCA:	Multichannel Analysis
NCBI:	National Center for Biotechnology and Information
OSA:	Order Sorting Aperture
PGM:	Plane Grating Monochromator
RF:	Radio Frequency
RT:	Room Temperature

Se:	Selenium
Se(0), Se^0	Elemental Selenium
SEM:	Scanning Electron Microscopy
SeMet:	Selenomethionine
SVD:	Singular Value Decomposition
SR:	Synchrotron Radiation
SSRL:	Stanford Synchrotron Radiation Lightsource
STXM:	Scanning Transmission X-ray Microscopy
TEM:	Transmission Electron Microscopy
LINAC:	Linear Accelerator
TR:	Thioredoxin Reductase
TMA:	Trimethylarsine
TMAO:	Trimethylarsine Oxide
TMSe:	Trimethylselenonium
TSA:	Tryptic Soy Agar
TSB:	Tryptic Soy Broth
UTM:	Universal Transverse Mercator
VLM:	Visual Light Microscopy
XAS:	X-ray Absorption Spectroscopy
XRF:	X-ray Fluorescence

CHAPTER 1. INTRODUCTION

Selenium (Z=34, Se) is an essential element, playing an important role in antioxidant enzymes in humans and other animals. Despite its crucial role, serious toxicity has been reported at elevated levels of selenium in biological systems. Although the level of selenium in the crust of the earth is low (0.09 ppm) [1], higher selenium concentrations in some areas or mining can result in toxic levels of selenium being released into the environment, particularly into aquatic ecosystems. The toxicity of selenium depends on which of its chemical forms, such as selenite or selenate, is present.

Arsenic (As, Z=33) is present all over the world in noticeable amounts depending on the areas [2]. Arsenic has been observed to be the most abundant and latent carcinogenic metalloid [3, 4]. Under normal ecological conditions, the arsenic level in soil typically ranges from 0.1 and 40 ppm unless anthropogenic activities have contributed [5, 6], e.g., arsenic-based pesticides [4] and mining [7]. Its adverse effects on the environment and humans are notorious. For example, many studies have shown that arsenic elevates the concentration of hydrogen peroxide in the apoptotic reaction [8] and causes modification of redox-sensitive signaling molecules by increased oxidative stress causing cellular injuries [9, 10].

High levels of selenium and arsenic from mining processing have been of considerable concern and reported in diverse regions of the world [11, 12]. For example, coal naturally contains 0.4 to 24 ppm [13] of selenium and as high as 35,000 ppm of arsenic [14]. These levels explain the inevitable release of high concentrations of selenium and arsenic during coal mining and processing. Concerted efforts have been made to cope with selenium and arsenic contamination for several decades using microorganisms [15-17]. Nevertheless, fundamental elucidation of how microorganisms resist and transform selenium and arsenic in the environment is limited.

The removal of excess selenium and arsenic from contaminated soil and water systems using bioremediation processes is receiving increased interest. In biotic systems, the outstanding ability of biofilm to detoxify toxic metals has drawn attention. Biofilms are the dominant form of microorganisms on the earth and 99 % of microorganisms are living in this state [18]. In general, biofilms consist of microorganisms and an extracellular polymeric substance (EPS). Typical

applications utilize biofilms from activated sludge to absorb heavy metals in wastewater [19]. Developed biofilms demonstrate a significant resistance to multimetal toxicity, providing 2 to 600 times more tolerance than planktonic forms [20, 21]. This complex microbial system with extensive EPS is believed to be the main structural architecture against chemical toxicity.

Considerable literature has shown that biofilms are readily related to the distribution, immobilization, and remobilization of inorganic metals in metal-contaminated areas [22]. However, difficulties in measuring the interrelationships of microenvironments and a lack of proper tools to investigate the local structures have been significant obstacles in biofilm research [22]. Throughout this research, synchrotron based X-ray spectroscopic techniques have been used to provide characterization of the microorganisms and local structural information associated with biotransformation of selenium and arsenic.

To simulate naturally generated biofilm, water samples were collected from mine-affected selenium contaminated Goddard Marsh (GM) near the Elkview Coal mine in British Columbia (BC), Canada. In addition, natural biofilms were collected after 1 month growth in the field. Selenium and arsenic speciation of the biofilm samples was examined using near-edge X-ray absorption spectroscopy and extended X-ray absorption fine structure (EXAFS) as well as more conventional confocal laser scanning microscopy technique to visualize biofilm structure. The results showed complex biofilm structure and biotransformation of selenium and arsenic in the biofilm. Further investigation of selenium biotransformation has been made in multispecies and pure culture biofilms. Synchrotron-based hard X-ray Micro X-ray fluorescence (μ-XRF) imaging and soft X-ray scanning transmission X-ray microscopy (STXM) techniques suggested biotransformation of selenium in biofilms occurs in a localized fashion. A novel experimental approach using both synchrotron techniques on the same areas of biofilms demonstrated a close relationship between selenium particles and the cellular and macromolecular structures of biofilms. Further microbiological and molecular biological techniques allowed identification of extremely selenium resistant microorganisms.

Overall, the following research topics will be discussed in each chapter: Chapter 1 gives an introduction to this research. A concise review on biofilms, selenium, and synchrotron-based techniques used in this research is presented in this chapter.

Chapter 2 presents a preliminary investigation of selenium species in natural biofilms collected from the coal mine-affected wastewater. Biofilm collectors were placed in the field and 1 month old natural biofilms were investigated using XAS techniques. This study aimed to examine what selenium chemical species were present in the naturally forming biofilm.

Chapter 3 extends the findings of Chapter 2 by investigating selenium and arsenic biotransformation in laboratory-controlled biofilms grown using the collected coal mine wastewater. The microbial population and nutrients present in the collected water from the field was used to generate biofilm. Biotransformation of selenium and arsenic, and selenium/arsenic were investigated using CLSM, XAS, and μ-XRF techniques. This study showed how multispecies biofilms cope with selenium and arsenic oxyanions.

Chapter 4 presents a more extensive study of the biotransformation of selenium in multispecies biofilm using synchrotron-based imaging techniques. Here, biofilms with microbial sources collected in Chapter 3 were grown with complex media and selenium biotransformation was investigated using nano-XRF, STXM, and transmission electron microscopy techniques. Selenium distribution in relation to the biofilm structure was investigated employing both synchrotron techniques on the same areas of the samples. This novel approach demonstrated how multispecies biofilm detoxifies selenium oxyanions by correlating biofilm structural components with selenium species present in the biofilm.

Chapter 5 investigates the biotransformation of selenium oxyanions by an extremely selenium resistant isolate, *Arthrobacter* sp. SASK-Se22 The pure-culture biofilm was generated using the extremely selenium resistant isolate from GM water and showed a superior ability in the biotransformation of the selenium oxyanion, selenite.

Chapter 6 concludes the thesis with an overall summary and the suggested future work.

Because this dissertation was prepared in a manuscript-based format and the same techniques were used in the studies, each chapter contains repetitive introduction, materials and methods. However, novel scientific findings were discussed in the results and discussion sections.

1.1. SELENIUM IN THE ENVIRONMENT

1.1.1. Source, toxicity and impact of selenium in the environment

Selenium (Z = 34) is a non-metal element present in several oxidation states (-II to +VI). Among these, selenate (SeO_4^{2-}) and selenite (SeO_3^{2-}) are present predominantly in soils, sediments, and water [23]. Selenium naturally occurs and is geochemically redistributed both by natural and human activities. The major natural sources of selenium are black shale, phosphate rocks and coals as well as volcanic activities. However, the major source of selenium exposure to the environment is anthropogenic activities such as mining and agricultural irrigation. These human activities re-distribute selenium into aquatic, atmospheric, sedimentary, and terrestrial phases causing chemical species changes of selenium [24]. A schematic illustration of selenium sources and the routes of exposure to the environment are shown in Figure 1.1. Selenium pollution has emerged as an issue in many places in the world including Canada, US, Brazil, Ecuador, Mexico, India, Russia, Japan, South Africa, Australia and more [13].

Selenium is an essential micronutrient as a component of certain antioxidant enzymes in animals and humans, [25] and beneficial functions are known in plants [26]. However, selenium has a very narrow margin between toxic and required levels [27]. Selenium toxicity varies considerably depending on its chemical species and can be very toxic to organisms with prolonged exposure even at low concentrations. Selenium toxicity is more serious in aquatic biota and the dominant route of exposure in animals is through uptake within the food web [28]. In addition, one serious problem with regard to selenium in environment is that it has a tendency to accumulate in organisms. Figure 1.1 shows exposure to selenium sources and the routes of exposure in the environment as well as biomagnification or bioaccumulation of selenium in higher trophic levels of aquatic organisms [29]. Selenium species observed in biological samples are shown in Table 1.1.

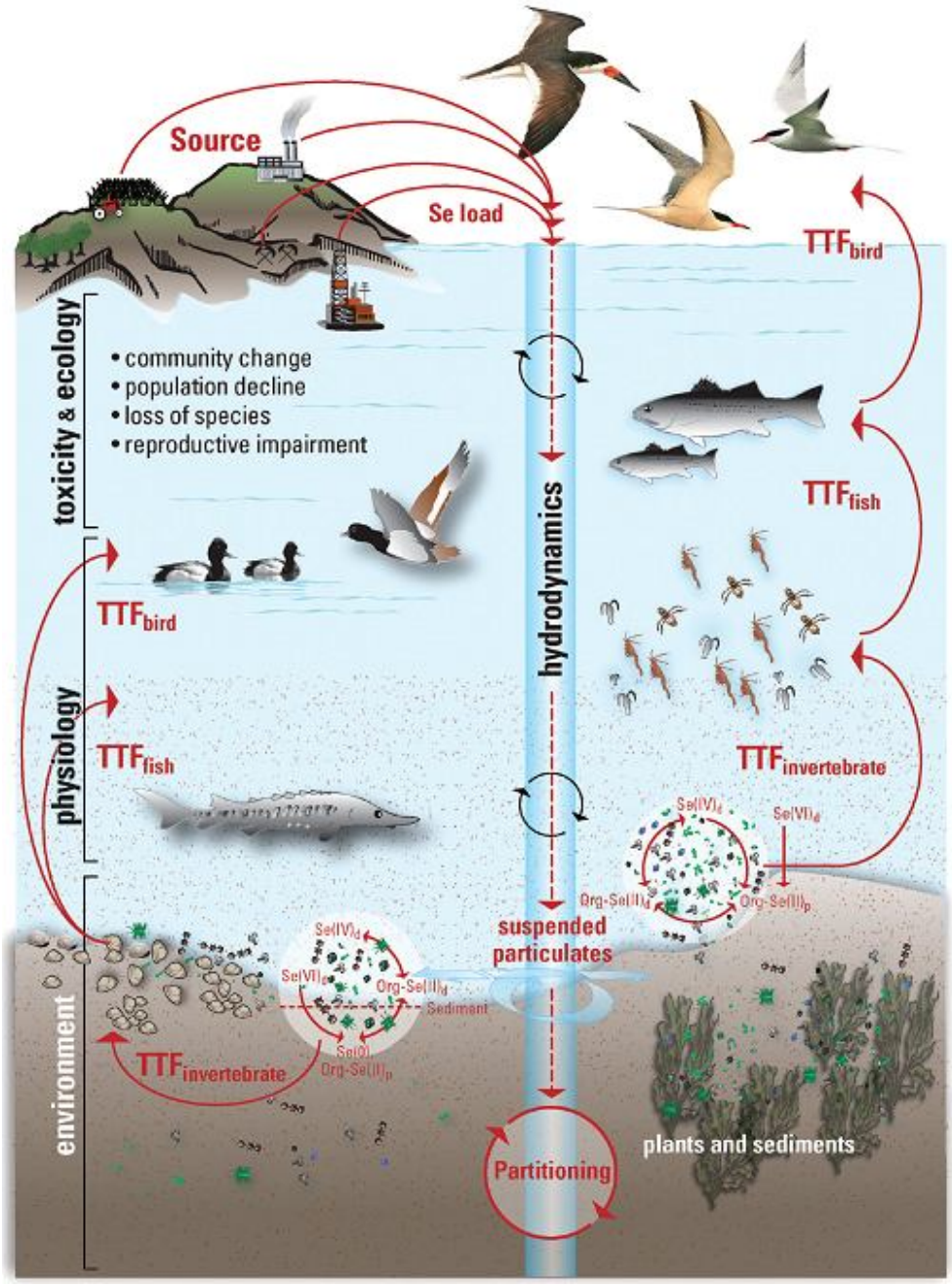

Figure 1.1. A schematic illustration of selenium sources and the routes of exposures to the environment. TTF, subscript d, and superscript p stand for trophic transfer factor, dissolved, and particulate, respectively (reprinted with permission) [29].

Table 1.1. Selenium species found in biological samples (table reproduced with permission [30])

Selenite	SeO_3^{2-}
Selenate	SeO_4^{2-}
Selenocysteine	$H_3N^+—CH(COO^-)—CH_2—SeH$
Selenocystine	$H_3N^+—CH(COO^-)—CH_2—Se—Se—CH_2—CH(COO^-)—NH_3^+$
Selenomethionine	$H_3N^+—CH(COO^-)—CH_2—CH_2—Se—Me$
Dimethyl selenide	Me_2Se
Trimethylselenonium ion	Me_3Se^+
Se-Methylselenocysteine	$H_3N^+—CH(COO^-)—CH_2—Se—Me$
γ-Glutamyl-*Se*-methylselenocysteine	$H_3N^+—CH_2—CH_2—CO—NH—CH(COO^-)—CH_2—Se—Me$
Selenocystathionine	$H_3N^+—CH(COO^-)—CH_2—CH_2—Se—CH_2—CH(COO^-)—NH_3^+$
Selenohomocysteine	$H_3N^+—CH(COO^-)—CH_2—CH_2—SeH$
Selenocystamine	$H_2N—CH_2—CH_2—Se—Se—CH_2—CH_2—NH_2$
5-[(Methylamino)methyl]-2-selenouridine	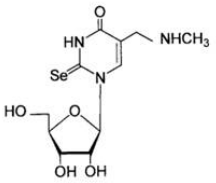
Se-Adenosylhomocysteine	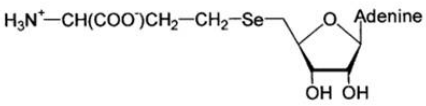

1.1.2. Biochemistry of selenium in microorganisms

A simplified proposed selenium metabolic pathway in *Escherichia coli* is shown as a model (Figure 1.2). Selenate is transported through the sulphate permease system, comprised of CysA, CysT and CysW which are believed to be the main selenate uptake routes. Selenite is transported through both the sulphate permease system and unknown transporters. Following uptake selenate is reduced to selenite and additional reduction occurs. The reduced selenium products include methylated forms as well as less toxic elemental selenium compounds (reviewed in [31]).

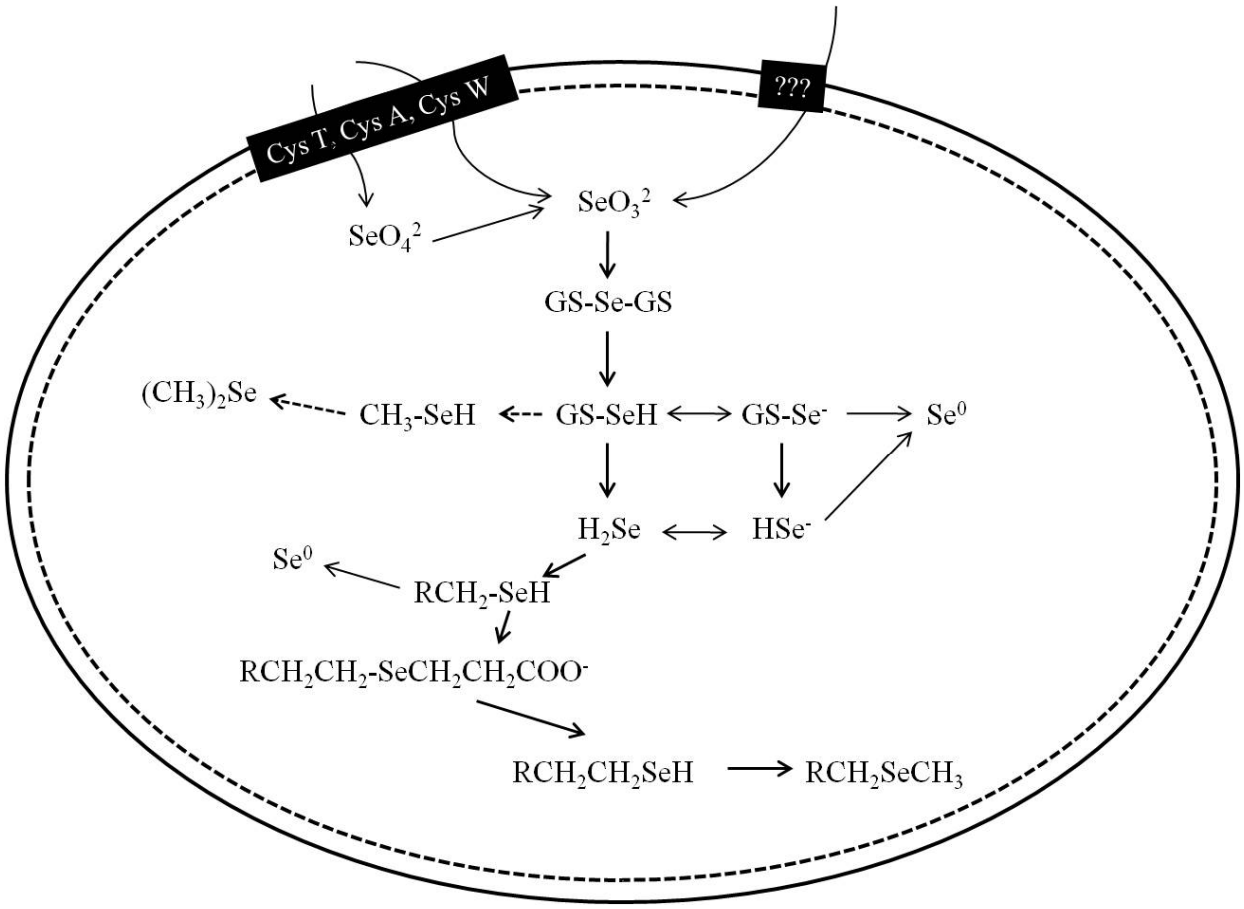

Figure 1.2. The selenium metabolism in *Escherichia coli*. This concise figure was redrawn based on a review by Turner *et al* [31] to show main metabolic intermediates and final selenium compounds. The dotted arrows indicate unproven pathways.

1.2. BIOFILM

1.2.1. Biofilm structure and physiology

A biofilm is a microbial consortium, which may consist of a single type of organisms (pure-culture) or multiple populations. In most cases, microorganisms are found as a mixed culture rather than as single cell floating planktonic forms [32]. Biofilms contain almost ~ 97 % of water and microbial populations in nature are diverse, including protozoa, bacteria, fungi, and algae. Biofilms consist of microorganisms with extracellular polymeric substances or slimy materials

and almost 99 % of microorganisms living on the earth are found in these ubiquitous communities. Biofilms have markedly higher resistance to physical, chemical, and antibiotic stress compared to free living forms of microorganisms. The physical properties of biofilms are determined by biomacromolecules present in biofilms, such as protein, lipid, and polysaccharides [22, 33]. The prominent capability of EPS to sorb metals has been observed and the sorption mechanisms include absorption, precipitation, and adsorption [22]. The structural moieties of biofilms and developmental stages are shown in Figure 1.3.

An important aspect of biofilms is that they can control the metabolisms of each individual or small community of microorganisms by a unique communication system, called quorum sensing. This communication mechanism is controlled by hormone-like chemicals called autoinducers (AI) making it possible to control a group of cells as a multicellular organism. Reported quorum sensing molecules in bacteria include *N*-Acyl-homoserine latones (AHL), oligopeptide, Streptomyces γ-butyrolactones, and Al-2 family autoinducers (reviewed in [34]).

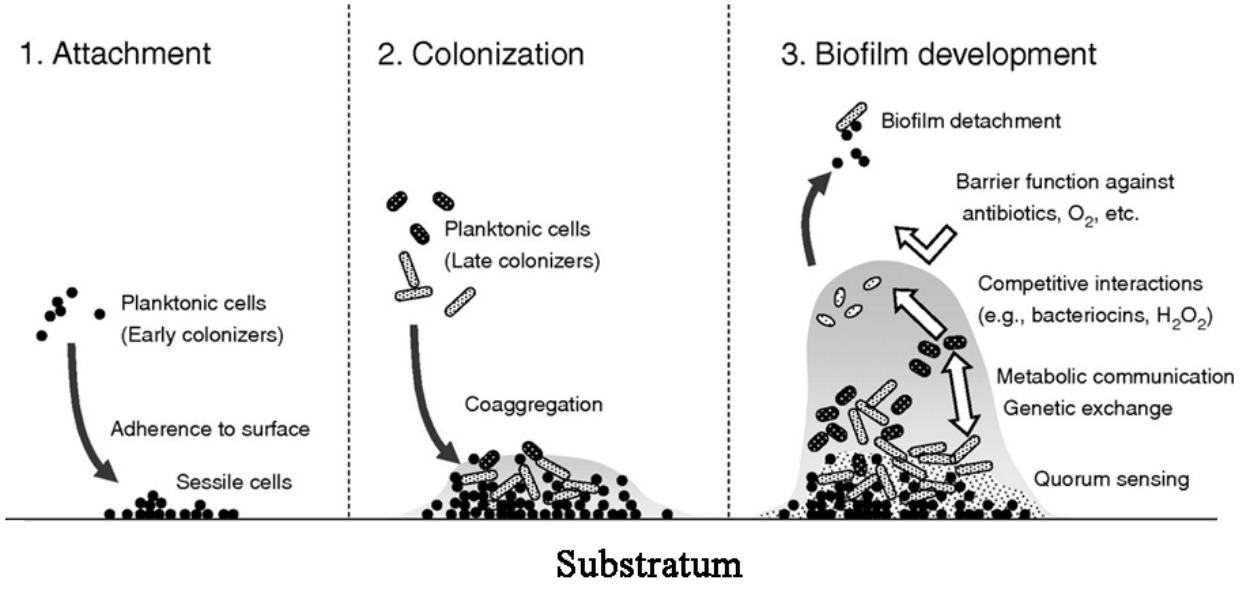

Figure 1.3. A concise illustration of biofilm development (image reproduced with permission [35])

1.2.2. Biofilm in the environment and its role in the bioremediation of toxic elements

In planktonic microorganisms, toxic metals are introduced into the cells by non-specific transport systems. The mode of actions for the initial uptake includes absorption and adsorption. For example, many divalent heavy metal cations have structural similarities to physiologically important ions, i.e. Mn^{2+}, Fe^{2+}, Co^{2+}, Ni^{2+}, Cu^{2+}, and Zn^{2+}, and the sizes of atoms all fall into 138 – 160 pm in ionic diameters. This structural similarity hinders the specific recognition ability of these transporters, and thus the non-specific transporters can deliver the toxic metals into the cytosol of microorganisms. Heavy metals may interact with other physiological elements and thiol groups in the active sites of important enzymes, thus interfering with essential enzymatic reactions. Because heavy metals cannot be degraded, microorganisms use the following detoxification or resistance mechanisms: efflux, utilizations of thiol complexes, modifications of oxidation states, and a combination of all of these methods (reviewed in [36]). However, the situation is more complex when groups of mixed microorganisms are considered for these resistance and detoxification or biotransformation.

It has not been a long time since the realization of the ubiquity and important roles of biofilms in geochemical cycling of elements in nature and their potential applications in bioremediation of heavy metals and toxic non-metal elements [22, 32]. As Teitzel *et al* [37] reported, biofilms are more resistant to heavy or toxic metals than their free living forms by 2 to 600 times. This increased resistance derives from the physical protection afforded by the biofilm matrix [22], as well as presumed gene transfer among microorganisms for resistance characteristics [38, 39]. With respect to bioremediation of toxic elements such as selenium, microbial consortia play an important role in the biogeocycling of elements in nature by detoxifying these elements by conversion to less toxic chemical species or relocating them by transformation to gaseous species [40, 41].

1.2.3. Microscopic techniques used in biofilm research

A comparison of common microscopic techniques used in biofilm research is shown in table 1.2.

Table 1.2. Microscopic techniques used in biofilm research*

Microscopic techniques	Source	Information	Merit	limitations
Light microscopy	visible light	microbial morphology thickness, density	simple, rapid	low resolution depth examination is impossible
Atomic force microscopy (AFM)	laser	tomographical information	real-time observation of biomolecular behavior	dehydration of biofilm, no compositional information
Confocal laser scanning microscopy (CLSM)	laser	*in-situ* monitoring of biofilm structure	internal structure by optical sectioning; cells and EPS can be distinguished ; detection of molecular reporters; possible to measure pH in biofilm.	expensive equipment, thickness limit, relatively lower resolution compared to electron microscopy techniques.
Scanning electron microscopy (SEM) [42]	electron	biofilm morphology (surface)	high resolution	surface probing, destructive sample preparation.
Transmission electron microscopy (TEM) [42]	electron	biofilm morphology	high resolution	sample thickness, destructive sample preparation.

* This table is based on the review by Denkhaus *et al* [43].

1.3. SYNCHROTRON-BASED EXPERIMENTAL TECHNIQUES

1.3.1. An overview of a synchrotron from a source to the brilliant beam

Synchrotron radiation is very intense light, which is almost a million times more intense than laboratory tube-sourced light and is tunable, vertically collimated, and polarized. Synchrotron radiation is generated when charged electrons (positrons or ions) are accelerated to near the speed of light in a magnetic field [44, 45]. The major components of the synchrotron include electron gun and linear accelerator (LINAC), booster ring, storage ring, and beamlines/end-stations (Figure1.4). The following information on compartments/ equipment of the synchrotron is available on Canadian Light Source (CLS, [46]) home page.

An electron gun generates electrons at 200,000 volts and the discrete bunches of generated electrons are emitted into the LINAC. Microwave radio frequency in the LINAC accelerates electrons to 99.9998 % of the speed of light by charging electrons to 250 million electron volts (MeV) and the electrons travel under 10^{-11} torr vacuum condition. The accelerated electrons are introduced into the booster ring, which consists of a recurring set of magnets and radio frequency-cavity (RF-cavity, it is also a part of the storage ring). The role of magnets is to direct electrons around the booster ring and to force the bunches of electrons into a fine beam. The lost energy of electrons by the generation of radiation is replaced or recharged by operation at a frequency of 500 MHz. In the CLS, electrons are injected into the storage ring when their energy reaches 2900 MeV. In the storage ring, there are a series of sets of magnets to keep directing and shaping electrons in the round shaped track consisting of straight sections. Radiation from the circulating electrons is generated by bending magnets and insertion devices, such as wigglers and undulators [46]. A comparison of spectral brightness and effective energy covered by various sources from an X-ray tube source to current bending magnets and insertion devices is shown in Figure 1.5 [47]. As shown in the figure, brightness increases in order from bending magnet, wiggler, to undulator. With respect to usable energy range, an undulator has the narrowest and wiggler the broadest.

The polychromatic or white beam generated by the sources stated above is introduced into the monochromator and a monochromatic (narrow range of wavelengths) beam is selectively chosen.

Mirrors are used to collimate and focus the beam (Figure 1.6). The size of the beam is controlled using slits. If a micro-beam is desired, the beam is further focused with additional optics, such as a Kirkpatrick-Baez (KB) mirror pair or a zone plate.

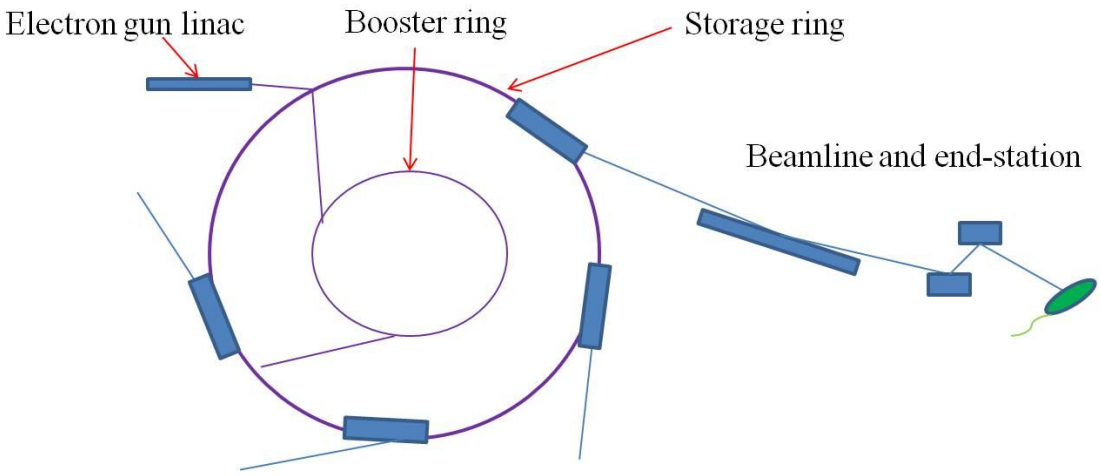

Figure 1.4. A schematic illustration of a synchrotron.

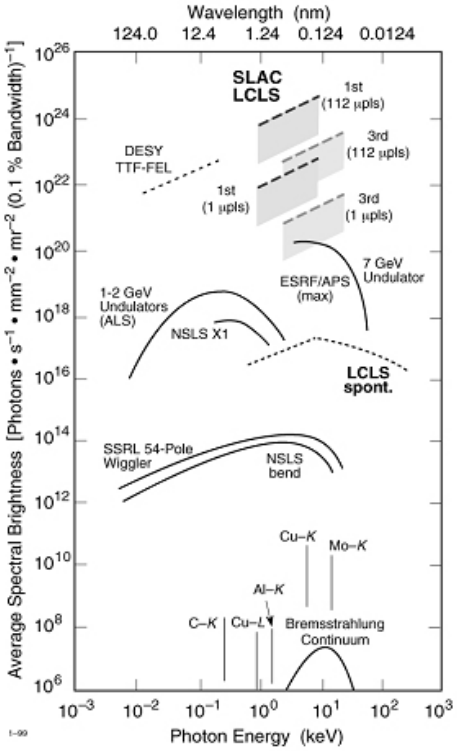

Figure 1.5. Brightness and energies of X-ray sources. Conventional X-ray tube brightness is shown at the bottom (image reproduced with permission) [47].

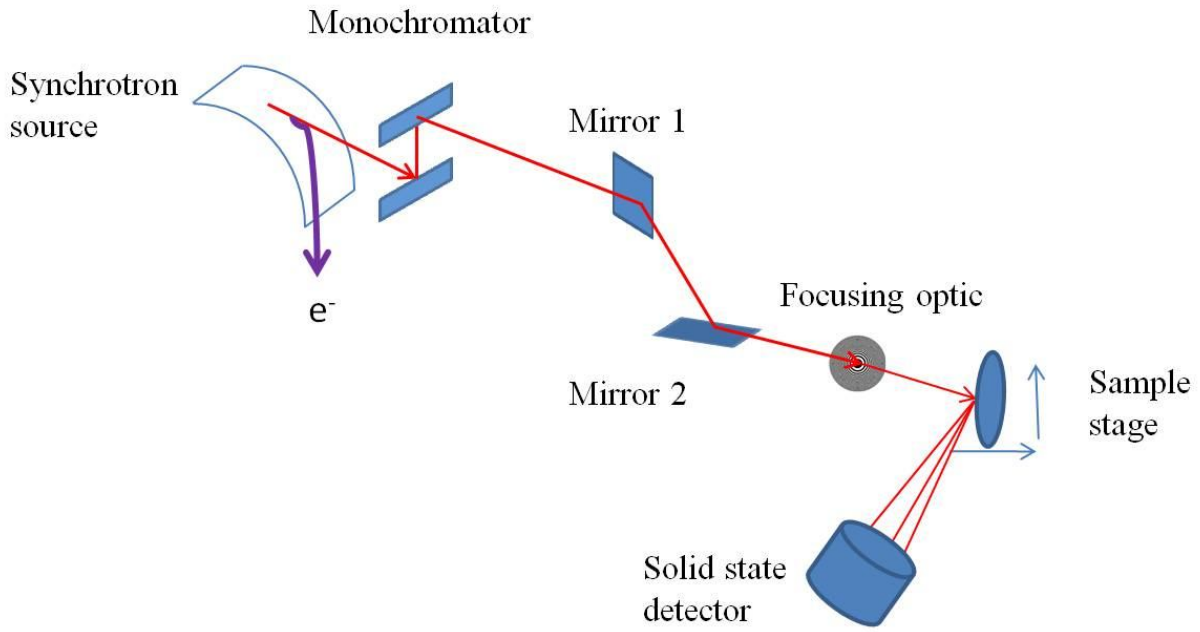

Figure 1.6. Beamline setup showing monochromator, mirrors, sample stage, and detector.

1.3.2. X-ray absorption spectroscopy

X-ray absorption spectroscopy (XAS) is an element-specific technique that can be used to investigate any phases of materials (gas, aqueous, solid) and even mixtures [48]. Based on extractable information, an XAS spectrum can be divided into 3 main regions as shown in Figure 1.7, where the selenium K near-edge (1*s* orbital excitation) spectrum is shown as an example. The first region is a pre-edge where core-electron X-ray absorption occurs (1*s* electrons in this case) and in this region the X-ray energy is not enough to eject the electrons out of the core-hole. In the near-edge region, bound-state transition of photoelectrons to higher molecular orbitals occurs and thus the spectrum contains unique information on the surrounding atoms. When the incident X-ray energy exceeds the edge energy threshold, photoelectron has enough energy to eject electrons into the continuum and the ejected photoelectrons are backscattered by neighboring atoms, leading to constructive or destructive interference depending on the energy. This results in oscillations in the high energy range of the XAS spectrum, which is termed the extended X-ray absorption fine structure (EXAFS). EXAFS can provide very accurate interatomic distance (accuracy better than 0.02 Å, [48][49]) between absorber and neighboring

(back scattering) atoms. Therefore, near-edge and EXAFS regions are useful for the determination of chemical characteristics of elements of interest.

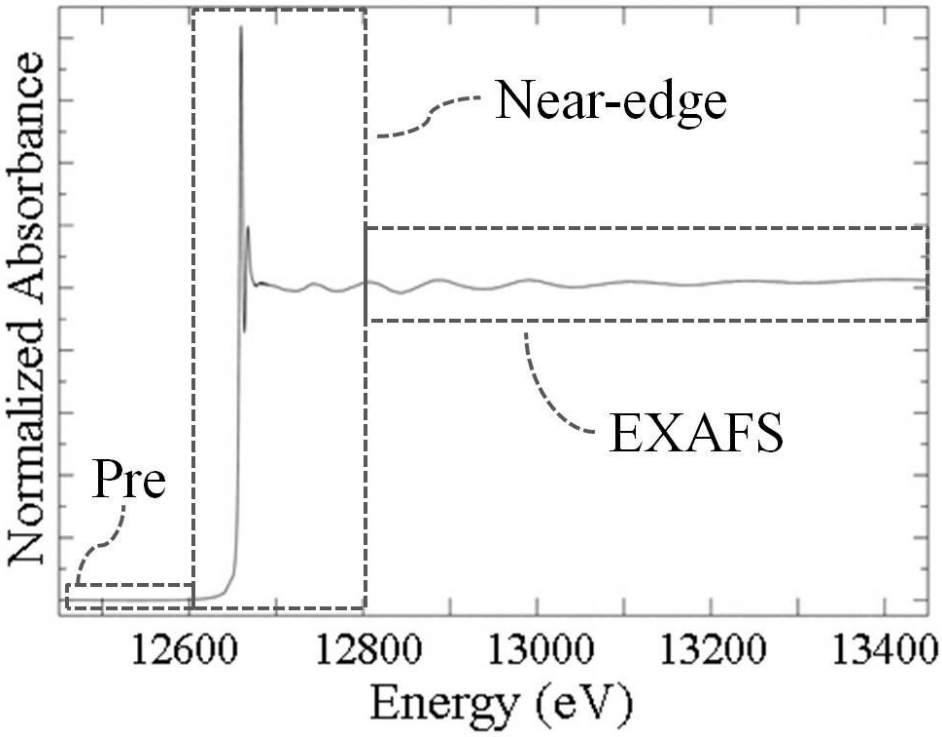

Figure 1.7. Selenium X-ray absorption spectrum. Pre-edge (Pre), near-edge, and extended X-ray absorption fine structure (EXAFS) regions are shown.

1.3.3. X-ray fluorescence (XRF) imaging

Compared to commonly used more conventional microprobe techniques, synchrotron-based hard X-ray XRF has several advantages, such as high sensitivity, capability to collect spectra and to conduct chemically specific imaging. In addition, samples under any condition (wet or dry, or thick) can be measured. In the early development in XRF imaging (1st generation synchrotron; in 1960 – mid 1970s), a slit or a pinhole assembly was used as collimation optics. This resulted in a decrease in the initially low flux as well as low spatial resolution. However, in the progression through 2nd generation synchrotron sources to the current (3rd generation) synchrotron facilities, the flux and optics for such experiments have improved dramatically [50, 51].

Currently, X-ray fluorescence imaging can produce an elemental map with moderate spatial resolution supported with high flux and state-of-art focusing optics, such as a KB mirror system or a Fresnel zone plate. Since X-rays have a 3-4 order of magnitude smaller wavelength than visible light, theoretically much higher resolution is achievable, where theoretically achievable spatial resolution is limited to 0.2 μm. This limit was overcome by current synchrotron-based hard X-ray optical set-ups. In addition, recently Mimura *et al.* [52] reported an advanced set-up at Spring-8, presenting better than 50 nm spatial resolution at 15 keV using elliptically focusing mirrors with tunable energy. However, it should be noted that the distance between the Si(111) monochromator and the sample is 1 km!

A state-of-art end-station set-up at beamline 2-ID-D of Advanced Photon Source (APS) is shown in Figure 1.8 as an example; this beamline was used for the nano-scale XRF presented in Chapters 4 and 5. The figure identifies the zone plate, which is used as a focusing optic, together with the Ge-detector, microscope, and sample stages. In normal cases, the sample and the detector are oriented at 15-45 and 90°, respectively from the incident beam to maximize the collection of emitted fluorescence from the sample [53].

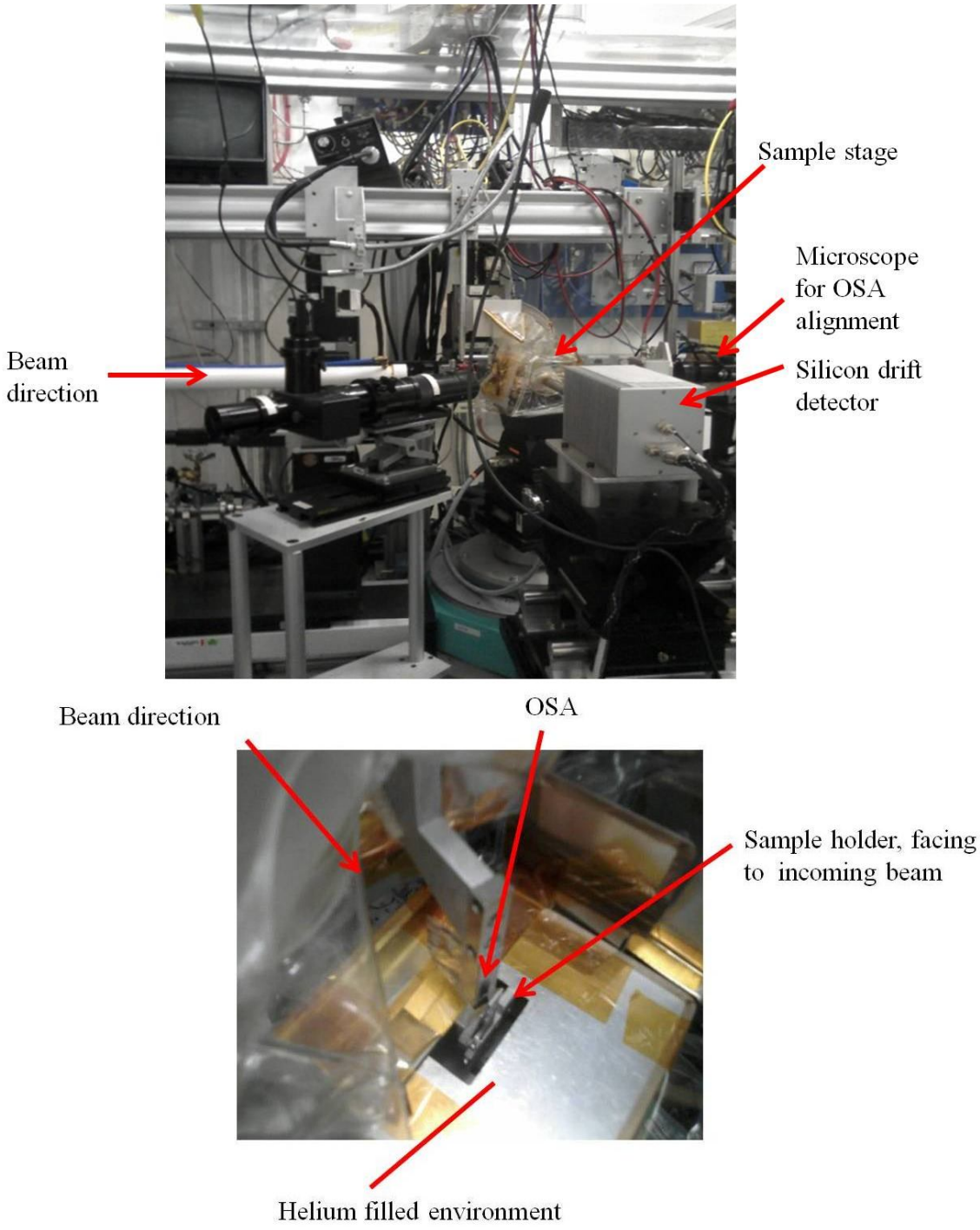

Figure 1.8. Experimental setup inside the experimental enclosure (upper image) and a mounted sample (lower image) at beamline 2-ID-D of Advanced Photon Source are shown. OSA stands for order sorting aperture.

1.3.4. Scanning transmission X-ray microscopy (STXM)

Scanning transmission X-ray microscopy (STXM) is a soft X-ray based synchrotron technique. The STXM setup at the Spectromicroscopy beamline of the Canadian Light Source (CLS) is shown in Figure 1.9 and 1.10; this beamline was used for the biofilm measurements presented in Chapters 4 and 5. Due to the high flux from an undulator, the photon-flux reaches 10^8 photons in a 50 nm spot with an available energy range of 130 - 2,500 eV. The zone plate makes it possible to focus the beam down to 30 nm in spatial resolution [54].

One of the major advantages of STXM for biological applications is that it can visualize the building blocks of organisms, carbon, nitrogen, and oxygen at their K-edges. This provides the opportunity to investigate biological structures with high spatial resolution. Even though sample preparation requires very thin sectioning of the sample (typically less than 1-3 μm section in biofilms) due to the need for transmission of X-rays, the technique can provide rich biological macromolecular compositional map, spectra, and morphology information at high resolution (~ 30 nm) which provide crucial information to understand biological interactions. Even though it has lower sensitivity to high atomic number elements compared to C, N, and O, STXM can image them if the elements of interest are localized in the biological system. This lower detection efficiency at higher atomic number elements is due to two main reasons: 1. lower absorption yield of L or M absorption edges compared to K-edge; 2. Transmission detection. A concise comparison between synchrotron hard X-ray XRF and soft X-ray STXM are shown in Table 1.3.

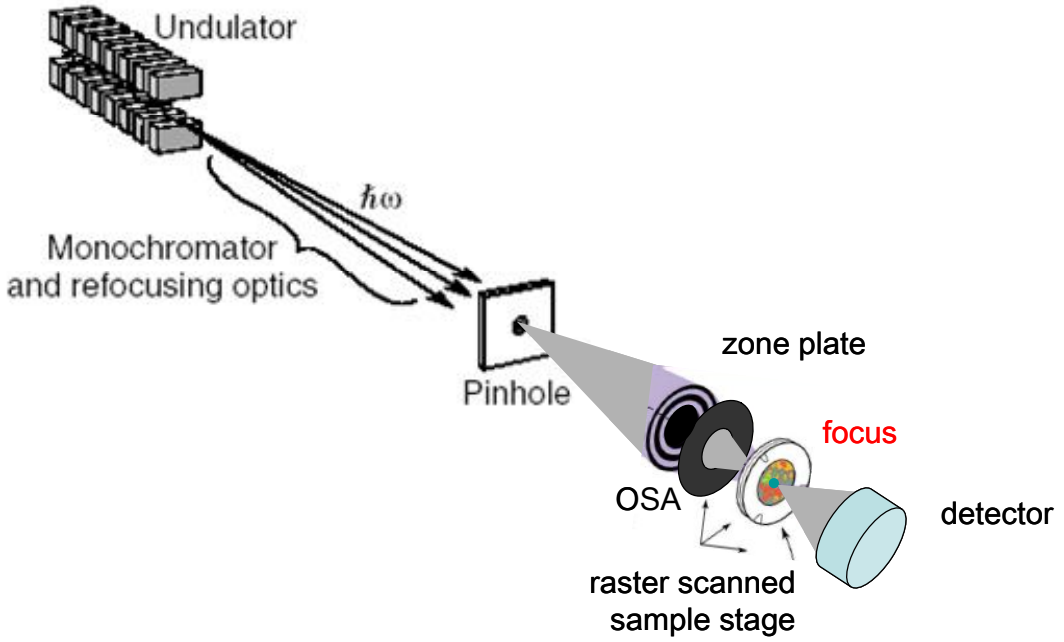

Figure 1.9. A schematic illustration of the scanning transmission X-ray microscopy set up at Spectromicroscopy beamline of Canadian Light Source. OSA stands for order sorting aperture [54].

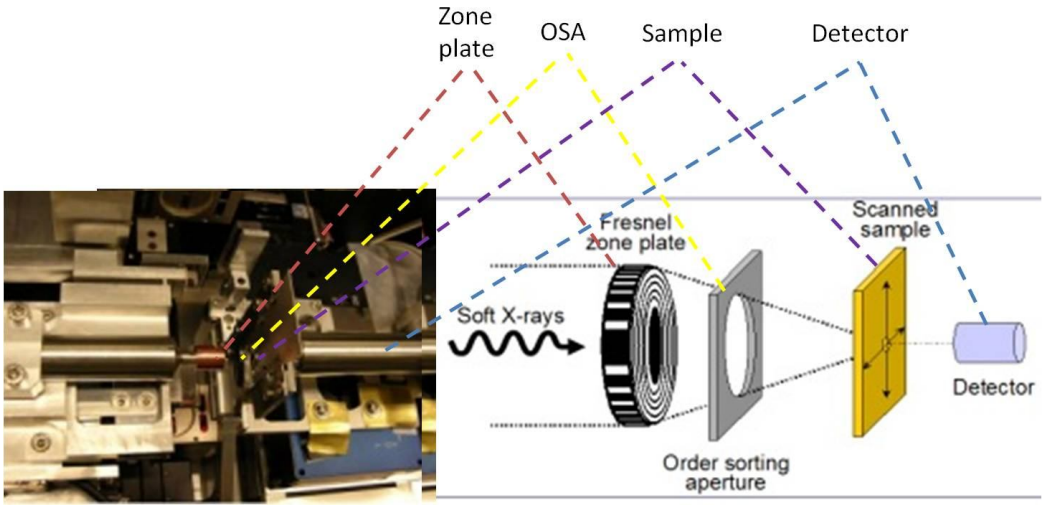

Figure 1.10. A photograph of the inside of a STXM chamber (left) and schematic diagram showing the optical elements (right)[54].

Table 1.3. Concise comparison between hard X-ray XRF and soft X-ray STXM.

	XRF[1]	STXM[2]
Source	Undulator	Undulator
Energy	6- 30 keV	0.13 - 2.5 keV
Flux	10^9 photons/0.3 × 0.25 μm^2/sec	10^8photons/0.05 × 0.05 μm^2/sec
Monochromator	Si(111), Si(220), Si(333)	Plane grating monochromator (PGM)
Detectors[3]	Silicon drift detector	Photomultiplier detector
Scanning mode	Unidirectional raster scan	Unidirectional raster scan
Resolution	200 nm	30 nm
Elemental map	Yes	No[4]
Spectrum	Yes	Yes
Advantages	Elemental map; fluorescence detention is more sensitive than transmission detection; Thickness of the sample is not a problem. K-edge (higher energy) fluorescence yield of biologically important transition metals (e.g., Zn, Cu) is higher than L-edges; Mass absorption coefficient of biological macromolecules is lower at higher energy (less destructive to biomolecules); XRF can visualize distribution of chemical species	STXM can visualize biologically important building blocks, such as protein, lipid, polysaccharide at carbon K-edge; Biologically important metals (e.g., transition metals) can be detected at L-M edges (mainly L-edges); very high resolution (~ 30 nm); chemically specific imaging at detectable concentration ;a stack of scans provides a whole set of spectra collected at each pixel; fast scan (e.g., 1 msec/point), wet cells can be examined.
Disadvantages	Can't show bio-macromolecules; more difficult to make beam smaller than soft X-ray; difficult to match biological information with elemental distribution if there are no indicator elements spread over the sample; photo-damage	Sample thickness should be less than 1-3 μm in case of biofilm to prevent distortion and thin sectioning can be challenging; L or M -edge detection are less sensitive than K-edge detection; photo-damage; transmission detection is less sensitive than fluorescence.

[1] APS 2-ID-D XRF beamline [55]

[2] CLS SM beamline [54]

[3] Only typical detectors are shown

[4] It is based on transmission detection (no fluorescence detection)

1.4. OBJECTIVES OF THIS RESEARCH

1. Characterization of selenium species in natural biofilm collected from coal mine-affected wastewater containing elevated selenium.

2. Investigation of selenium and arsenic biotransformation in laboratory-controlled biofilm grown using the collected coal mine wastewater.

3. Investigation of the selenium biotransformation in multispecies biofilm using nanoscale synchrotron-based imaging techniques.

4. Examination of the biotransformation of selenium oxyanions by an extremely selenium resistant isolate, *Arthrobacter* sp. SASK-22.

1.5. REFERENCES

[1] D. C. Ayres, D. G. Hellier, *in Dictionary of environmentally important chemicals* **1998**, pp. 270 (Blackie Academic & Professional: London).

[2] T. Clarkson, Health effect of metals: A role for evolution? *Environ Health Perspect* **1995,** *103,* 9.

[3] W. R. Cullen, K. J. Reimer, Arsenic speciation in the environment. *Chem. Rev.* **1989,** *89,* 713.

[4] P. Roy, A. Saha, Metabolism and toxicity of arsenic: A human carcinogen. *Curr. Sci.* **2002,** *82,* 8.

[5] J. M. Azcue, J. O. Nriagu, *in Arsenic in the environment* (Eds J. O. Nriagu) **1994**, pp. 1-15 (John Wiley and Sons: New York).

[6] H. Yan-Chu, *in Arsenic in the environment* (Eds J. O. Nriagu) **1994**, pp. 17-50 (John Wiley and Sons: New York).

[7] C. Choprapawan, A. Rodcline, *in Arsenic : exposure and health effects* **1997**, pp. xvi, 429 69-77 (Chapman & Hall: London).

[8] Y. Jing, J. Dai, R. M. E. Chalmers-Redman, W. G. Tatton, S. Waxman, Arsenic trioxide selectively induces acute promyelocytic leukemia cell apoptosis via a hydrogen peroxide-dependent pathway. *Blood* **1999,** *94,* 2102.

[9] G. S. Buzard, K. S. Kasprzak, Possible roles of nitric oxide and redox cell signaling in metal-induced toxicity and carcinogenesis: a review. *J Environ Pathol Toxicol Oncol* **2000,** *19,* 179.

[10] D. J. Thomas, M. Styblo, S. Lin, The cellular metabolism and systemic toxicity of arsenic. *Toxicol.Appl.Pharmacol.* **2001,** *176,* 127.

[11] I. Cano-Aguilera, B. E. Rubio-Campos, G. De la Rosa, A. F. Aguilera-Alvarado, Arsenic mobility from mining tailings of Monte San Nicolas to Presa de Mata in Guanajuato, Mexico. *World Academy of Science, Engineering and Technology* **2008,** *47,* 390.

[12] P. L. Orr, K. R. Guiguer, C. K. Russel, Food chain transfer of selenium in lentic and lotic habitats of a western Canadian watershed. *Ecotoxicol. Environ. Saf.* **2006,** *63,* 175.

[13] A. D. Lemly, Aquatic selenium pollution is a global environmental safety issue. *Ecotoxicol. Environ. Saf.* **2004,** *59,* 44.

[14] R. B. Finkelman, H. E. Belkin, B. Zheng, Health impacts of domestic coal use in China. *PNAS* **1999,** *96,* 3427.

[15] A. W. Cantafio, K. D. Hagen, G. E. Lewis, T. L. Bledsoe, K. M. Nunan, J. M. Macy, Pilot-scale selenium bioremediation of San Joaquin drainage water with *Thauera selenatis*. *Appl. Environ. Microbiol.* **1996,** *62,* 3298.

[16] W. T. Frankenberger, M. Arshad, Bioremediation of selenium-contaminated sediments and water. *Biofactors* **2001,** *14,* 241.

[17] K. A. Natarajan, Microbial aspects of acid mine drainage and its bioremediation. *Trans. Nonferrous Met. Soc. China* **2008,** *18,* 1352.

[18] J. W. Costerton, P. S. Stewart, E. P. Greenberg, Bacterial Biofilms: A Common Cause of Persistent Infections. **1999,** *284,* 1318.

[19] M. Su, D. K. Cha, P. R. Anderson, Influence of selector technology on heavy metal removal by activated sludge: Secondary effects of selector technology. *Water Research* **1995,** *29,* 971.

[20] D. H. Nies, S. Silver, Ion efflux systems involved in bacterial metal resistances. *Journal of Industrial Microbiology and Biotechnology* **1995,** *14,* 186.

[21] D. H. Nies, Microbial heavy-metal resistance. *Applied Microbiology and Biotechnology* **1999,** *51,* 730.

[22] E. van Hullebusch, M. Zandvoort, P. Lens, Metal immobilisation by biofilms: mechanisms and analytical tools. *Rev. Environ. Sci. Biotechnol.* **2003,** *2,* 9.

[23] A. Fernandez-Martinez, L. Charlet, Selenium environmental cycling and bioavailability: a structural chemist point of view. *Reviews in Environmental Science and Biotechnology* **2009,** *8,* 81.

[24] W. Maher, A. Roach, M. Doblin, T. Fan, S. Foster, R. Garret, G. Moller, L. Oram, D. Wallschlager, *in Ecological Assessment of Selenium in the Aquatic Environment* **2010**, pp. 47-92 (CRC Press: New York).

[25] K. Brown, J. Arthur, Selenium, selenoproteins and human health: a review. *Public Health Nutr.* **2001,** *4,* 593.

[26] H. Hartikainen, T. Xue, V. Piironen, Selenium as an anti-oxidant and pro-oxidant in ryegrass. *Plant Soil* **2000,** *225,* 193.

[27] A. G. Renwick, Toxicology of micronutrients: adverse effects and uncertainty. *J. Nutr.* **2006,** *136,* 493S.

[28] S. J. Hamilton, Review of selenium toxicity in the aquatic food chain. *Sci. Total Environ.* **2004,** *326,* 1.

[29] S. N. Luoma, T. S. Presser, Emerging opportunities in management of selenium contamination. *Environ.Sci.Technol.* **2009,** *43,* 8483.

[30] J. S. Edmonds, M. Morita, The identification of selenium species in biological samples. *Applied Organometallic Chemistry* **2000,** *14,* 133.

[31] R. J. Turner, J. H. Weiner, D. E. Taylor, Selenium metabolism in *Escherichia coli*. *Biometals* **1998,** *11,* 223.

[32] R. Singh, D. Paul, R. K. Jain, Biofilms: implications in bioremediation. *Trends Microbiol.* **2006,** *14,* 389.

[33] I. W. Sutherland, The biofilm matrix - an immobilized but dynamic microbial environment. *Trends Microbiol.* **2001,** *9,* 222.

[34] C. M. Waters, B. L. Bassler, Quorum Sensing: Cell-to-cell communication in bacteria. *Annu. Rev. Cell Dev. Biol.* **2005,** *21,* 319.

[35] K. Hojo, S. Nagaoka, T. Ohshima, N. Maeda, Bacterial interactions in dental biofilm development. *Journal of Dental Research}* **2009,** *88,* 982.

[36] D. H. Nies, Microbial heavy-metal resistance. *Appl.Microbiol.Biotechnol.* **1999,** *51,* 730.

[37] G. M. Teitzel, M. R. Parsek, Heavy metal resistance of biofilm and planktonic *Pseudomonas aeruginosa*. *Appl.Environ.Microbiol.* **2003,** *69,* 2313.

[38] A. Schluter, R. Szczepanowski, N. Kurz, S. Schneiker, I. Krahn, A. Puhler, Erythromycin resistance-conferring lasmid pRSB105, Isolated from a sewage treatment plant, harbors a new macrolide resistance determinant, an integron-containing Tn402-like element, and a large region of unknown function. *Appl.Environ.Microbiol.* **2007,** *73,* 1952.

[39] F. Baquero, J. Martínez, R. Cantón, Antibiotics and antibiotic resistance in water environments. *Curr.Opin.Biotechnol.* **2008,** *19,* 260.

[40] M. A. Rege, D. R. Yonge, D. P. Mendoza, J. N. Petersen, Y. Bereded-Samuel, D. L. Johnstone, W. A. Apel, J. M. Barnes, Selenium reduction by a denitrifying consortium. *Biotechnol.Bioeng.* **1999,** *62,* 479.

[41] C. B. Dissanayake, R. Chandrajith, C. B. Dissanayake, R. Chandrajith, Selenium- a new entrant to medical geology. **2009,** 205.

[42] M. J. Dykstra, *in Biological electron microscopy theory, techniques, and troubleshooting* **1992**, pp. 113-246 (Plenum Press: New York).

[43] E. Denkhaus, S. Meisen, U. Telgheder, J. Wingender, Chemical and physical methods for characterisation of biofilms. *Microchimica Acta* **2007,** *158,* 1.

[44] S. J. Maginn, Tutorial Review. Analytical applications of synchrotron radiation. *Analyst* **1998,** *123,* 19R.

[45] A. Iida, A. Yoshinaga, K. Sakurai, Y. Gohshi, Synchrotron radiation excited x-ray fluorescence analysis using total reflection of x-rays. *Anal.Chem.* **1986,** *58,* 394.

[46] Canadian Light Source, *2011,*http://www.lightsource.ca/education/whatis.php.

[47] G. E. Brown, N. C. Sturchio, An overview of synchrotron radiation applications to low temperature geochemistry and environmental science, reviews in mineralogy geochemistry. **2002**, *49*, 1.

[48] G. George, I. Pickering, X-ray absorption spectroscopy in biology and chemistry. **2007,** *13,* 97.

[49] G. N. George, I. J. Pickering, C. J. Doonan, M. Korbas, S. P. Singh, R. E. Hoffmeyer, *in Advances in Molecular Toxicology* (Eds J. C. Fishbein) **2008**, pp. 123-152 (Elsevier: Hungary).

[50] P. M. Bertsch, D. B. Hunter, Applications of synchrotron-based X-ray microprobes. *Chem.Rev.* **2001,** *101,* 1809.

[51] A. C. Thompson, D. T. Attwood, E. M. Gullikson, M. R. Howells, J. B. e. Kortright, *in X-Ray data booklet* **2001**, pp. 1-17 (Center for X-ray Optics and Advanced Light Source, Lawrence Berkeley National Laboratory: California).

[52] H. Mimura, S. Matsuyama, H. Yumoto, H. Hara, K. Yamamura, Hard X-ray diffraction-limited nanofocusing with unprecedentedly accurate mirrors. *Proceedings of the 8th international conference on X-ray microscopy* **2006,** *7,* 100.

[53] European Synchrotron Radiation Facility, Micro-spectroscopic experiments at ID22. *2011,*http://www.esrf.eu/UsersAndScience/Experiments/Imaging/ID22/BeamlineManual/Micro-Spectroscopy/Micro-Probe_Setup.

[54] SM beamline, STXM user manual. *2011,* http://exshare.lightsource.ca/sm/Pages/Manuals.aspx.

[55] S. Vogt, X-Ray microscopy and imaging: X-ray fluorescence mapping. *2011,*http://www.aps.anl.gov/Xray_Science_Division/Xray_Microscopy_and_Imaging/Science_and_Research/Techniques/Xray_Fluorescence_Mapping/index.html.

CHAPTER 2. INVESTIGATION OF SELENIUM CHEMICAL SPECIES IN NATURAL BIOFILMS

This study was designed to investigate biotransformation of selenium in naturally occurring biofilms. The information acquired here was used to design laboratory-based in-depth selenium biotransformation studies of multispecies and pure-culture biofilms in the following chapters. In addition, microbial sources used in chapter 3, 4, and 5 were collected and isolated from this study site.

2.1. ABSTRACT

In this study, biotransformation of selenium in natural biofilms was investigated. Natural biofilm was allowed to develop in the field for a month. Mature biofilms were recovered from 3 areas in Goddard Marsh, which receives coal mine-affected water. The collected Se-affected water contained 5.2 ppb of selenium, measured with an atomic absorption spectrometry. A speciation study conducted with selenium K X-ray absorption near-edge spectra and least-square fitting showed 80 % of selenium species observed in the biofilms were methylated or elemental selenium, demonstrating biotransformation of selenium in the natural biofilms. The information observed in this study was used to design and conduct laboratory-based research in later chapters.

2.2. INTRODUCTION

Selenium is an essential element to animals, yet it poses a very narrow gap between required and toxic levels [1]. In addition, a prolonged exposure of selenium even at a low level can cause toxicity problems in the environment. Environmental exposure of selenium occurs mainly through two routes: natural release in high selenium areas or anthropogenic release through agricultural drainage or mining activities [2, 3]. Coal mining, as an example, can release selenium into the environment during its mining and processing. Although the amount of selenium in the coal greatly depends on its types and geographical locations of mines, coal may contain up to 24 ppm of selenium [3].

Biofilms, microbial consortia, confer significant resistance to physical, chemical stress compared to their planktonic counterparts, as well as the ability to biotransform toxic elements [4]. Biofilms

consist of microorganisms and extracellular polymeric substances (EPS), and contain almost 95 % of water [5]. To investigate the role of naturally forming biofilm in the selenium transformation, biofilm reactors were distributed in Goddard Marsh (GM) of Elkview Coal mine in British Columbia (BC), Canada, within which elevated selenium levels previously were reported [6]. To investigate the role of naturally occurring biofilms in the geochemical cycling of selenium, the selenium species in the biofilms were studied using synchrotron-based X-ray absorption spectroscopy (XAS).

2.3. METHODOLOGY

2.3.1. Sample collections and biofilm acquisition

Sample collectors were designed using polycarbonate plastic materials to increase the biomass recovery as Kröpfl *et al* [7] reported. Six polycarbonate plastic slides (18 cm × 5 cm) were attached to concrete blocks (19 cm × 40 cm) and 5 blocks were aseptically prepared to collect natural biofilm from Goddard Marsh (Figure 2.1) in July 2008. The Universal Transverse Mercator (UTM) of the specific sampling area was zone 11, 0653165 (Easting), and 5514141 (Northing). GM was selected due to its high selenium level as Orr *et al* [8] previously reported. Five sets of collectors were distributed around the area and 30 slides were collected from 3 different spots within the areas (2, 2, and 1 blocks in 3 areas). The biofilms were collected from the field in August 2008 after allowing 1 month of biofilm formation (Figure 2.2).

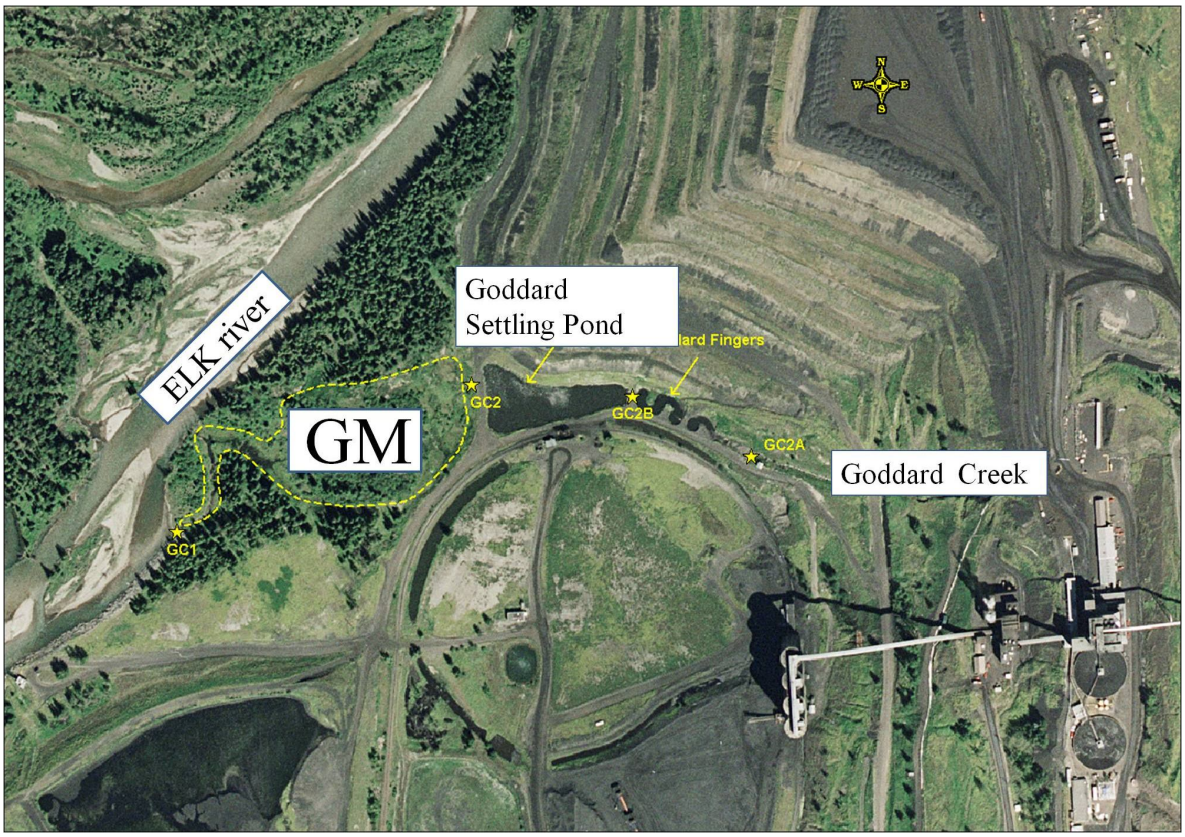

Figure 2.1. Satellite view of sampling area (Goddard Marsh, GM) in British Columbia, Canada (image courtesy of the Elkview Coal mine). GM is noted with a dotted line.

Figure 2.2. Placement of a natural biofilm collector (left) in July 2008 and recovery of the biofilm from the surface of polycarbonate substratum (right) in August 2008.

2.3.2. Natural biofilm preparation

Cultivated biofilms were recovered from the polycarbonate strips, transferred into micro-centrifuge tubes and kept with ice to prevent further biological reactions during overnight transportation to laboratories in Saskatoon. Following this, biofilms from each substratum were homogeneously mixed and packed into 2 mm XAS cuvettes followed by flash freezing in iso-pentane containing liquid nitrogen. The prepared samples were stored in a liquid nitrogen Dewar or -80 °C deep freezer until required.

2.3.3. Selenium speciation study of natural biofilm

Selenium speciation in natural biofilm was carried out using X-ray absorption spectroscopy at beamline 7-3 of the Stanford Synchrotron Radiation Lightsource (SSRL). An upstream Rh-coated bent flat mirror was used both to collimate the beam in the vertical direction and to provide harmonic rejection by adjusting the angle of incidence. The collimated polymeric beam was introduced into a Si(220) double crystal monochromator to produce monochromatic beam. A beam size of 1 mm x 8 mm was set using slits in the hutch. Incident and transmitted intensities were measured using ion chambers filled with nitrogen gas. The sample, prepared as described above, was set at 45° to the beam. During data collection, samples were maintained at approximately 10 - 13 K in a liquid helium flow cryostat (Oxford Instruments, Abingdon, UK). Selenium K_α fluorescence emission line was recorded using an energy dispersive 30 element germanium detector (Canberra Corp., Meriden, CT) at 90° to the incident beam. Scattered photons were reduced with the use of an arsenic filter, followed by Soller slits to remove filter fluorescence. Internal calibration was performed using a gray hexagonal elemental selenium foil located between the I_1 and I_2 ion chambers, downstream of the sample position. The first energy inflection of the foil was assumed to be 12,658 eV. Data processing including background subtraction and normalization was carried out using the EXAFSPAK program [9]. Quantitative analysis of the chemical speciation of selenium in the sample was performed as previously described [10].

2.3.4. Measurement of Selenium concentration

Selenium concentration of collected water samples was determined using atomic absorption spectrometry (AAS) as Mages *et al* [11] described. Proper modifications were made to the protocol as follows: ten milliliter of GM water was boiled to evaporate and the sample size was reduced to 500 µL, then 500 µL of nitric acid followed by 1/10 volume of hydrogen peroxide (30 %) was applied to digest organic materials and release bound selenium. The prepared sample solutions were ashed by boiling them on a hot plate. Afterwards, the ashed samples were dissolved in 10 mL of 3.7 % hydrochloric acid (10 × dilution from concentrated hydrochloric acid) for AAS measurements. The amount of recovered ashed biofilms were too little to measure using a conventional scale (micro gram or less unit) and inhomogeneous sample conditions due to sand, clay, and coal particles within biofilms caused difficulties in AAS sample preparation and prevented any measurements from being taken.

2.4. RESULTS AND DISCUSSION

The sampling area was previously reported to have an increased level of selenium [8], which greatly exceeds the water quality guidelines of both Canada (drinking water, HWC, 1 ppb [12]) and the US (USEPA, 5 ppb [13]). The average Se concentration of GM water in the samples collected at the time of biofilm harvest measured with AAS showed 5.2 ppb (± 1.1 ppb) and pH 7.4 (± 0.1). Our measured selenium level is much lower than that reported by both Orr *et al* [8] and Martin *et al* [14], where over 82 and 23.7 ppb of aqueous selenium were reported, respectively.

The selenium K near-edge spectrum collected from the harvested GM biofilm showed that it has 80 % of reduced species modelled as selenomethionine, the trimethylselenonium ion, and elemental selenium, with 20% as the oxyanion selenite (Figure 2.3, Figure 2.4, Table 2.1). Considering that oxyanions, such as selenate and selenite, are predominant in soil and aquatic systems [15] and selenate is the major dissolved selenium species in environmental water samples [16], the presence of methylated and zero oxidation state selenium species may suggest biotransformation of selenium oxyanions by the biofilms. However, possible sorption of reduced selenium species from the water by the naturally occurring biofilms cannot be ruled out from this observation alone.

Adsorption or absorption of methylated selenium by other organisms, such as plants, is also possible under natural conditions. However, it is very unlikely that elemental selenium is absorbed by biofilms due to its low solubility according to our conventional understanding of elemental selenium. These observations are slightly different from what Martin *et al* [14] reported for the top layer of sediment (< 1 cm) collected from GM area. In the natural environment, biofilms grow on the surface of materials, such as sediment and rocks, thus the surfaces of the sediment might provide a substrate analogous to the bioreactor in which the natural biofilms grew. The proportions of elemental and organo-selenium on the shallow sediment [14] and biofilm (this study) were very similar, both showing approximately 40 and 35 %, respectively. However, a higher proportion of selenite (< 5 %), and absence of FeSe and selenodisulfide in the biofilms may suggest that they grew in a more oxidizing environment compared to the sediment, which suggests the observation of elemental selenium may due to microbial activities. Of course, there are several additional differences between the two observations, which include the seasons of sampling, variable mining activities, and the fact that the bioreactors were left to equilibrate for just one month. Any of these factors may greatly affect the amount and chemistry of organic compounds and selenium as well as the dominant microbial species present, implying a direct comparison may be not adequate. However, observation of reduced selenium species in the biofilms suggests an important role of biofilms in the process of geochemical cycling of selenium in the environment.

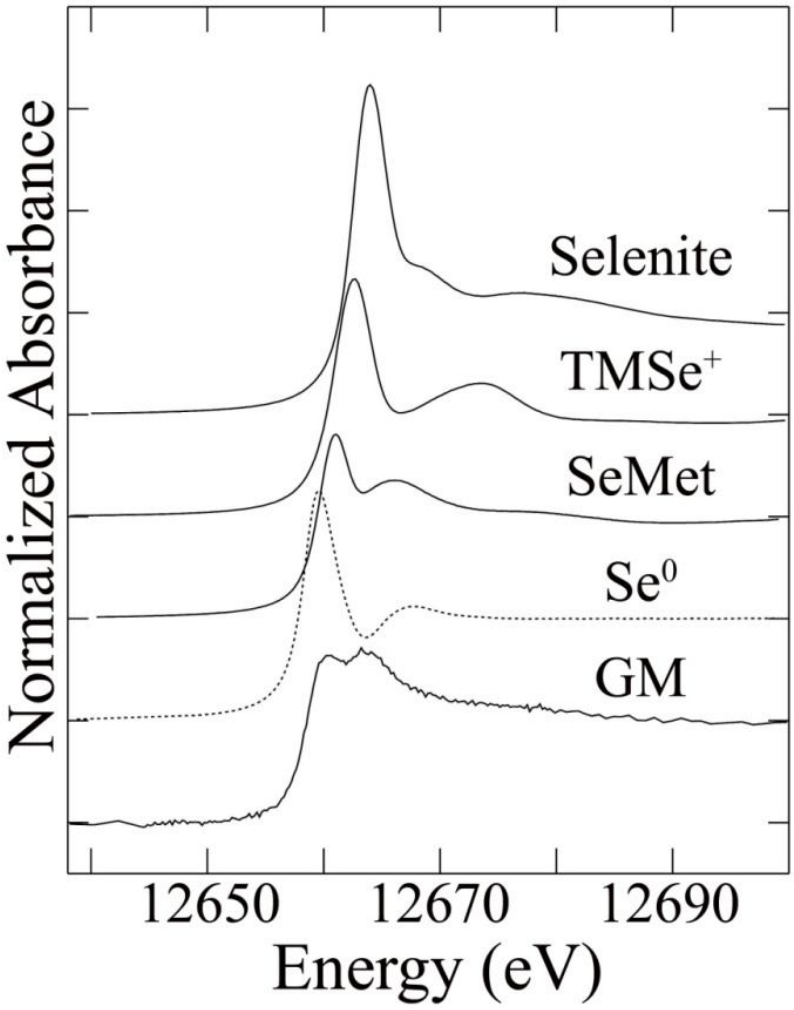

Figure 2.3. Selenium K X-ray absorption near-edge structure of natural biofilm grown and harvested from Goddard Marsh (GM), selenite, trimethylselenonium ion ($TMSe^{+}$), selenomethionine (SeMet), elemental selenium (Se^{0}) are shown.

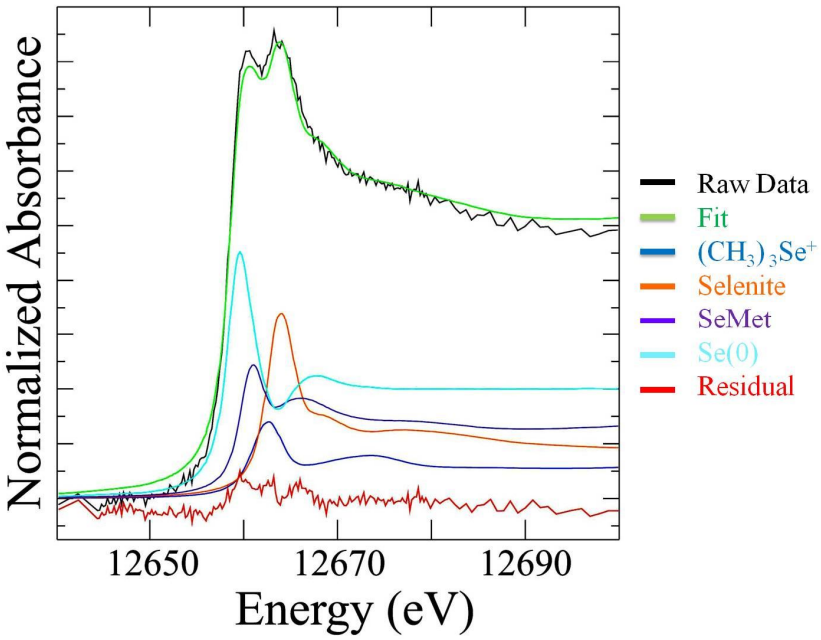

Figure 2.4. Selenium K near-edge spectra of mixed natural biofilms collected from Goddard Marsh (Raw Data, black) with a least square fit (Fit, green) from a linear combination of model compounds as shown. $(CH_3)_3Se^+$, Se(0), and residual represent trimethylselenonium ion, elemental selenium, and difference between data and fit. Component spectra have been scaled to show their contributions to the Fit spectrum.

Table 2.1. Selenium chemical species observed in natural biofilm collected from Goddard Marsh after 1 month growth*.

Observed selenium species	Fraction (%)	Fit error ($\times 10^{-4}$)**
Selenite	20(1)	3.6
$TMSe^+$	12(2)	
SeMet	27(3)	
Se(0)	41(2)	

* Three times estimated standard deviation is shown in the parenthesis.

** Fit error (f) is defined as $f = \frac{1}{n}\sum(A_{obs} - A_{cal})^2$, where 'n' (the number of data points within range), and 'obs' (observed) and 'cal' (calculated) absorbance (A) are shown.

2.5. CONCLUSIONS

This study showed natural biofilms play a role in the geochemical cycling of selenium in the environment. Because the major selenium species found in environmental water samples is selenate, the presence of elemental and methylated selenium species and their high proportion (80 %) implies the involvement of naturally forming biofilms in the process of selenium transformation. Thus, this study suggested further research on selenium biotransformation is required for better understanding of selenium biotransformation. In particular, there is an uncertainty as to whether the biofilms grown in the field might be adsorbing the reduced species from the environment, rather than performing the biotransformation themselves. Therefore, the growth of biofilms under much more controlled conditions in the laboratory is needed and this work will be described in the next chapter.

2.6. ACKNOWLEDGEMENTS

I thank Tech Coal Company (previously Elkview coal mine) for permission to work at this field site. I also appreciate Dr. Satya P. Singh of the Department of Geological Sciences for his assistance in collecting natural biofilms and transporting field water samples to the laboratory in Saskatoon. This research was supported by an NSERC Discovery Grant (to Pickering). Pickering is a Canada Research Chair. Yang is a CIHR-THRUST Fellow. Portions of this research were carried out at the Stanford Synchrotron Radiation Lightsource (SSRL), a national user facility operated by Stanford University on behalf of the U.S. Department of Energy, Office of Basic Energy Sciences. The SSRL Structural Molecular Biology Program is supported by the Department of Energy, Office of Biological and Environmental Research, and by the National Institutes of Health, National Center for Research Resources, Biomedical Technology Program.

2.7. REFERENCES

[1] A. G. Renwick, Toxicology of micronutrients: adverse effects and uncertainty. *J. Nutr.* **2006,** *136,* 493S.

[2] H. M. Ohlendorf, R. L. Hothem, C. M. Bunck, K. C. Marois, Bioaccumulation of selenium in birds at Kesterson Reservoir, California. *Arch.Environ.Contam.Toxicol.* **1990,** *19,* 495.

[3] A. D. Lemly, Aquatic selenium pollution is a global environmental safety issue. *Ecotoxicol. Environ. Saf.* **2004,** *59,* 44.

[4] D. H. Nies, Microbial heavy-metal resistance. *Appl. Microbiol. Biotechnol.* **1999,** *51,* 730.

[5] E. van Hullebusch, M. Zandvoort, P. Lens, Metal immobilisation by biofilms: mechanisms and analytical tools. *Rev. Environ. Sci. Biotechnol.* **2003,** *2,* 9.

[6] P. L. Orr, K. R. Guiguer, C. K. Russel, Food chain transfer of selenium in lentic and lotic habitats of a western Canadian watershed. *Ecotoxicology and Environmental Safety* **2006,** *63,* 175.

[7] K. Kröpfl, P. Vladár, K. Szabó, E. Ács, A. K. Borsodi, S. Szikora, S. Caroli, G. Záray, Chemical and biological characterisation of biofilms formed on different substrata in Tisza river (Hungary). *Environ Pollut* **2006,** *144,* 626.

[8] P. L. Orr, K. R. Guiguer, C. K. Russel, Food chain transfer of selenium in lentic and lotic habitats of a western Canadian watershed. *Ecotoxicol. Environ. Saf.* **2006,** *63,* 175.

[9] G. N. George, I. J. Pickering, EXAFSPAK: A Suite of computer programs for analysis of X-ray absorption spectra available at http://ssrl.slac.stanford.edu/exafspak.html. **2001,**.

[10] I. J. Pickering, G. N. George, V. Van Fleet-Stalder, T. G. Chasteen, R. C. Prince, X-ray absorption spectroscopy of selenium-containing amino acids. *J. Biol. Inorg. Chem.* **1999,** *4,* 791.

[11] M. Mages, W. v. Tümpling jun., d. V. van, M. Baborowski, Element determination in natural biofilms of mine drainage water by total reflection X-ray fluorescence spectrometry. *Spectrochimica Acta Part B: Atomic Spectroscopy* **2006,** *61,* 1146.

[12] Canadian Council of Misters of the Environment, Canadian environmental quality guidelines. *2011,*http://www.ccme.ca/publications/ceqg_rcqe.html.

[13] US-EPA, Current national recommended water quality criteria. *2007,*http://www.epa.gov/waterscience/criteria/wqcriteria.html.

[14] A. J. Martin, S. Simpson, S. Fawcett, C. I. E. Wiramanaden, I. J. Pickering, N. Belzile, Y. -. Chen, J. London, D. Wallschlager, Biogeochemical mechanisms of selenium exchange between water and sediments in two contrasting lentic environments. *Environ.Sci.Technol.* **2011,** *45,* 2605.

[15] V. Van Fleet-Stalder, T. G. Chasteen, I. J. Pickering, G. N. George, R. C. Prince, Fate of selenate and selenite metabolized by *Rhodobacter sphaeroides*. *Appl. Environ. Microbiol.* **2000,** *66,* 4849.

[16] D. Tanzer, K. G. Heumann, Determination of dissolved selenium species in environmental water samples using isotope dilution mass spectrometry. *Anal.Chem.* **1991,** *63,* 1984.

CHAPTER 3. BIOTRANSFORMATION OF SELENIUM AND ARSENIC IN MULTI-SPECIES BIOFILM

This chapter is a modified version of an article accepted in the journal Environmental Chemistry and is reproduced with permission from the journal (Soo In Yang, John R. Lawrence, George D. W. Swerhone, and Ingrid J. Pickering, 2011, Biotransformation of selenium and arsenic in multi-species biofilm, accepted). In this research paper, I planned, designed, conducted experiments and played a main role in preparing the paper. Other coauthors provided advice, help on experiment, and contributed to the preparation of the paper.

In this study, selenium and arsenic biotransformation was investigated in laboratory-grown biofilms using the collected coal mine wastewater. Microbial population and nutrients present in the collected water from chapter 2 were used to generate biofilms in the laboratory. The biotransformation of selenium and arsenic, and selenium/arsenic was investigated using CLSM, XAS, and μ-XRF techniques. This study showed how multispecies biofilms interact with high concentration of selenium and arsenic oxyanions.

3.1. ABSTRACT.

Arsenic and selenium are both elements of concern especially when released into the environment by anthropogenic activity. Biofilms, or communities of microorganisms, can play important roles in biotransforming elements to less toxic chemical forms. This study used novel tools to characterize the fate of oxyanions (selenate, selenite, arsenate or arsenite) in multispecies biofilms inoculated from a source receiving coal mine effluent. Confocal laser scanning microscopy (CLSM) demonstrated distinct biofilm morphology at elevated oxyanion concentrations. Selenium and arsenic K near-edge X-ray absorption spectroscopy (XAS) showed biofilm biotransformation of oxyanions; extended X-ray absorption fine structure (EXAFS) confirmed elemental selenium as a product. Micro X-ray fluorescence imaging combined with CLSM revealed highly localized reduced selenium species in the biofilm. Isolation and partial 16S rRNA gene sequencing suggested 4 principal bacterial genera were responsible. Biofilms can both detoxify and sequester selenium and arsenic, playing critical roles in their fate and effects in aquatic environments.

3.2. INTRODUCTION

Selenium plays an essential role in metabolism[1] as a constituent of antioxidant enzymes, such as glutathione peroxidase (GPx), thioredoxin reductase (TR), iodothyronine deiodinase and others in humans.[2, 3] In spite of this important role, the toxic effects of higher concentrations represent a concern not only for humans, but also in aquatic ecosystems.[4-6] One notorious example of selenium toxicity in the environment is the Kesterson Reservoir case, where increased levels of selenium in water caused deformity of fish and seriously disturbed physiological functions in birds.[7-9] Arsenic is another element of environmental concern; typically present in soils at levels between 0.1 and 40 ppm, higher levels may indicate contamination by anthropogenic sources such as mining.[10, 11]

High levels of selenium and arsenic from mining activities have been of considerable concern and reported in diverse regions of the world.[12, 13] For example, coals generally contain close to 10 and 50 ppm of selenium and arsenic, respectively,[14, 15] which can lead to release of these elements during coal mining and processing. Arsenic and selenium are readily metabolized by prokaryotes and attempts have been made to exploit this capability in order to mitigate selenium and arsenic contamination.[16-18] Progress has been made in understanding the fundamental mechanisms of selenium biotransformation in many planktonic bacteria, such as the aquatic bacterium *Thauera selenatis*,[19] *Bacillus* sp,[20] *Pseudomonas fluorescens* K27,[21] *Rhodobacter sphaeroides*[22] and others. In the environment, microorganisms are most commonly found not in planktonic forms but in biofilms, which are communities of microbial cells surrounded by or embedded in extracellular polymeric substances (EPS).[23, 24] Despite the importance of biofilms, there is limited fundamental information on how they resist and transform potentially toxic elements such as selenium and arsenic.

In general, cells in biofilms are better protected from chemical, physical, and biological stress than in planktonic forms.[24] Biofilms are known to play a vital role in detoxification of environmentally hazardous chemical species and the utilization of biofilms for bioremediation has drawn attention for a long time.[25] However, there are challenges in characterizing biofilms. Most of the available microscopy-based research approaches require the use of probe conjugated fluorophores or staining. This may limit assessment of the interrelationships of microbial cells,

EPS, and microenvironments particularly in relation to metals and metalloids.[26] Therefore, the present research implemented less destructive synchrotron based techniques as well as conventional confocal microscopy and culture-based analytical methods to characterize the biofilms.

This study was aimed at characterizing biofilms from a source with elevated levels of selenium and arsenic in order to investigate the biotransformation of these elements at high levels in the cultivated biofilms. Biofilms were generated in the laboratory using effluent affected water collected from a coal mine tailings site. The chemical species of selenium and arsenic present in the biofilms were investigated using X-ray absorption spectroscopy (XAS). Biofilm physical structure was examined by confocal laser scanning microscopy (CLSM) and the distribution of selenium in the biofilms was investigated using micro X-ray fluorescence (μ-XRF) imaging. This research was designed to answer fundamental questions on how biofilms biotransform and sequester high levels of selenium and arsenic, and may contribute to the development of bioreactors to treat selenium or arsenic affected areas or waters.

3.3. EXPERIMENTAL METHODS

3.3.1. Acquisition of mining effluent

Forty liters of water was collected using polyethylene plastic bottles in August 2008 from Goddard Marsh (GM), a lentic environment in British Columbia, Canada that receives effluent from a coal mine with high levels of selenium.[4]. Water samples were collected from 3 random points including an influx point into which effluent from coal processing flows directly. The universal transverse mercator (UTM) of GM is zone 11, 0653165(Easting), and 5514141(Northing). Water was transported to laboratories in Saskatoon and stored at 4 ºC for 7 days until required.

3.3.2. Identification of selenium resistant isolates

Bacterial genomic DNA from cultured selenium resistant microorganisms was isolated (GenElute Bacterial Genomic DNA kit, Sigma) and 16S rRNA genes were amplified using PCR primers (fD1, rP2;[27] Integrated DNA Tech., IA, USA). PCR conditions used were as follows:

initial denaturation (94 ºC, 3 min), denaturation (94 ºC, 30 sec), annealing (63 ºC, 45 sec), extension (72 ºC, 2 mins, additional 30 sec per cycle), and final extension (72 ºC, 15 min). The conservative 1.5 kbp 16S rRNA genes were examined on 1 % agarose gel and purified (Qiagen PCR purification kit, Qiagen, ON, Canada). DNA sequencing was performed using ABI 3730 capillary electrophoresis DNA analyzer at NRC Plant Biotechnology Institute (Saskatoon, Canada). The resultant DNA sequences were blasted for identification at NCBI website (http://blast.ncbi.nlm.nih.gov/Blast.cgi).

3.3.3. Selection of biofilm treatment conditions

Laboratory-generated biofilms were inoculated using effluent impacted water collected in GM. Atomic absorption spectroscopy measurements of selenium and arsenic indicated that both were lower in the collected water (< 0.06 μM; equivalent to < 5 ppb of selenium and arsenic) than reported.[5] Biofilms were treated with selenate or selenite, alone or in combination with arsenate or arsenite, as these oxyanions are the most common forms found in aqueous environments. Treatment concentrations of 0.63, 6.33, and 12.6 mM Se and/or As (approximately equivalent to 50, 500, 1000 ppm, respectively) were selected. These concentrations were chosen to conduct fundamental investigations of the response of the biofilms to relatively high yet physiologically tolerable levels of the oxyanion while providing readily detectable selenium and/or arsenic levels for speciation of chemical forms.

3.3.4. Preparation of biofilm

Biofilms were generated by circulating 10 L of GM water mixed from 3 random points as inoculum using rotating (160 rpm) annular bioreactors[28] supplied with water at a flow rate of 1.4 mL·min^{-1} by a peristaltic pump (Watson-Marlowe; Fisher Scientific). Prior to inoculation, all equipment surfaces were disinfected by circulating 5 % sodium hypochlorite for 30 min followed by rinsing with excess autoclaved distilled water. Biofilms were grown for 30 days at room temperature (22 ± 3 ºC) and the biofilm development was examined using confocal laser scanning microscopy (see below). Mature biofilms were rinsed 5 times with filtered (0.2 μm, Nalgene) GM water before transferring to 50 mL conical tubes containing the As and/or Se treatment and placing on a gyratory shaker (100 rpm). Each tube contained 50 mL of GM water

which had been filtered (Whatman #1 and Sterfil Aseptic System equipped with 0.2 μm filter, Millipore) to eliminate planktonic bacteria. Afterwards, aliquots from the filtered (0.2 μm) stock solution of arsenic and selenium with sodium counter cations were applied into the GM water. Additional biofilm growth under amendment with As and/or Se species was allowed for either 20 days for a short term or 90 days for a long term exposure at 100 rpm on a gyratory shaker at room temperature. No additional nutrients were added in order to avoid providing nutritional selection pressure. To monitor possible chemical species change of arsenite in absence of biofilm, 1 mM arsenite (final concentration) dissolved in the filtered (0.2 μm) GM water was incubated under the same condition.

3.3.5. Confocal laser scanning microscopy (CLSM) and molecular probes

Biofilm structure was examined as reported by Lawrence *et al.*[29] Briefly, a 1 cm × 1 cm polycarbonate substratum with biofilm was rinsed 3 times with filtered (0.2 μm pore size) GM water to prevent osmotic shock and contamination. The rinsed samples were stained using fluorescent probes (DNA specific SYTO-9, Invitrogen; *Triticum vulgaris* lectin, Sigma-Aldrich) according to the manufacturers' instructions. Images were obtained using red, green, and far red fluorescence.[29] Quantitative analyses of image stacks were performed using macros created in Image J.[30] Statistical analysis was performed using one way ANOVA (analysis of variance).

3.3.6. Colony counts and isolation of selenium tolerant microorganisms

Viable cell counting was carried out by applying 100 μL of GM water onto 10 % tryptic soy agar (TSA) plates containing up to 200 mM sodium selenate and incubating for 7 days at room temperature. Higher concentrations of sodium selenate, 400 and 500 mM, incubated for 30 days, were used subsequently to investigate resistance/tolerance at higher concentration. The microbial species isolated through this process are culturable microorganisms and this process reflects selective microbial populations, which can grow aerobically on TSA plates. Statistical analysis was performed using one way ANOVA.

3.3.7. X-ray absorption spectroscopy (XAS)

Biofilms for XAS analysis were rinsed at least 3 times using filtered (0.2 μm filter) GM water to eliminate planktonic bacteria. Biofilms were removed from the polycarbonate substrata using a sterile piece of silicon tubing as a scraper, and then quickly packed into 2 mm path length XAS cuvettes followed by flash freezing in slurry of iso-pentane and liquid nitrogen. Frozen samples were preserved in liquid nitrogen up to 60 days. Data collection was carried out at the Stanford Synchrotron Radiation Lightsource (SSRL) as previously described.[31-34] Reference spectra consisted of dilute (1 mM) aqueous solutions of biologically relevant species collected in fluorescence with the exception of elemental selenium, which was measured in transmittance. Data processing including background subtraction and normalization was carried out using the EXAFSPAK program.[35] Quantitative analysis of the chemical speciation of selenium and arsenic in the sample was carried out as previously described with minor modifications.[31-34] The total curve-fitting method was carried out by fitting the spectrum of a biofilm or related unknown sample to a linear combination of reference selenium or arsenic spectra. The percentage contribution of the reference spectrum to the biofilm spectrum is equivalent to the contribution of that chemical species to the total Se or As in the biofilm. A small component for which the 95 % confidence limit exceeded the fitted value was considered not significant; the component was removed and the fit was performed again without this component.

3.3.8. Extended X-ray absorption fine structure (EXAFS)

For EXAFS, the reddish precipitate produced by a multi-species community was prepared by growth in 3 ml of 10 % tryptic soy broth (TSB) with 280, 290, and 300 mM sodium selenate for 20 days with 1 % inoculum of GM water. Cells were harvested by centrifuging at 8,000 g for 30 seconds and were rinsed 5 times with 10 % autoclaved TSB to remove any excess selenate loosely associated with precipitates. Washed precipitates were combined in a 2 mm pathlength XAS cuvette and flash frozen in slurry of iso-pentane and liquid nitrogen. EXAFS analysis was carried out using EXAFSPAK according to standard procedures with phase and amplitude functions calculated using *ab initio* calculation code, FEFF 7.0.[36]

3.3.9. Micro X-ray fluorescence (μ-XRF)

Biofilms for μ-XRF imaging were grown on 50 nm thick silicon nitride windows (0.5 mm × 0.5 mm, NX5050B, Norcada Inc). The wells of 24-well plates (Nunclon Multidish, Nalgene) were disinfected using 5 % sodium hypochlorite and rinsed by circulating excess autoclaved distilled water. Silicon nitride windows were placed in the wells and the open tops were sealed with rubber stoppers. GM water was circulated and biofilms developed for 20 days; following this, 50 mL of GM medium was spiked with sodium selenate (6.33 mM final concentration) and circulated for 60 days. The biofilms were subsequently rinsed at least 5 times and air-dried. Data were collected at beamline 2-3 of SSRL with a Si(220) double crystal monochromator and using a Kirkpatrick-Baez (KB) mirror system to vertically and horizontally focus the beam to a spot size of 2.5 μm × 2.5 μm on the sample. Nitrogen gas-filled ion chambers were located upstream and downstream of the sample to monitor the intensity of the incident and absorbed beams. The silicon nitride window was supported on an aluminum frame positioned at 45º to the beam. A single element Vortex® silicon drift detector (SII NanoTechnology USA Inc., Northridge, CA) was located at 90° to the incident beam to measure the fluorescence emission spectrum from the sample. Data were processed using the SMAK software.[37] Following the micro X-ray fluorescence mapping, selenium K near-edge spectra were collected on selected high-selenium pixels. Five identical sweeps at the same pixel were averaged to provide acceptable signal to noise. The individual sweeps were identical within the signal to noise, indicating no temporal changes to the selenium speciation during data collection.

3.4. RESULTS AND DISCUSSION

3.4.1. Effect of arsenic and selenium on biofilm structure

Figure 3.1 shows the results of confocal laser scanning microscopy (CLSM) of biofilms treated with arsenic and selenium oxyanions together with a control. The biofilms showed reduced diversity of morphological populations in the presence of 0.63, 6.33, and 12.6 mM selenium and arsenic when compared with the control biofilm. Figure 3.2 displays population density and shows that the total number of microorganisms also decreased relative to the control biofilm in the presence of selenium and arsenic. Moreover, optical sectioning by CLSM showed a decrease in biofilm thickness as a function of concentration. Conversely, when selenate and arsenate were used together an increase in the total number of microorganisms was observed with increasing

metalloid oxyanion concentration (Figure 3.1 and 3.2). This might be explained by selection of resistant microorganisms within the biofilm, and is consistent with the observed decrease of morphological diversity concomitant with an increased count of morphologically similar microorganisms. Identification using partial 16S rRNA gene sequencing (500 bps) of highly selenium resistant culturable microorganisms, which were selected from the presumable elemental selenium-containing dark red colonies, indicated that *Rhodococcus* sp (Gene Bank ID, AP0008957), *Pseudomonas* sp (FJ652605.1), *Bacillus* sp (GQ495047), and *Arthrobacter* sp (FJ517623.1) are present in the community.

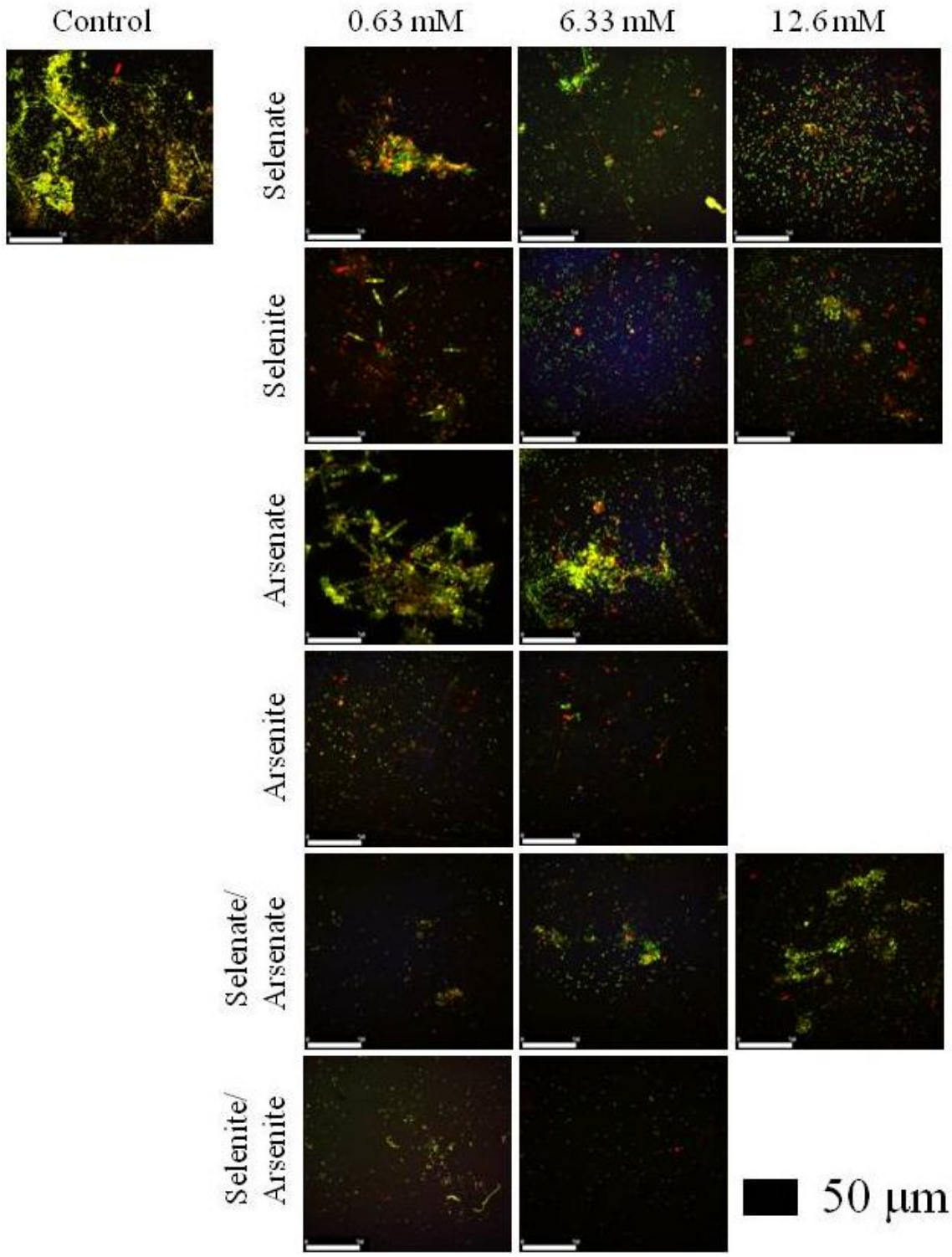

Figure 3.1. Selected representative stacked confocal laser scanning microscopy (CLSM) images of biofilms treated for 20 days with selenate, selenite, arsenate and/or arsenite. Laser-induced fluorescence images of microorganisms (green), polysaccharide and EPS (red), and co-localized microorganisms and EPS (yellow) are shown at forty times magnification (scale bar, 50 µm).

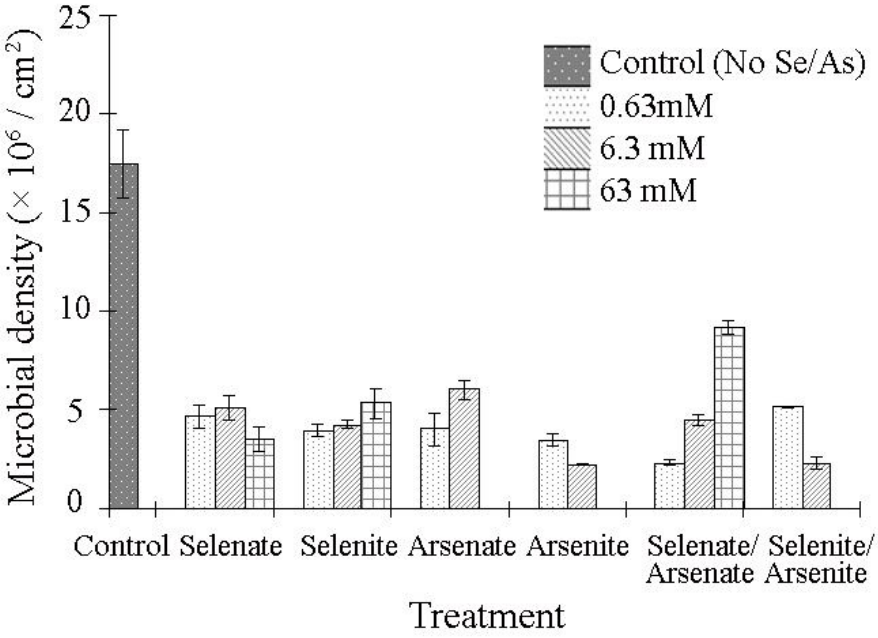

Figure 3.2. Microbial populations observed in each stacked confocal laser scanning microscopy (CLSM) biofilm image after treatment for 20 days with selenate, selenite, arsenate and/or arsenite at As and/or Se concentrations of 0.63, 6.33, or 12.6 mM. The populations were detected and visualized using DNA specific probe SYTO-9 and measured in 2 to 3 areas. Error bars indicate standard deviations.

3.4.2. Biotransformation of selenium

Selenium and arsenic K near-edge X-ray absorption spectroscopy (XAS) were used to probe the biotransformation of selenium and arsenic oxyanions by biofilms. XAS is sensitive to the local chemical environment around a central absorbing atom.[32] Bulk XAS can be used to investigate the chemical species averaged over the total biofilm communities sampled by the X-ray beam and can be carried out essentially without pretreatment of the biofilm, preserving the chemical integrity. Least-squares fitting of the biofilm and media near-edge spectra to linear combinations of the spectra of standard species is a standard method that can be used to quantitatively analyze the percentages of chemical species present.[32] In both biofilms and media a variety of chemical species were observed, specifically, selenate, selenite, Se(0) (elemental selenium), TMSe

(trimethylselenonium), SeMet (selenomethionine), arsenate, arsenite, MMA(V) (monomethylarsonate), MMA(III) (monomethylarsinite), and TMAO (trimethylarsine oxide) were observed (Figure 3.3). Normalized spectra from biofilms and media after treatment with 6.33 mM selenium and arsenic are shown in Figure 3.3.

In selenate-spiked biofilms using short term incubation (20 days), selenium located within the biofilms showed 15 % and 36 % biotransformation in the absence and presence of arsenate, respectively (Table 3.1). With longer exposure time the proportion of selenate in the biofilms which was converted to other forms increased, although there was no detectable change in the Se species in the medium. With selenate treatment increased concentrations favored production of elemental selenium over other species such as methylated or organic selenium, and elemental selenium appeared to be the final product with concentrations over 6.33 mM. The proportion of elemental selenium observed in the biofilms treated with selenate alone was smaller in the presence of arsenate, implying a more efficient reduction in the absence of arsenate. However, for the 12.6 mM treatment the observed number of microorganisms was higher in the presence of arsenate (Figure 3.2). This may be due to an increase of arsenate-reducing bacteria that are also resistant to selenate since the observed number of microorganisms in the co-treated biofilms also increased with concentration (Figure 3.2) and significant arsenate biotransformation was evident with co-treatment (Table 3.2). Comprehensive understanding of these results is far from straightforward in multispecies biofilms; but similar sensitivities have been reported for planktonic microorganisms.[38]

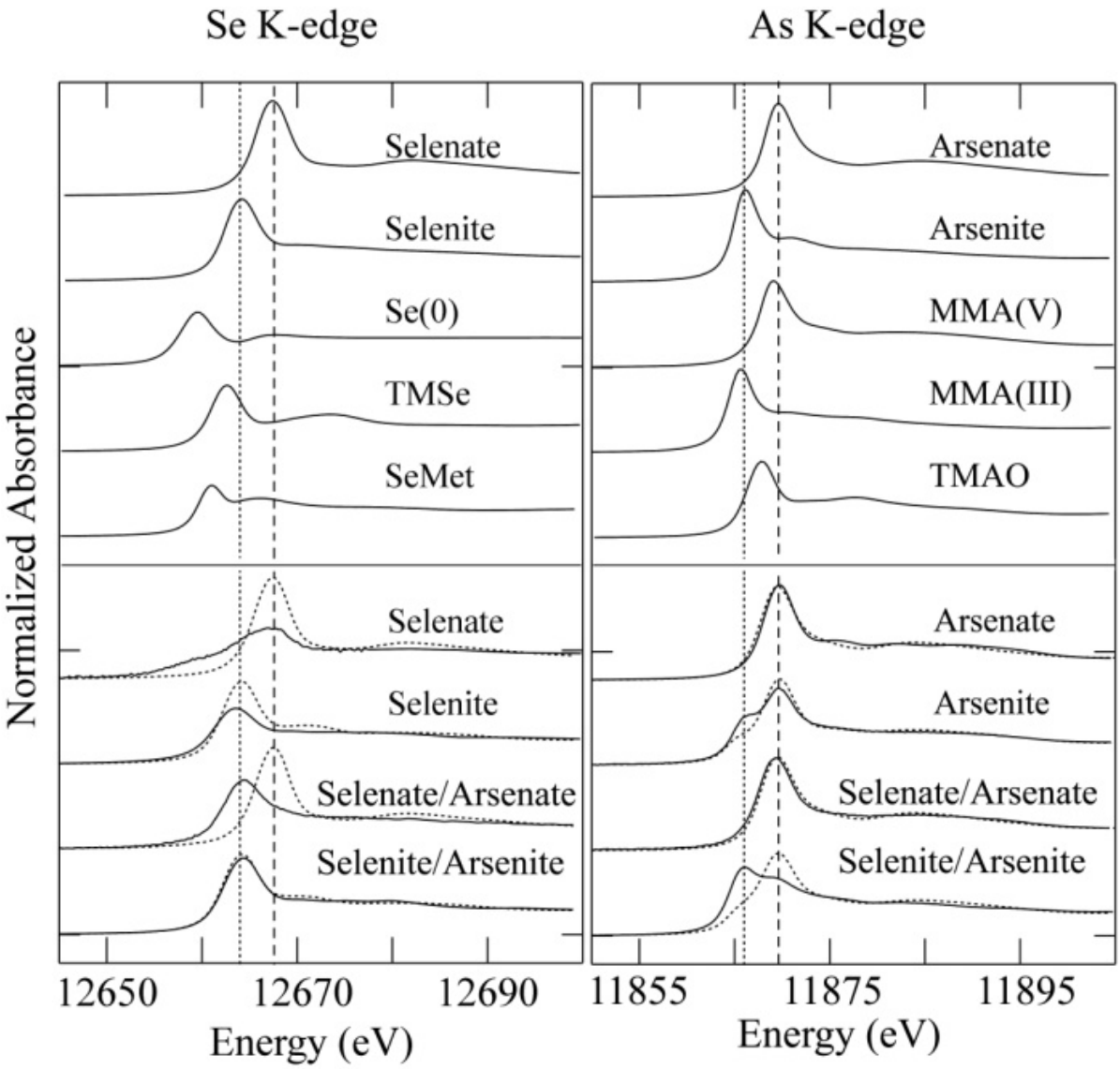

Figure 3.3. Selected selenium (left) and arsenic (right) K near-edge X-ray absorption spectra of biofilms (solid lines, lower panel) and media (dotted lines) after 90 days of incubation at 6.33 mM. Upper panels show spectra of standards. For selenium: selenate; selenite; Se(0), red elemental selenium; TMSe, trimethylselenonium; SeMet, selenomethionine. For arsenic: arsenate; arsenite; MMA(V), monomethylarsonate; MMA(III), monomethylarsinite; TMAO, trimethylarsine oxide. Peak positions of selenate and arsenate (dashed lines), and selenite and arsenite (dotted lines) are indicated.

In contrast to the selenate treatment, biofilms spiked with selenite for short-term showed no detectable proportions of biotransformed selenium species in either biofilm or medium (Table 3.1). Little biotransformation was observed in the 0.63 and 12.6 mM selenite treatment in the long term incubation, although 15 % of elemental selenium was observed in biofilms after the 6.33 mM selenite treatment, possibly due to the dominance of certain selenite reducing microbes as suggested above (Figure 3.1 and 3.2). To date, only a limited number of selenite reducing bacteria have been reported, the majority of which are anaerobes, and only a few aerobic selenite reducers are known including *Pseudomonas* sp. CA5[39] and *Rhizobium* sp. B1.[40] The aerobic selenite reducing abilities of microorganisms isolated from these biofilms are currently being confirmed (Yang et al., unpublished data). Our results of low selenite biotransformation compared with selenate are in contrast to what has been observed with planktonic bacterial systems,[21, 22] where selenite reduction was more significant than selenate. The planktonic results are also consistent with what is expected from simple chemical considerations as selenate is somewhat more challenging to reduce than selenite.[41] Thus, it seems likely that transport and availability within the EPS of the biofilm may play an important role in determining these differences. Moreover, molecular mimicry can allow selenate to utilize sulfate transporters[42] and viable biofilms must allow molecular-level access to sulfate, as this is an essential sulfur nutrient. In addition, reductions of selenium oxyanions by nitrate[33] and nitrite[34] reductases has been reported. Unfortunately, extremely low biomass recovery (μg to mg units) of biofilm from sample strips prohibited quantification of total selenium in the biofilms under these conditions.

Table 3.1. Selenium species observed in biofilms.

Percentages of selenium species in biofilms determined from near-edge spectra. Three times estimated standard deviations, as determined from the least square fit, are ± 3 % or less. All percentages in the media samples were unchanged (NC) from 100% of the amended species.

[Se], concentration [mM] of Se in amendment; NC, no change from 100 % of the selenium species in amendment; dash (–), value not detectable.

Amendment conditions			Observed species in biofilm[A]		
Species	[Se][B]	Time [days]	Selenate	Selenite	Elemental Selenium
Selenate	6.33	20	85	11	4
Selenite	6.33	20	–	NC	–
Selenate/Arsenate	6.33	20	64	16	20
Selenite/Arsenite	6.33	20	–	NC	–
Selenate[C]	0.63	90	56	–	–
Selenate	6.33	90	32	32	36
Selenate	12.6	90	30	48	22
Selenite	0.63	90	–	NC	–
Selenite[D]	6.33	90	–	45	15
Selenite	12.6	90	–	94	6
Selenate/Arsenate	0.63	90	6	66	28
Selenate/Arsenate	6.33	90	10	79	11
Selenate/Arsenate	12.6	90	83	17	–
Selenite/Arsenite	0.63	90	–	NC	–
Selenite/Arsenite	6.33	90	–	94	6

[A]Other selenium chemical species tested include: TMSe, trimethylselenonium; SeMet, selenomethionine; selenourea; selenocysteinate; selenocysteine; selenocystine; selenodiglutathione; Se-methylselenocysteine; seleno-bis (*S*-glutathionyl) arsinium ion.

[B]Where applicable, [As] = [Se]

[C]Other species in biofilm: TMSe, 18 ± 4 %; SeMet 26 ± 6 %

[D]Other species in biofilm: TMSe, 40 %

3.4.3. Biotransformation of arsenic

In arsenic-spiked biofilms, both oxidation of arsenite and reduction of arsenate, together with biotransformation to produce methylated species were observed (Table 3.2). While it is not clear that the methylation process directly follows the formation of less reactive chemical species in the complex multispecies biofilm, some interpretation is possible. In the arsenic methylation pathway of biological systems,[43-45] arsenate and arsenite are thought to be bioconverted in the following pathway: arsenate → arsenite → MMA(V) → MMA(III) → DMA(V) → DMA(III) → TMAO → TMA (trimethylarsine). There are a large number of reports of studies upon the mechanism of arsenic toxicity. Firstly, trivalent arsenicals with two or more OH groups can act as a respiratory poison by binding to reduced lipoic acid in enzymes such as pyruvate dehydrogenases.[46] Other toxic responses include tumor promotion in vertebrates, DNA damage, and increase of reactive oxygen species.[47-50] Among these, the most harmful one may be DNA damage, which varies with chemical type, decreasing in the following order:[51, 52] TMA[53] > DMA(III) > MMA(III) > arsenite, arsenate > MMA(V) > DMA(V) > TMAO. Therefore, if the reduction is driven by detoxification, the process will tend to the formation of TMAO, which is a relatively non-toxic arsenic species.[45, 54] Detectable amounts of TMAO were observed in the majority of long term exposures (Table 3.2), suggesting detoxification of arsenic by biofilm. The As(III) *tris*-glutathione species observed in plants[34, 55] and insects[31, 56] was not observed in any arsenic-treated biofilms or media. Likewise, the seleno-bis (S-glutathionyl) arsinium ion reported as a detoxification molecule in mammals[57] was not observed in the arsenic and selenium co-treated systems.

Biofilms spiked with arsenate for an extended period (90 days) exhibited an increased level of methylation showing chemical species change from MMA(III) to TMAO in both biofilms and media. In the presence of a 1:1 equimolar ratio of selenate, arsenate biotransformation was more extensive. This is consistent with the apparent proliferation of arsenate reducing microorganisms, which are also resistant to selenate and do not use selenate as electron acceptor[58] as indicated by a lower ratio of reduced selenium species observed in selenium K edge spectra (Table 3.1 and 3.2).

In arsenite-spiked biofilms, microbial arsenite oxidation was observed (Figure 3.3). No oxidation of arsenite was observed in the medium of the control sample which was incubated under the same conditions in the absence of biofilm. However, under short-term exposure, 100 % oxidation to arsenate in biofilm and 54 % in media was observed. It is also notable that 46 % of arsenite was methylated to MMA(III) in the media, indicating coexistence of arsenate or arsenite biotransformations in the biofilm as well as excretion of MMA(III) and arsenate to the media. However, this observation contrasts with reported arsenic metabolism in microorganisms because MMA(III) is an intermediate product with low cellular permeability and is generated during a methylation cascade inside the cell in microbial systems.[45, 59, 60] This result could be attributed to leakage of MMA(III) from dead microorganisms, which were also involved in the reduction of arsenite in the biofilm as reported in the *Apiotrichum humicola* pure culture system.[60] This observation would be consistent with the decreased microbial numbers in biofilms (Figure 3.1 and 3.2) and hampered methylation of arsenite in the longer exposure. This phenomenon was also observed in selenite/arsenite-spiked biofilms. The observation of arsenite oxidation and presence of TMAO suggests the possible application of this biofilm for arsenite removal in heavily arsenite contaminated aquatic environments, such as mining/processing waste water.

Table 3.2. Arsenic species observed in biofilms and media.

Percentages of arsenic species determined from near-edge spectra. Three times the estimated standard deviations, as determined from the least square fit, are ± 3 % or less.

[As], concentration [mM] of As in amendment; MMA(III), monomethylarsinite; TMAO, trimethylarsine oxide; Bio, measured in biofilm; Med, measured in medium; NC, no change from 100 % of the arsenic species in amendment; dash (–), value not detectable.

Amendment Conditions			Observed Species[A]							
Species	[As][B]	Time [days]	Arsenate		Arsenite		MMA(III)		TMAO	
			Bio	Med	**Bio**	Med	**Bio**	Med	**Bio**	Med
Arsenate	0.63	20	**90**	100	–	–	**10**	–	–	–
Arsenate	6.33	20	**NC**	96	–	–	–	4	–	–
Arsenite	6.33	20	**NC**	54[C]	–	–	–	46[C]	–	–
Selenate/Arsenate	6.33	20	**82**	79	–	21	**18**	–	–	–
Selenite/Arsenite	6.33	20	**11**	5	**59**	95	**30**	–	–	–
Arsenate	0.63	90	**87**	84	–	–	–	–	**13**	16
Arsenate	6.33	90	**92**	87	–	–	–	–	**8**	13
Arsenite	0.63	90	**95**	–	–	96	–	–	**5**	4
Arsenite	6.33	90	**54**	74	**46**	26	–	–	–	–
Selenate/Arsenate	0.63	90	**67**	92	–	–	–	–	**33**	8
Selenate/Arsenate[D]	6.33	90	–	92	–	8	–	–	–	–
Selenate/Arsenate	12.6	90	**83**	93	–	–	–	–	**17**	7
Selenite/Arsenite	0.63	90	**67**	92	–	–	–	–	**33**	8
Selenite/Arsenite	6.33	90	**18**	71	**82**	29	–	–	–	–

[A]Other arsenic chemical species tested and not significant: MMA(V), monomethylarsonate; DMA(III), dimethylarsinite; DMA(V), dimethylarsinate; As(III) *tris*-glutathione; seleno-bis (*S*-glutathionyl) arsinium.

[B]Where applicable, [Se]=[As]

[C]Three times estimated standard deviation for this fit was ± 6 %

[D]Biofilm fit: 100 % MMA(V)

3.4.4. Selenium resistant microorganisms at very high selenate concentrations

The total counts and the colony forming units of the community of microorganisms changed significantly (P-value < 0.001) as selenate concentration increased (Figure 3.4). The total number of colonies detected in GM water and culturable using tryptic soy agar (TSA) plates using the described methods decreased by 3.7 fold under exposure to 200 mM selenate compared to the control. White colored colonies (elemental selenium negative) also decreased by 13 fold under the same conditions. However, the number of red colonies (elemental selenium positive) showed an increase and accounted for 79 % of colonies at 200 mM selenate. This phenomenon has been observed in some selenium-respiring pure culture systems in which the red color was believed to be due to red elemental α-selenium.[39, 40, 61] The population of these red colonies increased with selenate concentration up to 100 mM. We observed no red colonies on the negative control samples over the same period, indicating the red color was not a microbial pigment formed under the incubation conditions. After an extended incubation for 30 days exposed to 0.4, 0.5 or 1 M selenate, distinctive intense dark red colonies were observed, suggesting the presence of extremely selenate resistant microorganisms, which can grow aerobically on TSA plates.

Extended X-ray absorption fine structure (EXAFS) (Figure 3.5) was used to confirm the identity of the red precipitates formed when multispecies biofilms were exposed to extremely high concentrations (280-300 mM) of selenate for 20 days. The EXAFS curve fitting results (Figure 3.5) showed two selenium atoms at an interatomic distance of 2.336 ± 0.003 Å. This distance is substantially identical to the average Se-Se distance observed in our red elemental selenium reference (2.335 ± 0.003 Å) as well as the interatomic distance (2.334 ± 0.015 Å) of red monoclinic cyclo-octaselenium determined by crystallography.[62] Thus, EXAFS indicates that the precipitate has an identical selenium environment to that of red elemental selenium. This finding suggests possible applications of the multispecies biofilm for elemental selenium production, which is in great demand for example in the semiconductor industry,[63] as well as in environmental bioremediation.[25, 39] Due to its low reactivity derived from its insolubility, elemental selenium is generally considered as either non-toxic or much less toxic than other chemical forms, and is sought after as a final product in selenium bioremediation processes along with gaseous methylated forms.

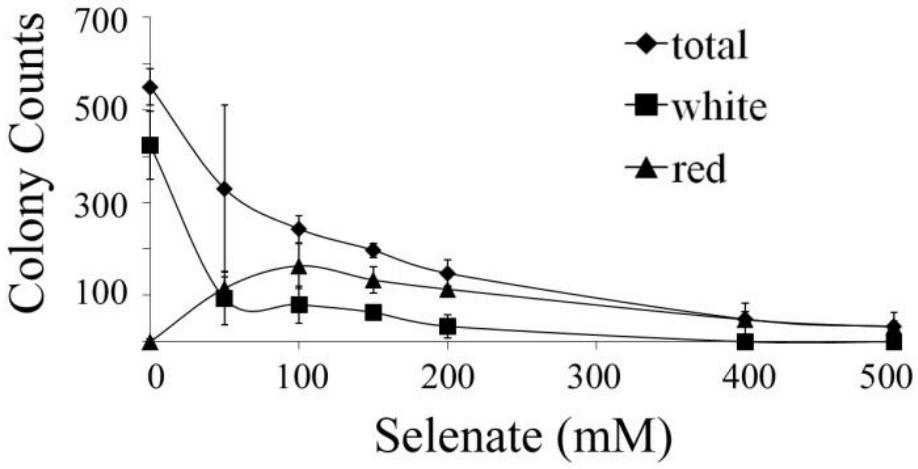

Figure 3.4. The number of red, white and total colonies observed on 10 % tryptic soy agar medium as a function of the concentration of selenate in the medium. After applying 100 µL aliquot of Goddard Marsh water the medium was incubated at room temperature for 7 days (0-200 mM) or for 30 days (400-500 mM). Total count includes yellow colored colonies, which only appeared in the absence of selenate. One way analysis of variance (ANOVA) test indicated p-value < 0.001.

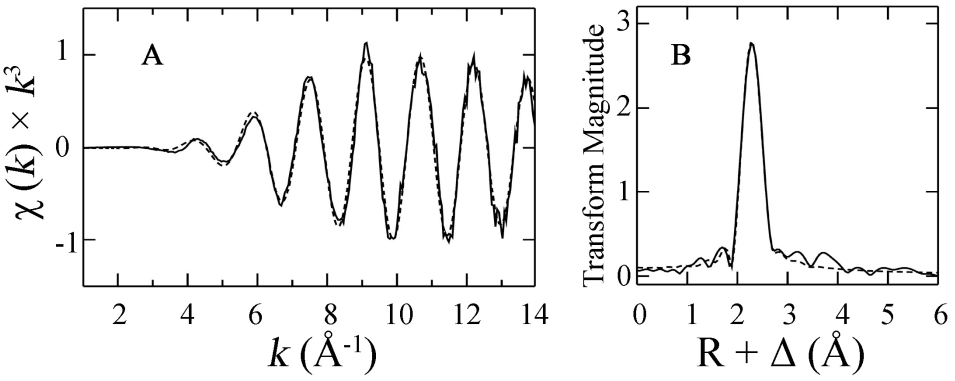

Figure 3.5. Extended X-ray absorption fine structure (EXAFS) spectrum (A) and EXAFS Fourier Transform (B) for the microbial precipitate showing experimental data (solid) and the best fit (dotted) corresponding to a single selenium-selenium shell: coordination number (N), 2; inter atomic distance (R), 2.336 ± 0.003 Å; Debye Waller factor (σ^2), 0.0025 ± 0.0003 Å^2; refined offset to nominal threshold energy of 12675 eV (ΔE_0), -14.0 ± 1.5 eV (parameter ± three times estimated standard deviation in the fit).

3.4.5. Distribution of selenium in multispecies biofilm

The results presented so far indicate that selenium and arsenic species induced structural changes in the cultivated biofilm community. This would be consistent with adaptation through the selection and proliferation of resistant microbes within the community as suggested by 16S rRNA sequencing results. However, there is some uncertainty in this observation due to a lack of available techniques to detect a certain type of microorganism specifically in the multi-species biofilm without interfering with the chemical/biological conditions of the biofilm. A complementary approach is to combine measurements of biofilm structure using CLSM with selenium distribution and speciation information from micro X-ray fluorescence imaging (μ-XRF) and micro X-ray absorption spectroscopy (μ-XAS).

Using μ-XRF, highly localized selenium was observed in the multispecies biofilm exposed to selenate for 60 days (Figure 3.6), suggesting that accumulation of selenium occurred in localized colonies within the biofilm. Selenium K-edge μ-XAS collected with a micro-focused beam on the most intense selenium spots revealed that the selenate had been reduced in the biofilm environment and was present predominantly as selenite with 16 % or less of elemental selenium (Figure 3.6). Averaged over the whole sample using bulk XAS (Table 3.1), the percentage of selenate was much higher (32 %) than observed in these high selenium areas in the μ-XRF map (5 % at most; Figure 3.6), even though the μ-XRF treatment time was 30 days shorter which might result in less conversion of selenate (Table 3.1). Thus, the results suggest that selenate is broadly distributed at low levels, possibly bound to EPS. These findings suggest how multispecies biofilms deposit selenium in a selenate contaminated environment. To our knowledge, this is the first report upon the localization of selenium and its biotransformation in a multispecies biofilm.

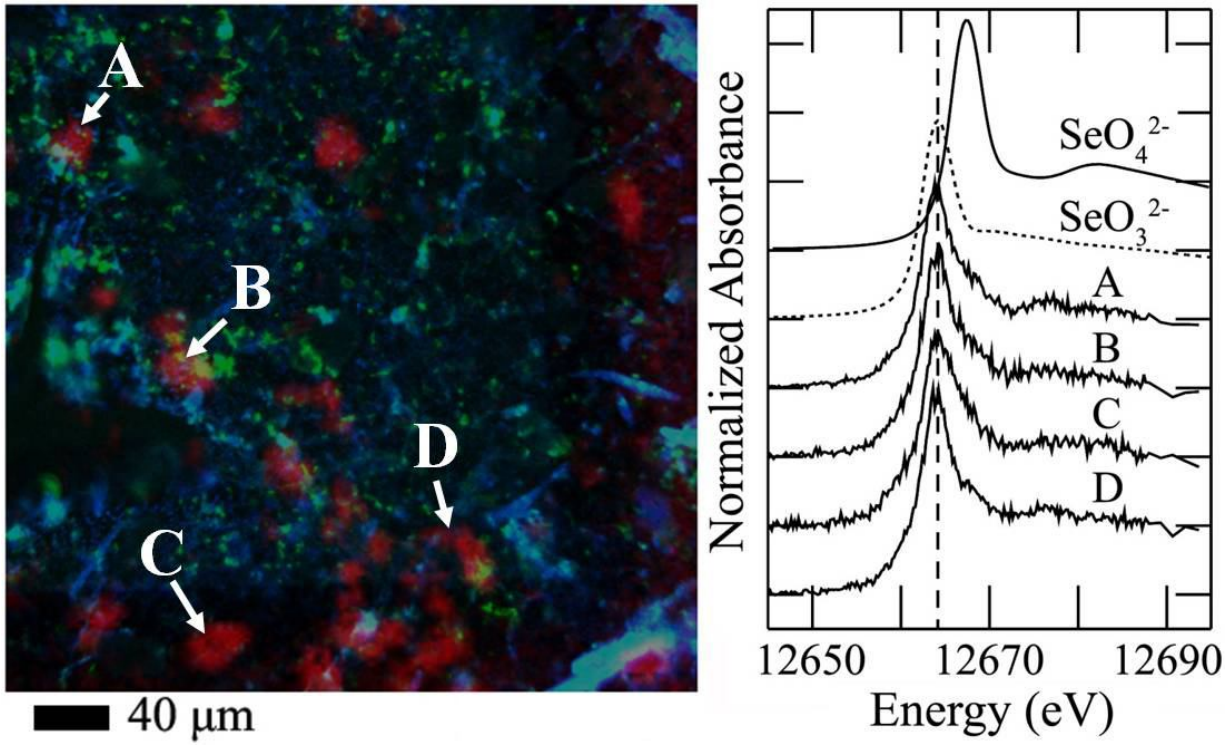

Figure 3.6. Superimposed confocal laser scanning microscopy (CLSM) and micro X-ray fluorescence (μ-XRF) images of biofilm incubated under 6.33 mM selenate for 60 days (left) showing CLSM (pixel size 0.799 μm × 0.799 μm; microorganisms, blue; polysaccharide, green) and selenium μ-XRF image (pixel size 2.5 μm × 2.5 μm at 13,450 eV, red). Scale bar, 40 μm; intensity scale for selenium μ-XRF image shows highly localized selenium as red spots. Selenium K near-edge spectra from selected intense selenium spots (right); the spectrum of selenite and the position of the peak are shown in dashed lines. Near-edge fit results for A, C and D show 12, 16 and 13 % elemental selenium, respectively with the balance as selenite. B shows 11 % elemental selenium, 5 % selenate and 84 % selenite. Three times the estimated standard deviation is 3-4 % in all cases.

3.5. CONCLUSIONS

Our study shows that selenium and arsenic oxyanions significantly affect both microbial diversity and structure in the multispecies biofilms studied. Investigations using CLSM showed dominance of morphologically simplified populations in the multispecies biofilms in the presence of selenium or arsenic species. We have used synchrotron-based XAS to demonstrate that biofilms biotransform selenium and arsenic oxyanions to chemically more stable or less

toxic species. Imaging using μ-XRF indicated that selenium was highly localized in the biofilm in the form of reduced chemical species. In addition, results from CLSM and μ-XRF techniques have been combined in a unique correlative microscopy approach. We believe that such combined methodology will be useful in future investigations of metal or metalloid distributions in biological samples. We have shown that complex biotransformations of selenium and arsenic occur within a multispecies biofilm, but several outstanding unresolved questions remain, including what microorganisms are resistant to selenium and how they differ phylogenetically and which are involved in the biotransformation of selenium to generate environmentally more benign selenium forms. These questions will be the subjects of future research, as will a comparison of monoculture and multispecies biofilms.

3.6. ACKNOWLEDGEMENTS

We express our gratitude to Drs. Graham George and Helen Nichol, as well as the Pickering/George research group at the University of Saskatchewan. This research was supported by an NSERC Discovery Grant (to Pickering) and by Environment Canada. Pickering is a Canada Research Chair. Yang is a CIHR-THRUST Fellow. Portions of this research were carried out at the Stanford Synchrotron Radiation Lightsource (SSRL), a national user facility operated by Stanford University on behalf of the U.S. Department of Energy, Office of Basic Energy Sciences. The SSRL Structural Molecular Biology Program is supported by the Department of Energy, Office of Biological and Environmental Research, and by the National Institutes of Health, National Center for Research Resources, Biomedical Technology Program.

3.7. REFERENCES

[1] J. R. Arthur, G. J. Beckett, Symposium 2 Newer aspects of micronutrients in at risk groups. *Proc. Nutr. Soc.* **1994,** *53,* 615.

[2] R. Abdulah, K. Miyazaki, M. Nakazawa, H. Koyama, Chemical forms of selenium for cancer prevention. *J. Trace Elem. Med. Biol.* **2005,** *19,* 141.

[3] K. Brown, J. Arthur, Selenium, selenoproteins and human health: a review. *Public Health Nutr.* **2001,** *4,* 593.

[4] A. D. Lemly, Aquatic selenium pollution is a global environmental safety issue. *Ecotoxicol. Environ. Saf.* **2004,** *59,* 44.

[5] P. L. Orr, K. R. Guiguer, C. K. Russel, Food chain transfer of selenium in lentic and lotic habitats of a western Canadian watershed. *Ecotoxicol. Environ. Saf.* **2006,** *63,* 175.

[6] S. J. Hamilton, Review of selenium toxicity in the aquatic food chain. *Sci. Total Environ.* **2004,** *326,* 1.

[7] H. M. Ohlendorf, D. J. Hoffman, M. K. Saiki, T. W. Aldrich, Embryonic mortality and abnormalities of aquatic birds: Apparent impacts of selenium from irrigation drainwater. *Sci.Total Environ.* **1986,** *52,* 49.

[8] D. J. Hoffman, G. H. Heinz, Embryotoxic and teratogenic effects of selenium in the diet of mallards. *J. Toxicol. Environ. Health* **1988,** *24,* 477.

[9] H. M. Ohlendorf, R. L. Hothem, D. Welsh, Nest success, cause-specific nest failure, and hatchability of aquatic birds at selenium-contaminated Kesterson Reservoir and a reference site. *The Condor* **1989,** *91,* 787.

[10] J. M. Azcue, J. O. Nriagu, *in Arsenic in the environment* (Eds J. O. Nriagu) **1994**, pp. 1-15 (John Wiley and Sons: New York).

[11] H. Yan-Chu, *in Arsenic in the environment* (Eds J. O. Nriagu) **1994**, pp. 17-50 (John Wiley and Sons: New York).

[12] I. Cano-Aguilera, B. E. Rubio-Campos, G. De la Rosa, A. F. Aguilera-Alvarado, Arsenic mobility from mining tailings of Monte San Nicolas to Presa de Mata in Guanajuato, Mexico. *World Academy of Science, Engineering and Technology* **2008,** *47,* 390.

[13] R. B. Finkelman, H. E. Belkin, B. Zheng, Health impacts of domestic coal use in China. *PNAS* **1999,** *96,* 3427.

[14] Y. E. Yudovich, M. P. Ketris, Arsenic in coal: a review. *Int. J. Coal Geol.* **2005,** *61,* 141.

[15] Y. E. Yudovich, M. P. Ketris, Selenium in coal: a review. *Int. J. Coal Geol.* **2006,** *67,* 112.

[16] A. W. Cantafio, K. D. Hagen, G. E. Lewis, T. L. Bledsoe, K. M. Nunan, J. M. Macy, Pilot-scale selenium bioremediation of San Joaquin drainage water with *Thauera selenatis*. *Appl. Environ. Microbiol.* **1996,** *62,* 3298.

[17] W. T. Frankenberger, M. Arshad, Bioremediation of selenium-contaminated sediments and water. *Biofactors* **2001,** *14,* 241.

[18] K. A. Natarajan, Microbial aspects of acid mine drainage and its bioremediation. *Trans. Nonferrous Met. Soc. China* **2008,** *18,* 1352.

[19] J. M. Macy, S. Rech, G. Auling, M. Dorsch, E. Stackebrandt, L. I. Sly, *Thauera selenatis* gen. nov., sp. nov., a member of the beta subclass of Proteobacteria with a novel type of anaerobic respiration. *Int. J. Syst. Bacteriol.* **1993,** *43,* 135.

[20] R. Burra, G. A. Pradenas, R. A. Montes, C. C. Vásquez, T. G. Chasteen, Production of dimethyl triselenide and dimethyl diselenenyl sulfide in the headspace of metalloid-resistant *Bacillus* species grown in the presence of selenium oxyanions. *Anal. Biochem.* **2010,** *396,* 217.

[21] S. Hapuarachchi, J. Swearingen, T. G. Chasteen, Determination of elemental and precipitated selenium production by a facultative anaerobe grown under sequential anaerobic/aerobic conditions. *Process Biochem.* **2004,** *39,* 1607.

[22] V. Van Fleet-Stalder, T. G. Chasteen, I. J. Pickering, G. N. George, R. C. Prince, Fate of selenate and selenite metabolized by *Rhodobacter sphaeroides*. *Appl. Environ. Microbiol.* **2000,** *66,* 4849.

[23] J. W. Costerton, K. J. Cheng, G. G. Geesey, T. I. Ladd, J. C. Nickel, M. Dasgupta, T. J. Marrie, Bacterial biofilms in nature and disease. *Annu. Rev. Microbiol.* **1987,** *41,* 435.

[24] C. de Carvalho, Biofilms: recent developments on an old battle. *Recent Patents on Biotechnology* **2007,** *1,* 49.

[25] R. Singh, D. Paul, R. K. Jain, Biofilms: implications in bioremediation. *Trends Microbiol.* **2006,** *14,* 389.

[26] E. van Hullebusch, M. Zandvoort, P. Lens, Metal immobilisation by biofilms: mechanisms and analytical tools. *Rev. Environ. Sci. Biotechnol.* **2003,** *2,* 9.

[27] W. G. Weisburg, S. M. Barns, D. A. Pelletier, D. J. Lane, 16S ribosomal DNA amplification for phylogenetic study. *J. Bacteriol.* **1991,** *173,* 697.

[28] J. R. Lawrence, G. D. W. Swerhone, T. R. Neu, A simple rotating annular reactor for replicated biofilm studies. *J. Microbiol. Methods* **2000,** *42,* 215.

[29] J. R. Lawrence, G. D. W. Swerhone, G. G. Leppard, T. Araki, X. Zhang, M. M. West, A. P. Hitchcock, Scanning transmission X-ray, laser scanning, and transmission electron microscopy mapping of the exopolymeric matrix of microbial biofilms. *Appl. Environ. Microbiol.* **2003,** *69,* 5543.

[30] M. D. Abramoff, P. J. Magelhaes, S. J. Ram, Image processing with Image J. *Biophoton Int.* **2004,** *11,* 36.

[31] R. Andrahennadi, I. J. Pickering, Arsenic accumulation, biotransformation and localisation in bertha armyworm moths. *Environ. Chem.* **2008,** *5,* 413.

[32] R. Andrahennadi, M. Wayland, I. J. Pickering, Speciation of selenium in stream insects using X-ray absorption spectroscopy. *Environ. Sci. Technol.* **2007,** *41,* 7683.

[33] I. J. Pickering, G. N. George, V. Van Fleet-Stalder, T. G. Chasteen, R. C. Prince, X-ray absorption spectroscopy of selenium-containing amino acids. *J. Biol. Inorg. Chem.* **1999,** *4,* 791.

[34] I. J. Pickering, R. C. Prince, M. J. George, R. D. Smith, G. N. George, D. E. Salt, Reduction and coordination of arsenic in Indian mustard. *Plant Physiol.* **2000,** *122,* 1171.

[35] G. N. George, I. J. Pickering, EXAFSPAK: A Suite of computer programs for analysis of X-ray absorption spectra available at http://ssrl.slac.stanford.edu/exafspak.html. **2001,**.

[36] S. I. Zabinsky, J. J. Rehr, A. Ankudinov, R. C. Albers, M. J. Eller, Multiple-scattering calculations of x-ray-absorption spectra. *Phys. Rev. B* **1995,** *52,* 2995.

[37] S. Webb, MicroAnalysis Toolkit. *2010,*http://home.comcast.net/~sam_webb/smak.html.

[38] G. A. Burton Jr, T. H. Giddings, P. DeBrine, R. Fall, High incidence of selenite-resistant bacteria from a site polluted with selenium. *Appl. Environ. Microbiol.* **1987,** *53,* 185.

[39] W. Hunter, D. Manter, Reduction of selenite to elemental red selenium by *Pseudomonas* sp. strain CA5. *Curr. Microbiol.* **2009,** *58,* 493.

[40] W. Hunter, L. Kuykendall, Reduction of selenite to elemental red selenium by *Rhizobium* sp. strain B1. *Curr. Microbiol.* **2007,** *55,* 344.

[41] W. T. Frankenberger Jr, U. Karlson, *in Selenium in the environments* (Eds W. T. Frankenberger Jr, S. Benson) **1995**, pp. 369-387 (Marcel Dekker Inc: New York).

[42] G. N. George, I. J. Pickering, C. J. Doonan, M. Korbas, S. P. Singh, R. E. Hoffmeyer, *in Advances in Molecular Toxicology* (Eds J. C. Fishbein) **2008**, pp. 123-152 (Elsevier: Hungary).

[43] F. Challenger, Biological methylation. *Chem. Rev.* **1945,** *36,* 315.

[44] D. J. Thompson, A chemical hypothesis for arsenic methylation in mammals. *Chem. Biol. Interact.* **1993,** *88,* 89.

[45] R. Bentley, T. G. Chasteen, Microbial methylation of metalloids: arsenic, antimony, and bismuth. *Microbiol. Mol. Biol. Rev.* **2002,** *66,* 250.

[46] M. G. Ord, L. A. Stocken, A contribution to chemical defence in World War II. *Trends Biochem.Sci.* **2000,** *25,* 253.

[47] J. A. Imlay, S. M. Chin, S. Linn, Toxic DNA damage by hydrogen peroxide through the Fenton reaction *in vivo* and *in vitro*. *Science* **1988,** *240,* 640.

[48] H. Wiseman, B. Halliwell, Damage to DNA by reactive oxygen and nitrogen species: role in inflammatory disease and progression to cancer. *Biochem. J.* **1996,** *313,* 17.

[49] S. Yamamoto, Y. Konishi, T. Murai, M. Shibata, T. Matsuda, K. Kuroda, G. Endo, S. Fukushima, Enhancing effects of an organic arsenic compound, dimethylarsinic acid (cacodylic acid), in a multi-organ carcinogenesis bioassay. *Appl. Organomet. Chem.* **1994,** *8,* 197.

[50] D. Sinha, S. Mukherjee, S. Roy, R. K. Bhattacharya, R. Roy, Modulation of arsenic induced genotoxicity by curcumin in human lymphocytes. *JECE* **2009,** *1,* 001.

[51] E. Dopp, L. M. Hartmann, A. M. Florea, U. von Recklinghausen, R. Pieper, B. Shokouhi, A. W. Rettenmeier, A. V. Hirner, G. Obe, Uptake of inorganic and organic derivatives of arsenic associated with induced cytotoxic and genotoxic effects in Chinese hamster ovary (CHO) cells. *Toxicol. Appl. Pharmacol.* **2004,** *201,* 156.

[52] N. Eguchi, K. Kuroda, G. Endo, Metabolites of arsenic induced tetraploids and mitotic arrest in cultured cells. *Arch. Environ. Contam. Toxicol.* **1997,** *32,* 141.

[53] P. Andrewes, K. T. Kitchin, K. Wallace, Dimethylarsine and trimethylarsine are potent genotoxins *in vitro* . *Chem. Res. Toxicol.* **2003,** *16,* 994.

[54] l. R. de, J. G. Parsons, A. Martinez-Martinez, J. Peralta-Videa, J. Gardea-Torresdey, Spectroscopic study of the impact of arsenic speciation on arsenic/phosphorus uptake and plant growth in tumbleweed (*Salsola kali*). *Environ. Sci. Technol.* **2006,** *40,* 1991.

[55] H. Yamauchi, T. Kaise, K. Takahashi, Y. Yamamura, Toxicity and metabolism of trimethylarsine in mice and hamsters. *Toxicol. Sci.* **1990,** *14,* 399.

[56] C. J. Langdon, A. J. Morgan, J. M. Charnock, K. T. Semple, C. N. Lowe, As-resistance in laboratory-reared F1, F2 and F3 generation offspring of the earthworm *Lumbricus rubellus* inhabiting an As-contaminated mine soil. *Environ. Pollut.* **2009,** *157,* 3114.

[57] J. Gailer, G. N. George, I. J. Pickering, R. C. Prince, S. C. Ringwald, J. E. Pemberton, R. S. Glass, H. S. Younis, D. W. DeYoung, H. V. Aposhian, A metabolic link between arsenite and selenite: the seleno-bis(S-glutathionyl) arsinium ion. *J. Am. Chem. Soc.* **2000,** *122,* 4637.

[58] J. F. Stolz, P. Basu, J. M. Santini, R. S. Oremland, Arsenic and selenium in microbial metabolism. *Annu. Rev. Microbiol.* **2006,** *60,* 107.

[59] D. Páez-Espino, J. Tamames, V. de Lorenzo, D. Cánovas, Microbial response to environmental arsenic. *Biometals* **2009,** *22,* 117.

[60] W. R. Cullen, H. Li, G. Hewitt, K. J. Reimer, N. Zalunardo, Identification of extracellular arsenical metabolites in the growth medium of the microorganisms *Apiotrichum humicola* and *Scopulariopsis brevicaulis*. *Appl. Organometal. Chem.* **1994,** *8,* 303.

[61] L. Lortie, W. D. Gould, S. Rajan, R. G. L. McCready, K. J. Cheng, Reduction of selenate and selenite to elemental selenium by a *Pseudomonas stutzeri* isolate . *Appl. Environ. Microbiol.* **1992,** *58,* 4042.

[62] O. Foss, V. Janickis, Crystal structure of [gamma]-monoclinic selenium. *J. Chem. Soc., Dalton Trans.* **1980,** *4,* 624.

[63] B. Cheng, E. T. Samulski, Rapid, high yield, solution-mediated transformation of polycrystalline selenium powder into single-crystal nanowires. *Chem. Commun.* **2003,** 2024.

CHAPTER 4. MULTISPECIES BIOFILMS BIOTRANSFORM SELENIUM OXYANIONS INTO NANO PARTICLES

This manuscript will be submitted for publication in the *Proceedings of the National Academy of Sciences* with the following author list: Soo In Yang, Graham N. George, John R. Lawrence, Susan G. W. Kaminskyj, James J. Dynes, Barry Lai, Ingrid J. Pickering. In this research, I planned, designed, conducted experiments, and played a main role in preparing the manuscript. Other coauthors provided advice, help on experiment, and contributed to the preparation of the manuscript.

In this study, biotransformation of selenium was investigated using synchrotron-based imaging techniques in multispecies biofilms grown using the same source as the previous chapters, yet under enriched conditions. Biofilms were grown under complex media and selenium biotransformation was investigated using nano-XRF, STXM, and transmission electron microscopy techniques. Selenium distribution related with biofilm structure was demonstrated employing both synchrotron techniques on the same spot of the sample. This novel approach showed how multispecies biofilms transform selenium oxyanions by correlating biofilm structural components with selenium species present in the biofilm.

4.1. ABSTRACT

Naturally, occurring microbial consortia, biofilms, play important roles in the biogeochemical cycling of toxic elements in aquatic systems. Despite their important role, the complexity of naturally forming multispecies biofilms hinders biofilm research due to essential chemical and physical modifications, which occur in conventional microscopic techniques. We have employed a set of synchrotron-based techniques with minimum sample preparation to investigate biotransformations of selenium oxyanions, the selenium species commonly present in the aquatic environment. Biotransformation of selenium oxyanions to elemental selenium and subsequent sequestration in biofilms were observed using synchrotron-based nano-scale scanning transmission X-ray microscopy (STXM) and X-ray fluorescence (XRF) imaging techniques at the selenium L and K near-edges. STXM at the carbon K-edge demonstrated a close association of selenium particles with lipid. The unique distributions of selenate and selenite as well as

elemental selenium within this complex multispecies biofilm structure were investigated using a novel application of STXM and XRF on identical areas of biofilms. The biogenic elemental selenium examined with transmission electron microscopy was sub-micron-sized, ranging from 50-700 nm in diameter, and closely associated with the microbial structures. The biosynthesis of submicron-sized elemental selenium may suggest possible applications of the biofilms for the semiconductor industry where micro- to nano- sized selenium particles are in great demand.

4.2. INTRODUCTION

Selenium (Se, Z=34) is as an essential micronutrient in animals and certain microorganisms. Selenium serves as a catalytic element within the active site of several types of antioxidant enzymes important for health, such as thioredoxin reductase [1, 2]. In addition, a positive role of selenium in certain plants, e.g. an increase of yield, has been also suggested [3, 4]. Despite its beneficial role, selenium can be toxic at elevated level and it tends to have a narrow margin between required and toxic levels [5]. With respect to its toxic mechanisms, selenium can be toxic by mimicking or disturbing sulfur metabolism [6] and damaging cells by oxidative stress [7] in most organisms, including humans.

In the aqueous environment, microorganisms favor growing as communities known as biofilms by forming and incorporating a slimy matrix of extracellular polymeric substances (EPS). Biofilms have shown a high resistance to toxic elements compared with the free-living planktonic forms of microorganisms [8, 9]. One advantage of the biofilm community is ease of metabolic control using cell-to-cell communication in response to environmental changes [10]. Hence, the prevalent yet complex structure of biofilms typically leads to increased tolerance to physical, chemical, and biological stress compared to free-living microorganisms [8, 9]. Therefore, biofilm formation is evolutionally significant for microorganisms, increasing their sustainability or survival.

Although advances in microscopy and molecular biological techniques have expanded our understanding of processes in biofilms, the investigation of toxic substance interaction and resistance of biofilms presents special challenges, in particular in maintaining both structure and essential chemistry of the biofilm. With this in mind, we used synchrotron-based transmission

and fluorescence imaging techniques with Se L and K near-edge X-ray absorption structures to examine selenium biotransformation in biofilms. We demonstrated a novel approach using synchrotron-based hard and soft X-ray imaging techniques on the same areas of the samples to allow exploration of chemistry in the context of the biology. The results indicated that specific regional communities in biofilms carry out selenium detoxification, as shown by the localized distribution of biologically less reactive selenium species including elemental selenium, which was deposited as sub-micron-sized particles closely associated with the microorganisms.

4.3. MATERIALS AND METHODS

4.3.1. Growth of biofilm

Biofilms were cultivated as described by Yang *et al*. (2011) [11] with the following modifications. One percent of a microbial pre-culture incubated overnight in 10 % tryptic soy broth (TSB) at room temperature (RT, 22 ± 3 °C) was used as inoculum. Biofilm growth occurred on the surface of polycarbonate strips (10 cm × 1 cm) for 10 days or 1 month. Biofilms were subsequently transferred to test tubes containing 16 mL of fresh 10 % TSB, which also contained selenate or selenite (0.63 – 63 mM). Tubes were further incubated aerobically on a gyratory incubator at 100 rpm for 20 days or 2 months. Thus, total incubation periods were 1 or 3 months. All experimental procedures were carried out in sterile conditions.

4.3.2. Nano X-ray fluorescence imaging (n-XRF)

Biofilm samples were rinsed at least 3 times using autoclaved 10 % TSB and excess liquid was removed. Biofilms were then harvested using a sterile scraper made with silicon tubing. One micro liter aliquot of the collected biofilm was applied onto silicon nitride windows (0.5 mm × 0.5 mm, NX5050B, Norcada Inc, AB, Canada) and allowed to air-dry. The prepared biofilm samples were brought to the beamline 2-ID-D of the Advanced Photon Source, USA. Regions of interest were recorded using an optical light microscope (Leica DMR, Leica, IL, USA). The silicon nitride window was mounted on an aluminum frame positioned at 15° to the incident beam and a Vortex® silicon drift detector (SII Nano Technology USA Inc., CA, USA) was located at 90° to the incident beam to measure fluorescence emission spectrum. The beam size was fixed at 200 nm × 200 nm using the Fresnel zone plate. The sample was maintained in a

helium gas filled environment and raster scanned at 0.5 seconds on each pixel. Data were processed using MAPS software [12]. Further image processes were conducted using aXis2000 [13].

4.3.3. Determination of selenium concentration

Ten percent of maximum concentration was used as a threshold to determine selenium concentration in both XRF and STXM data.

4.3.4. Co-localization map

Co-localization maps of elements and Mander's overlap coefficients were processed using MAPS [12] and macros created in Image J [14], respectively.

4.3.5. Selenium chemically specific nano X-ray fluorescence imaging

The regions of interest in the biofilms were scanned at the energies of the most intense absorption peaks of elemental selenium (12,659.5 eV), selenite (12,663.9 eV), and selenate (12,667.3 eV). The observed selenium distribution maps at each energy of selenium species was separately generated as image data files. To calculate the pure distribution map of each selenium chemical species each image was processed as shown in Figure 4.5 and Table 4.2. Thus, the pure intensity of each selenium species was obtained by subtracting the contribution of each selenium species from the intensity of selenium species of interest. For example, the pure selenite distribution map was obtained by subtracting calculated elemental selenium and selenate distribution intensity at 12,663.9 eV. For some of selenate-amended biofilms (Figure 4.6 c, d), selenate intensity at most intense peak energy (12,667.3 eV) was computed, based on the observed intensity at 12680 eV. Following this, the intensity contribution from selenite and elemental selenium was subtracted to show only selenate intensity. The contribution of selenium intensity and calculated values are shown in Figure 4.5 and Table 4.2. Spectra used in this estimation were collected from beamline 7-3 and 9-3 of Stanford Synchrotron Radiation Lightsource (SSRL). The data was processed using MAPS [12], aXIS2000 [13], and EXAFSPAK software [15].

4.3.6. nano X-ray K-edge absorption spectroscopy

The intense selenium spots were investigated using a 200 nm × 200 nm beam by scanning energies from 12,620 – 12,740 eV in duplicate. Each spectrum was examined for any photo-damage (oxidation or reduction) by checking for any spectral changes between duplicate data collection scans. Data was processed using EXAFSPAK [15].

4.3.7. Investigation on photo-reduction of selenium oxy anions

Photo-damage on selenium species was investigated by collecting spectra on spots of selenate and selenite powder samples under the same condition, yet exposing longer time (120 seconds per a scan) over 12,620 - 12,740 eV, in triplicate. Data was processed using EXAFSPAK [15]. All K-edge selenium reference spectra were collected from beamline 7-3 and 9-3 of SSRL.

We carefully screened for any possible radiation damage by inspecting selenium K edge absorption spectral positions during XRF measurements and did not observe any noticeable changes (Figure 4.1). We also measured XRF first and revisited the identical areas with STXM to minimize possible photo damage to the sample. The higher energy X-rays have a low X-ray mass absorption coefficient resulting in a lower dose to the thin sample. In contrast, at the lower energies of the C K-edge used on STXM, a substantial proportion of the beam is absorbed, potentially leading to greater radiation damage. Thus, employing high energy XRF first followed by low energy STXM was appropriate since it minimized damage to both biofilms and selenium oxyanions.

4.3.8. Scanning transmission X-ray microscopy (STXM)

STXM images and spectroscopy were carried out at the Soft X-ray Spectromicroscopy beamline (SM) at the Canadian Light Source (CLS). Data were collected using point, line scan spectral, and whole scanning modes at a sequence of energies. The raw data were converted into optical density images and were further processed using aXis2000 [13] as reported by Dynes *et al* [16]. For the quantitative analyses of selenium and biofilm macromolecular structures, singular value decomposition (SVD) [17] was used. The spectra of selenium references including selenate, selenite, selenomethionine, selenocysteine, selenocystine, and elemental selenium were collected

under the same conditions and used for quantitative analysis of selenium in biofilms. Spectra from carbon K and selenium L-edge were extracted and background subtracted, and normalized to the highest absorbance points.

4.3.9. Transmission electron microscopy (TEM)

TEM studies were carried out using the method as described by Shi *et al*. [18].

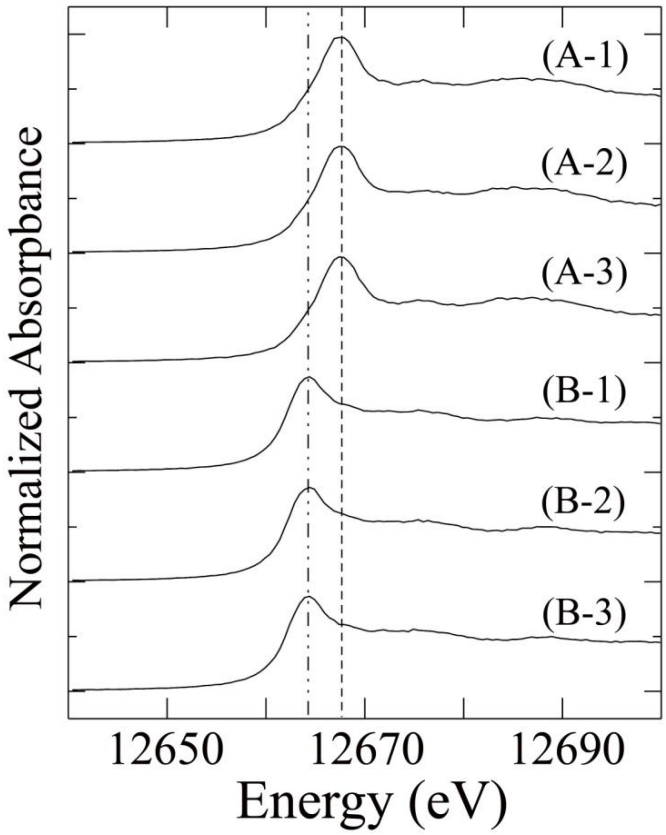

Figure 4.1. Selenium K near-edge spectra of selenate (A) and selenite (B) prepared as powder forms. Numerical numbers after A and B represent the order of each scan on the same area (200 nm × 200 nm). Each scan was 120 seconds long. Dotted and broken lines indicate the most intense peak positions of selenate and selenite.

4.4. RESULTS AND DISCUSSION

4.4.1.Element distribution in selenate amended multispecies biofilms

We used synchrotron-based X-ray fluorescence (XRF) imaging to examine the distribution of selenium and other elements within the biofilms. Figure 4.2 shows examples of the images for different concentrations of selenate, with fields of view corresponding to one or a few microorganisms. We observed highly localized selenium in selenate amended multispecies biofilms incubated for 3 month with 63 mM selenate (Figure 4.2). The intense selenium spots, consistent with sub micron-sized objects substantially smaller than the cells, were only present in the highest (63 mM) of the selenate-amended biofilms.

XRF allows the simultaneous measurement of distributions of other elements in the biofilm. Cu and Zn were highly co-localized in certain regions of the biofilms. The morphologies of the Cu and Zn rich areas suggest that they are not distributed in the EPS, but restricted to cells. In contrast, P is evenly distributed throughout the biofilms. The P distribution also differs from that of microbiologically important nonmetal elements S and Ca, which appear highly co-localized with each other. In addition, concentrations of S and Ca were significantly elevated compared with the control under the all examined selenate amended conditions (Table 4.1, Figure 4.2). These nonmetal ions are strictly controlled in microorganisms and we do not know why these elements are accumulated in biofilms under high selenate concentration.

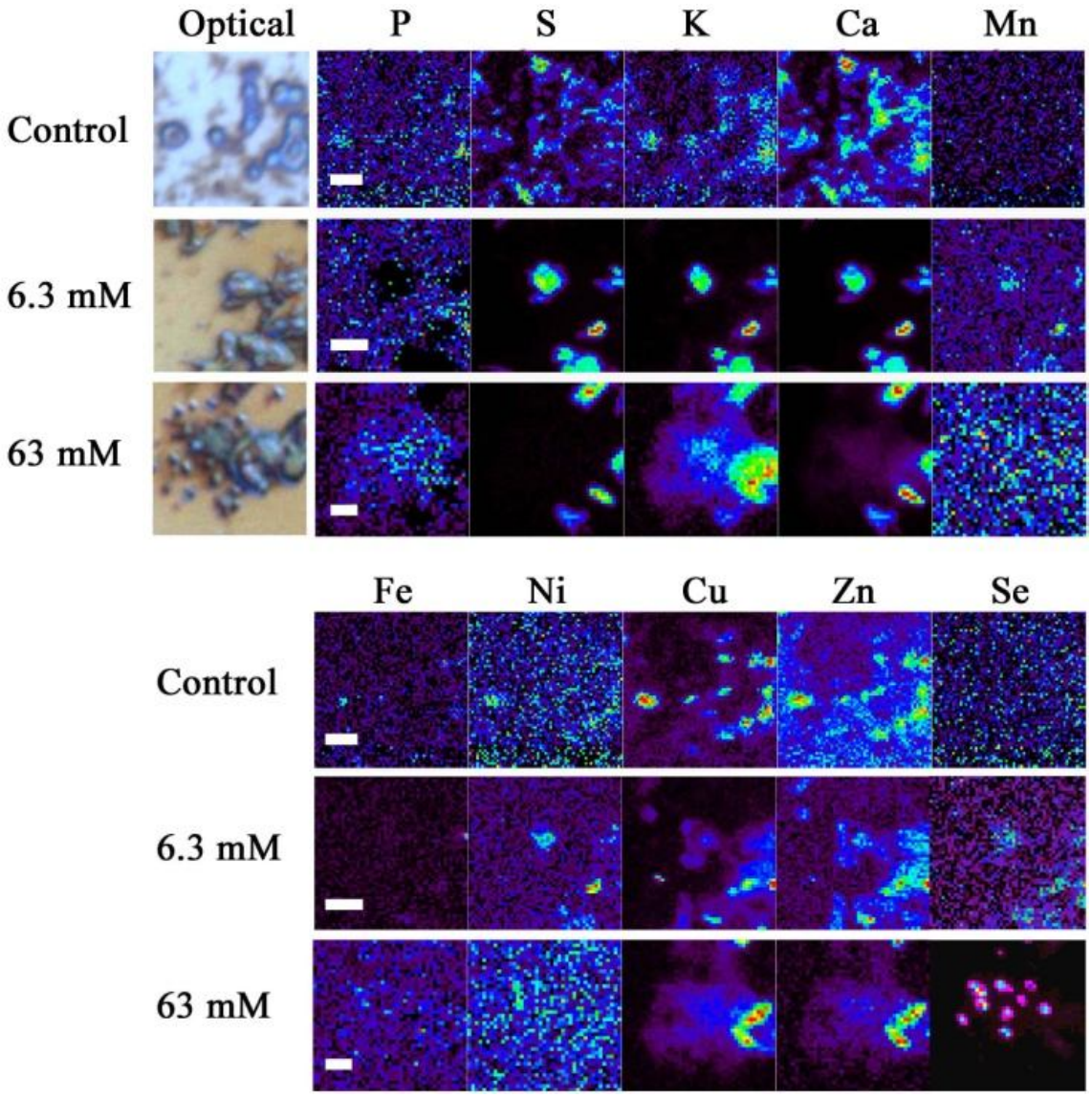

Figure 4.2. False color micro-XRF elemental distribution maps of control (no selenium), 6.3 and 63 mM selenate amended biofilms. Optical microscopic images on the scanned areas are shown on left. Biofilms were grown for 3 months in the presence of selenate and measured at 12,680 eV. Scale bars show 2 μm, respectively.

Table 4.1. Observed elemental maximum concentrations in multispecies biofilms shown in Figure 4.2 and 4.3*

		Observed maximum elemental concentration (μg/cm^2)										
	Concentration (mM)	P	S	K	Ca	Mn	Fe	Ni	Cu	Zn	Se	Se (avg)
Selenate	Control**	2.24	8.53	0.57	3.93	0.06	0.09	0.02	0.56	0.22	0.01	N/O
	6.3**	1.74	119	16.8	132	0.09	0.32	0.09	1.11	0.18	0.02	0.02 (0.01)
	63**	3.61	58.3	2.54	30.6	0.04	0.11	0.03	0.82	0.23	14.2	0.75 (0.50)
Selenite	0.63#	9.60	94.3	64.9	61.7	0.29	0.51	0.28	1.46	0.35	301	32.5 (24.9)
	6.3 (1 month)#	6.56	395	17.7	119	0.23	2.21	0.13	0.36	0.50	41.1	2.10 (1.45)
	6.3#	5.64	9.18	1.33	4.08	1.33	19.6	0.64	16.6	9.00	14.7	10.6 (9.68)

*Maximum and average (only for selenium) concentrations are shown. All biofilms were incubated for 3 months unless otherwise noted. Average concentrations were calculated by applying 10 % threshold of maximum selenium concentration observed. N/O stands for not observed. Standard deviations are in shown in parentheses.

**Figure 4.2.

#Figure 4.3.

4.4.2. Element distribution in selenite amended multispecies biofilms

When multispecies biofilms were incubated under extremely high selenite conditions (0.63 – 63 mM) for either 1 or 3 months (Figure 4.3), we observed an elemental distribution pattern similar to that shown in selenate-amended biofilms. However, the selenium concentration was considerably greater and more intensely localized within the biofilm (Figure 4.3, Table 4.1), suggesting a highly concentrated phase. Se K nano-X-ray absorption near-edge structure spectra measured from these intense selenium spots indicated that their chemical form is elemental selenium (Figure 4.4). A consequence of the highly concentrated selenium was that self-absorption distortions of the fluorescence signal caused a reduction in intensity of the prominent 1*s* to 4*p* transition peak (Figure 4.4). This reduction of intensity was more obvious in pt 2 and 3 than pt 1, which had much lower concentration. The relation between the distortion in fluorescence signal and selenium particle size was previously simulated by Wiramanaden *et al.* [19], with larger particle sizes of elemental selenium causing greatly decreased fluorescence intensities of spectra.

The maximum selenium concentration was substantially higher than those of other biologically significant elements present in both selenite and selenate-amended biofilms. The maximum values of these elemental selenium particles ranged from 14.7 - 301 μg/cm^2 in the examined biofilm areas (Figure 4.3, Table 4.1). It may suggest selenium bioaccumulation as a consequence of bio-detoxification or utilization of selenite as an electron acceptor by members of the multispecies biofilms.

Biotransformation of selenite to elemental selenium has been observed using conventional analytical methods in many free-living microorganisms, such as *Rhodospirillum rubrum*, *Bacillus subtilis*, *Exiguobacterium* sp, *Rhizobium* sp strain B1, *Pseudomonas* sp. strain CA5, and *Escherichia coli* [20-24]. However, information on production of elemental selenium from selenite in complex multispecies biofilms is limited. Indeed, the complex multispecies biofilm, which is inherently more challenging to characterize, may more closely represent how microbial consortium may cope with these toxic selenium oxyanions. In general, selenite is more biochemically reactive than selenate in biofilms [21-23] and thus, microorganisms may convert it to less reactive elemental selenium as a result of detoxification and utilization.

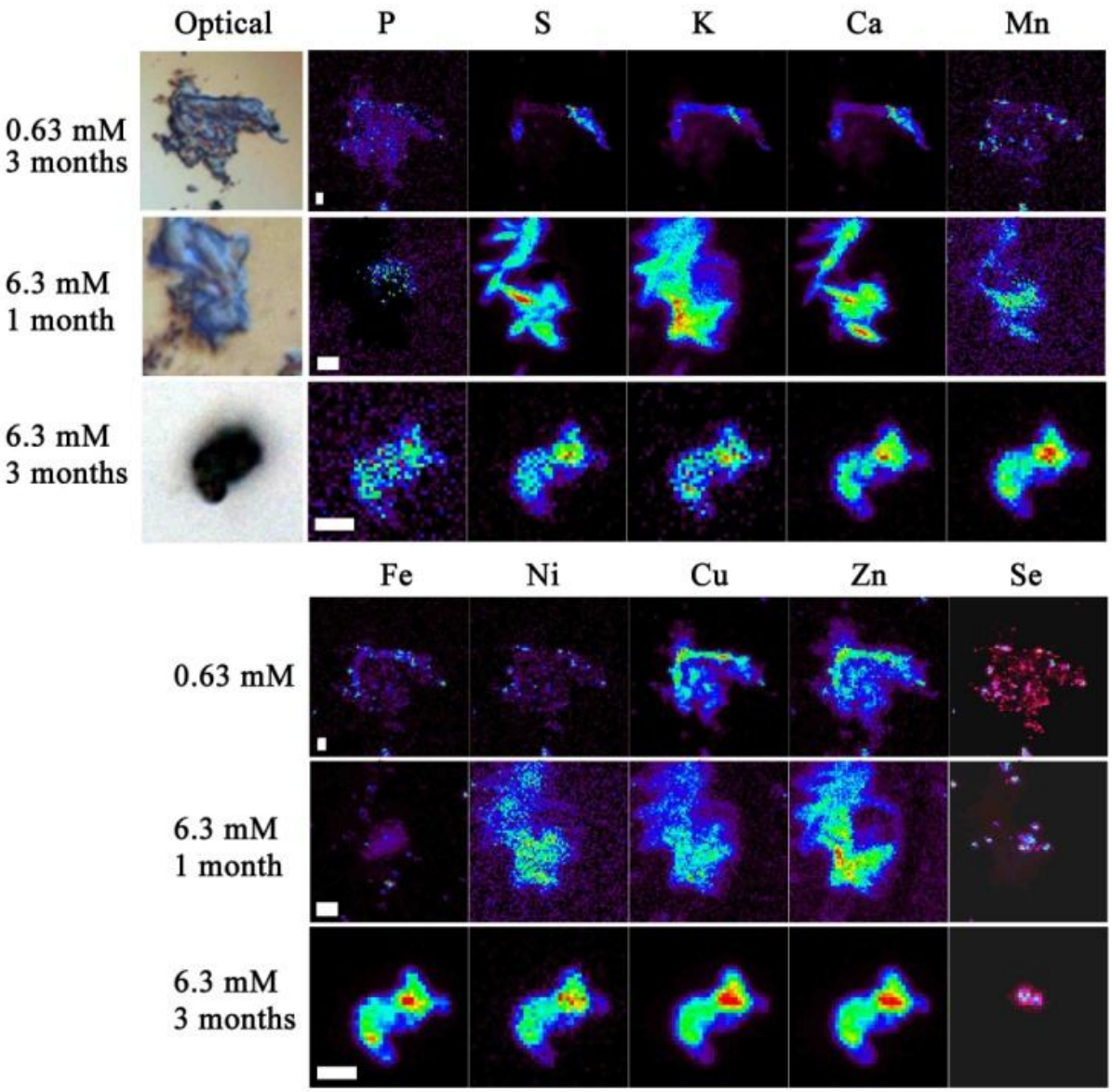

Figure 4.3. False color micro-XRF elemental distribution maps of 0.63 and 6.3 mM selenite amended biofilm samples and measured at 12,680 eV. Optical microscopic images on the scanned areas are shown on left. Incubation length is shown in months. Scale bars indicate 2μm.

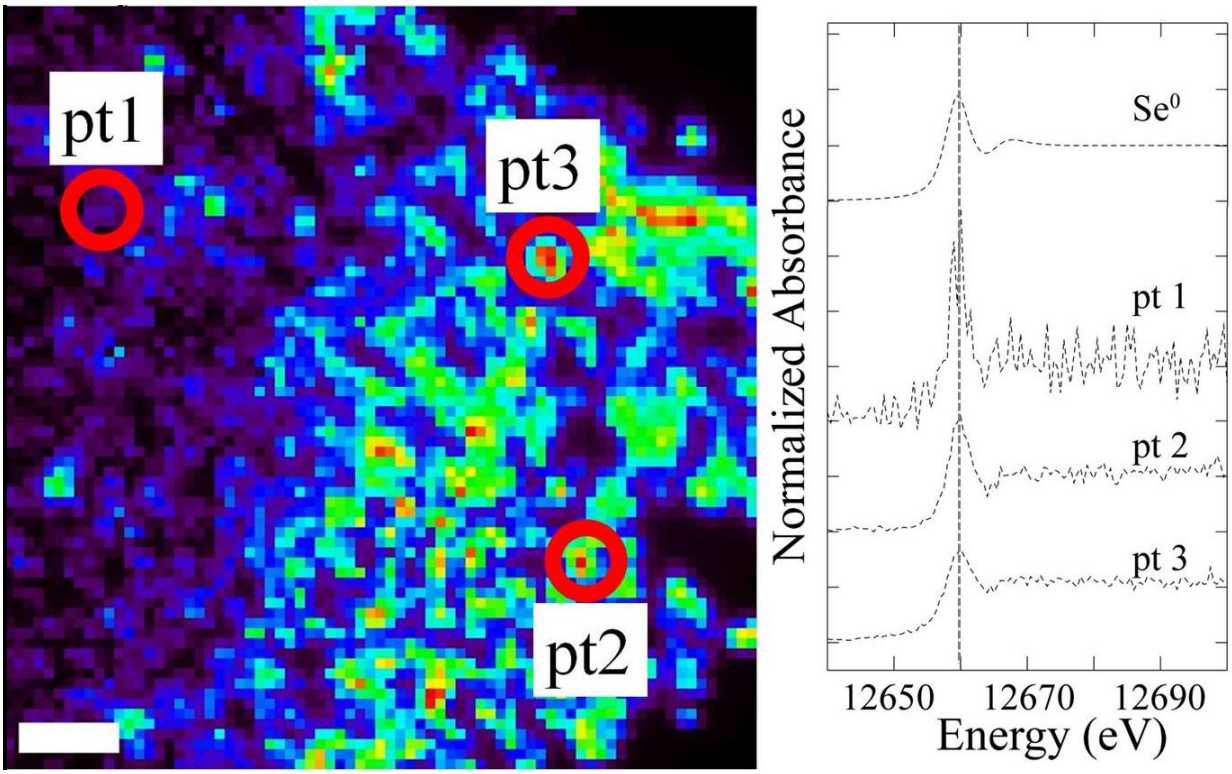

Figure 4.4. Selenium distribution in biofilm (left) incubated for 1 month under 6.3 mM and normalized Se K near-edge spectra (right) on 200 nm spots as indicated by pt 1- pt 3, in comparison with reference spectra, elemental selenium (Se^0) and selenite. The broken line indicates the peak position of elemental selenium. The scale bar shows 2 μm and selenium intensity bar is shown at the bottom of the image.

4.4.3. Chemically specific selenium X-ray fluorescence imaging in biofilms

The distribution of amended and biotransformed selenium species in the biofilms was investigated using chemically specific XRF imaging by adjusting the incident energy to the highest absorbance intensity of selenate or selenite, and elemental selenium on identical areas. The detailed spectral peak positions of each selenium species and intensity contributions used in this study are shown in Figure 4.5 and Table 4.2. Biotransformed selenium species are shown in each of the XRF results (Figure 4.6). Both selenate and selenite have been observed to be distributed broadly over the biofilm, whereas elemental selenium was found in the highly localized distributions within the biofilm.

We also observed that the average concentration of elemental selenium in biofilms differed greatly between selenite and selenate amended conditions, 22.8 μg/cm^2 (Figure 4.6-a) and 0.8 μg/cm^2 (Figure 4.6-c), respectively. This is consistent with the intense selenium signal observed in Figure 4.3 being primarily due to elemental selenium. Selenium species observed in Figure 4.6 also demonstrated that selenate is present over the EPS and is presumably absorbed or adsorbed into the biofilm without being further processed even under extremely high selenate exposure.

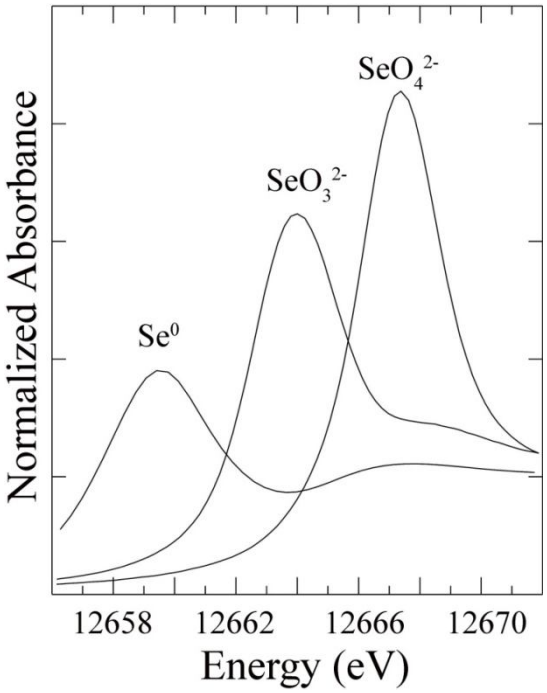

Figure 4.5. Selenium K near-edge spectra of elemental selenium (Se^0), selenite (SeO_3^{2-}), and selenate (SeO_4^{2-}). The intensity contributions of each selenium species are shown in Table 4.2.

Table 4.2. Intensity contributions of selenium species at scanned peak energies in the mixed system[A]

			Percent contribution of [B]		
Species	Peak Energy (eV)	Intensity at peak	Elemental	Selenite	Selenate
Elemental	12,659.5	1.89		11.7	3.8
Selenite	12,663.9	3.26	46.6		19.7
Selenate	12,667.3	4.26	58.5	46.0	
Selenate[C]	12,680.0	1.27	52.9	35.9	

[A] Peak energies, contribution of fluorescence intensities from each selenium species shown in Figure 4.5. Elemental stands for elemental selenium. Peak energy represents the energy where the most intense peak of each selenium species was observed. Intensities at peaks were measured by recording the values at the most intense peak position after background subtraction and normalization of spectral signal to 1. These maximum intensity values were used to evaluate the relative contribution of other selenium species.

[B] The percent intensity contribution from other selenium species at each peak energy position is shown. For example, at 12,663.9 eV (selenite peak), elemental selenium and selenate contribute 46.6 and 19.7 % of their max intensities to selenite signal when present in a mixed condition. These contributions were calculated and subtracted from the observed selenite intensity to present only selenite intensity. In calculation of elemental selenium fluorescence signal, the contributions from selenite and selenate were disregarded due to their minor contributions.

[C] Some (Figure 4.6-a and b) of the intensity values at 12,667.3 eV was calculated from selenate intensity observed at 12,680.0 eV and percent contribution of selenate at 12,667.3 eV was calculated accordingly.

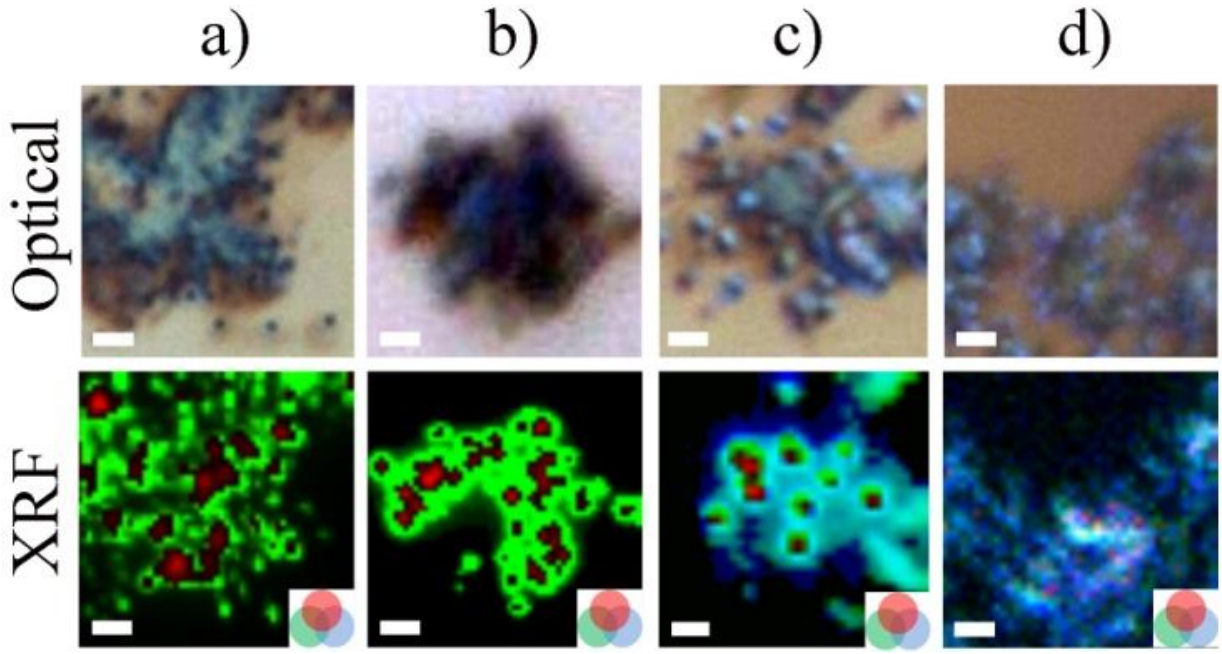

Figure 4.6. False color micro-XRF chemically specific images of biofilms amended with 6.3 mM selenite for 1 month (a) and 3 months (b), and biofilms amended with selenate for 3 months at 63 mM selenate (c, d). (c) is the same area shown in Figure 4.2. Optical microscopic images (optical) on the scanned areas are shown on top and X-ray fluorescence signals are shown below the optical images. Elemental selenium (red), selenite (green), and selenate (blue) are shown as a relative intensity color scale in each image. Scale bars indicate 2μm.

4.4.4. Biotransformations of selenium oxyanions and biofilm macromolecular structure

We used STXM to investigate the biotransformation products of selenium oxyanions and their possible associations with the biofilm structures. STXM can specifically image for proteins, polysaccharides, and lipids that are used as markers for microbial cells, EPS, and lipid, respectively in biofilms [16, 25] at the carbon K edge [26]. In addition, imaging using the Se L-edges can give information about the selenium distribution and speciation. Thus, information from STXM can be used to examine how selenium oxyanions and biotransformed species are associated with microbial cells and EPS without the need for any physical or chemical modifications of biofilms.

The areas in biofilms (Figure 4.7) that were initially investigated using XRF were further examined with STXM by revisiting the same areas. The result indicated how microorganisms

and EPS interact and biotransform with selenium oxyanions. Comparisons between selenium map (XRF) and elemental selenium/bio-macromolecule map (STXM-B) indicated that elemental selenium particles are closely localized with microorganisms and tend to be deposited in biofilms. We also found precipitated red elemental selenium at the bottom of the bioreactors, suggesting biofilms also release elemental selenium particles into the environment. Thus, the results clearly indicated that the amended selenium oxyanions were biotransformed by the biofilms and the majority of selenium species present under the exposed incubation is the detoxified product, elemental selenium.

As shown in Figure 4.7, lipid (red, STXM-A) was found associated with elemental selenium (red, STXM-B), showing average 0.53 Mander's overlap coefficient (co-localization) in 6.3 mM selenite amended biofilms. There have been a large number of reports on the role of sulfur containing peptides or proteins in elemental selenium synthesis *in vitro* [24, 27], but not on the role of lipids. Although the reduction of selenium oxyanions can induce lipid peroxidation through the generation of reactive oxygen species, we do not know whether the associated lipid was oxidized during the reduction process of selenium oxyanions. However, the strong association of lipid with elemental selenium suggests that lipid might be involved in the formation and stability of elemental selenium to a certain degree as thiol groups [24, 28].

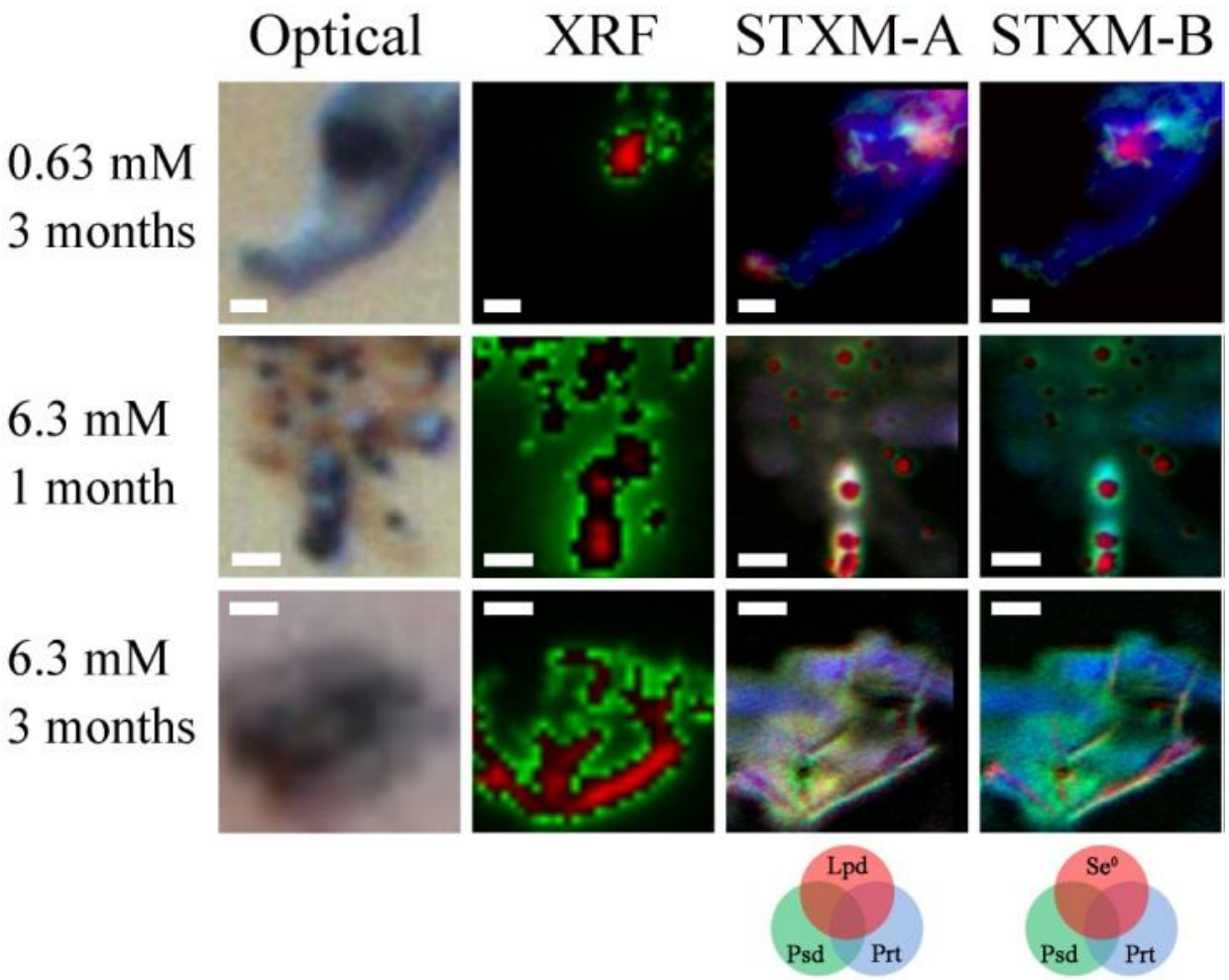

Figure 4.7. Optical, XRF and STXM images of biofilms treated with selenite. Treatments were with 0.63 mM for 3 months (large area shown in Figure 4.3), and with 6.3 mM for 1 and 3 months. Optical microscopic images on the scanned areas are shown on left (optical). XRF results shows upper 90 % and lower 10 % of the selenium intensity in red and green, respectively. STXM-A shows the distributions of protein (bacterial cells, red), polysaccharide (EPS, green) and lipid (blue). STXM-B combines selenium and macromolecular distributions showing elemental selenium (red), EPS (green) and microbial cells (blue). The areas were investigated first using XRF and revisited by STXM. Scale bars indicate 1 μm. In tricolor maps of STXM-A and –B, lipid (Lpd), polysaccharide (Psd), protein (Prt), and elemental selenium (Se^0) are shown.

4.4.5. Investigations of selenium chemical species using XRF and STXM

Investigation of selenium chemical species using two synchrotron-based techniques on the same areas of the biofilm demonstrated complementary and consistent results. In Figure 4.8, nano X-ray K near-edge structures with XRF and selenium L_3 near-edge structure with STXM on selenium intense spots in biofilms both showed elemental selenium to be the intense selenium species.

Using STXM, selenium concentrations in the examined area were determined to be 152 and 62.9 $\mu g/cm^2$ at maximum and average intensity, respectively. XRF imaging on the same area, scanned using the energy of the maximum intensity of the elemental selenium K absorption edge, indicated 135 and 52.1 $\mu g/cm^2$ at the most intense spot and at the average concentration, respectively. Thus, the two methods provided results that were consistent and reproducible over the investigated areas. This novel combination may be useful for other research in microbiology and cell biology for example, in which tools with high resolution and chemical sensitivity with minimal sample destruction would be an asset.

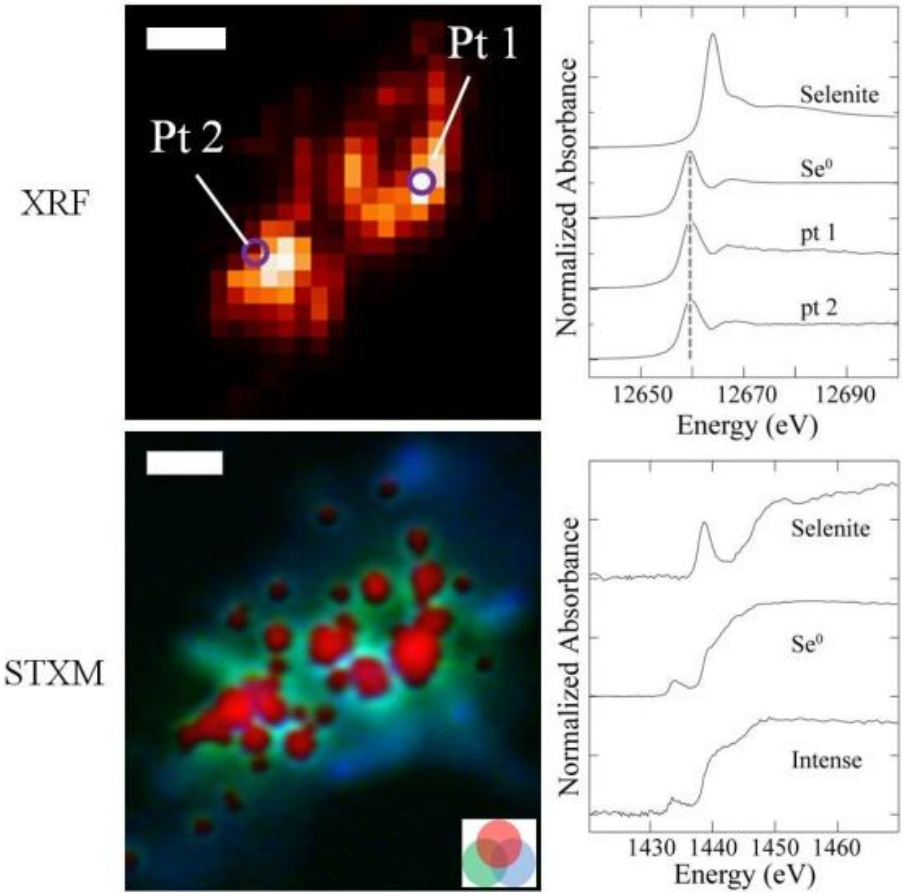

Figure 4.8. XRF and STXM images of biofilm amended with 6.3 mM selenite for 1 month. The same area of the biofilm was investigated using XRF for selenium distribution followed by STXM for selenium and macromolecular structure of biofilm. In XRF, selenium distribution is shown in relative intensity scale, thus selenium in low concentration with broad distribution is not clearly shown in the selenium map. Nano X-ray absorption Se K near-edge structures (n-XAS) are shown on right. The dotted line indicates the peak position of elemental selenium. In STXM, the "Intense" Se L_3 near-edge spectrum was extracted from the areas of intense selenium shown in red. Protein and polysaccharide are shown in blue and green, respectively. Scale bars indicate 1 μm.

4.4.6. Biogenic selenium nano-particles

Further investigation using transmission electron microscopy (TEM) with 70 nm biofilm sections suggested that biogenic elemental selenium occurs as nano particulates, ranging from 50 to 700 nm in diameter (Figure 4.9). Some selenium particles were found inside of the cells although they were mostly within the EPS. This result agrees with our observation from STXM (Figure 4.7 and Figure 4.8). Further investigation with least square curve fitting of the observed spectrum in Figure 4.10 demonstrated it is indeed elemental selenium with less than 2 % error. This result also suggested active biotransformation of selenite to elemental selenium over selenate (Figure 4.9 and Figure 4.11). This multispecies biofilm may be useful in the application of bioremediation in selenium contaminated areas and semiconductor industries where selenium nanoparticles are in great demand.

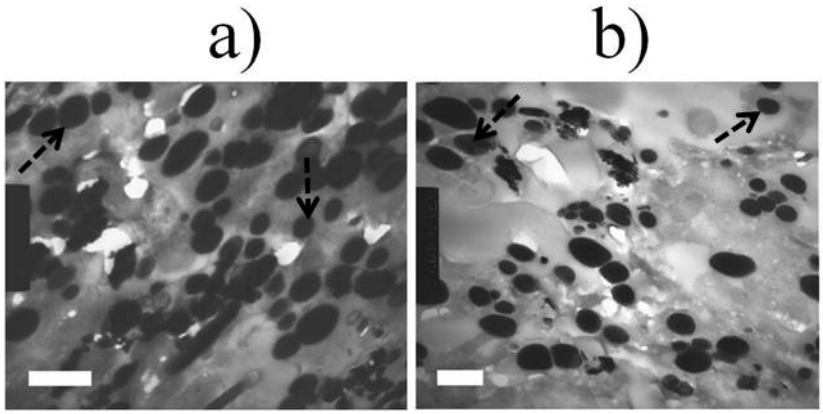

Figure 4.9. Thin sectioned (70 nm) electron micrographs of 6.3 mM (a) and 63 mM selenite (b) amended biofilms incubated for 3 months. Electron dense areas shown in black and indicated with broken arrows suggest elemental selenium nano particles. Scale bars indicate 0.5 μm.

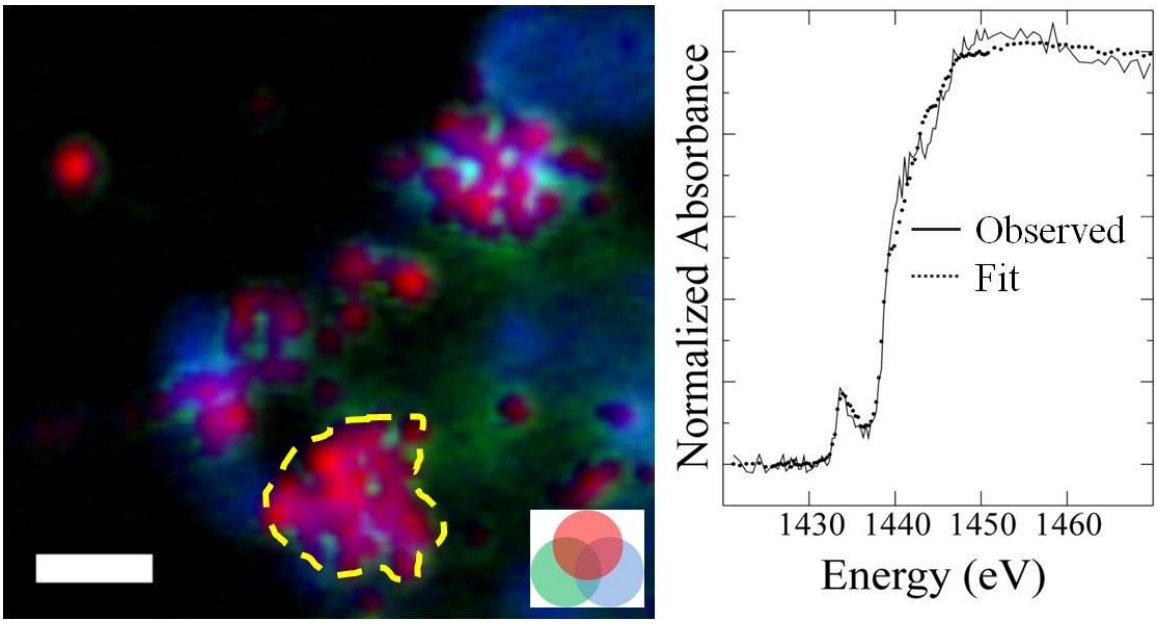

Figure 4.10. STXM image (left) and observed selenium L-edge spectra (right) from biofilm amended with 6.3 mM selenite for 1 month. In STXM image, red (elemental selenium), green (polysaccharide; extracellular polymeric substances), and blue (protein; microbial cells) are shown. The yellow broken line in STXM image outlines the region from which the observed spectrum was extracted. The least square fitting result of the observed spectrum is shown in a dotted line. Scale bar indicates 1 μm.

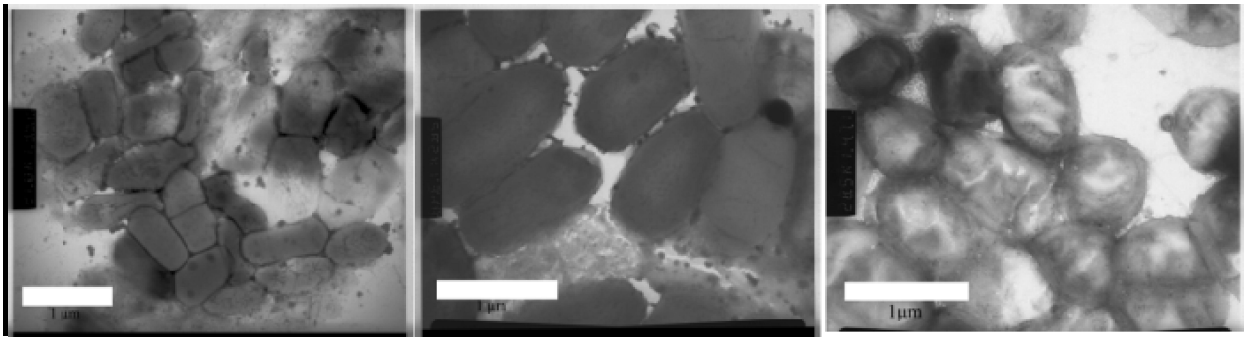

Figure 4.11. Transmission electron micrographs of negative stained control (no selenium; left) and 63 mM selenate amended biofilms incubated for 1 month (middle), and 3 months (right). Scale bars indicate 1 μm.

4.4.7. Carbonate deposit in multispecies biofilm

We examined carbonate deposit using synchrotron-based soft X-ray scanning transmission X-ray microscopy (STXM) at the carbon K edge (Figure 4.12). The spectrum averaged over the biofilm showed broadly distributed carbonate (CO_3^{2-}). The strong transition peak at 290.5 eV is an indicator of carbonate, arising from the C 1s to $\pi^*_{C=O}$ transition of carbonate [26], and thus it can be used to identify its presence in the mixed system. Carbonate mainly accumulated in EPS at average concentration of 66.8 (± 28.2) μg/cm^2 in the examined carbonate-rich area (3 μm × 3 μm) shown in Figure 4.12. This suggests carbonate biomineralization in the biofilms.

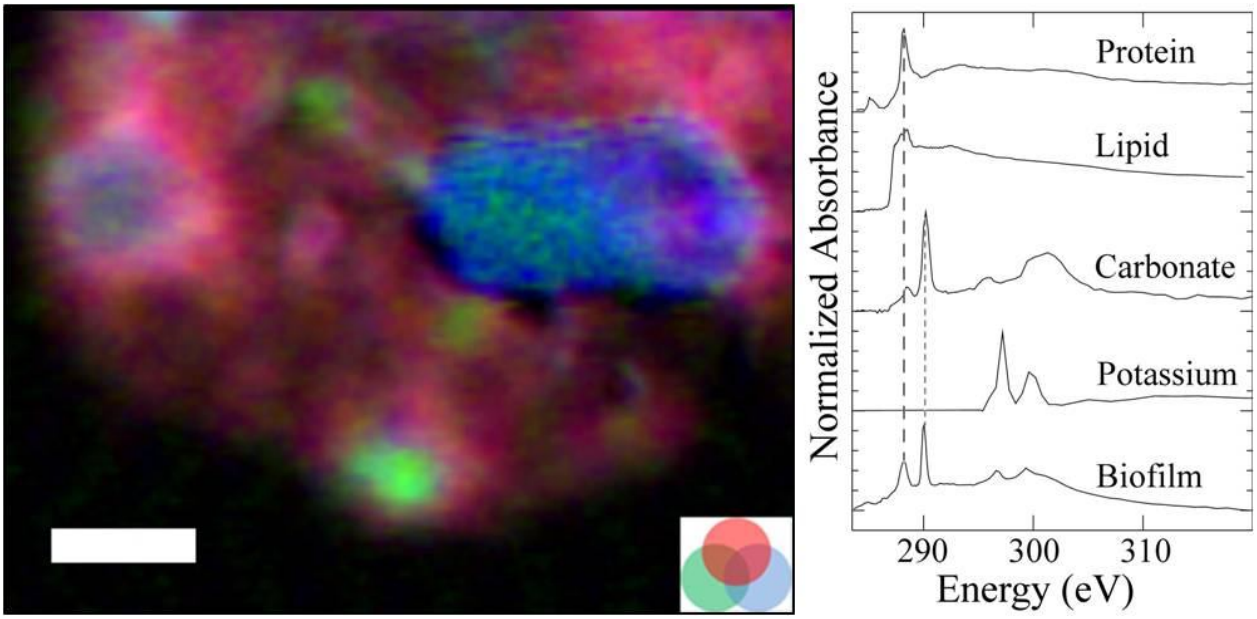

Figure 4.12. STXM image of 1 month incubated biofilm under 6.3 mM of selenite (left). Red, green, and blue represent carbonate, lipid, and microbial cells, respectively. Scale bars indicate 0.5 μm. Spectrum (biofilm) collected from the whole area is shown with reference protein, lipid, carbonate (CO_3^{2-}), and carbon K near-edge spectra (right). The broken line at 288.2 eV indicates the C 1s to π* transition in C=O of carboxyamide. The dotted line shows C 1s to π* transition in C=O in carbonate.

4.5. ACKNOWLEDGMENTS

The authors thank to all the Pickering/George group members at University of Saskatchewan and George Swerhone at Environment Canada. This research is supported by an NSERC Discovery Grant (to Pickering) and by Environment Canada. Pickering is a Canada Research Chair and Yang is a CIHR-THRUST Fellow. STXM was carried out at the Canadian Light Source (CLS) and XRF at the Advanced Photon Source (APS). The CLS is supported by the Natural Sciences and Engineering Research Council of Canada, the National Research Council Canada, the Canadian Institutes of Health Research, the Province of Saskatchewan, Western Economic Diversification Canada, and the University of Saskatchewan. Use of the APS, an Office of Science User Facility operated for the U.S. Department of Energy (DOE) Office of Science by Argonne National Laboratory, was supported by the U.S. DOE under Contract No. DE-AC02-06CH11357.

4.6. REFERENCES

[1] L. Letavayová, D. Vlasáková, J. E. Spallholz, J. Brozmanová, M. Chovanec, Toxicity and mutagenicity of selenium compounds in *Saccharomyces cerevisiae*. *Mutat Res* 2008, *638,* 1.

[2] K. Brown, J. Arthur, Selenium, selenoproteins and human health: a review. *Public Health Nutr.* 2001, *4,* 593.

[3] H. Hartikainen, T. Xue, V. Piironen, Selenium as an anti-oxidant and pro-oxidant in ryegrass. *Plant Soil* 2000, *225,* 193.

[4] Z. Pedrero, Y. Madrid, H. Hartikainen, C. Cámera, Protective effect of selenium in broccoli (*Brassica oleracea*) plants subjected to cadmium exposure. *J.Agric.Food Chem.* 2008, *56,* 266.

[5] A. G. Renwick, Toxicology of micronutrients: adverse effects and uncertainty. *J. Nutr.* 2006, *136,* 493S.

[6] A. Sekowska, H. Kung, A. Danchin, Sulfur metabolism in *Escherichia coli* and related bacteria: facts and fiction. *J. Mol. Microbiol. Biotechnol.* 2000, *2,* 145.

[7] K. B. Miklós Mézes, Prooxidant mechanisms of selenium toxicity – a review. *Acta Biologica Szegediensis* 2009, *53,* 15.

[8] E. van Hullebusch, M. Zandvoort, P. Lens, Metal immobilisation by biofilms: mechanisms and analytical tools. *Rev. Environ. Sci. Biotechnol.* 2003, *2,* 9.

[9] J. R. Lawrence, T. R. Neu, Microscale analyses of the formation and nature of microbial biofilm communities in river systems. *Rev. Environ. Sci. Biotechnol.* 2003, *2,* 85.

[10] C. M. Waters, B. L. Bassler, Quorum Sensing: Cell-to-cell communication in bacteria. *Annu. Rev. Cell Dev. Biol.* 2005, *21,* 319.

[11] S. I. Yang, J. R. Lawrence, D. W. G. Swerhone, I. J. Pickering, Biotransformation of selenium and arsenic in multi-species biofilm. *Environ. Chem.* Accepted on September, 2011.

[12] S. Vogt, MAPS: A set of software tools for analysis and visualization of 3D X-ray fluorescence data sets. *J Phys IV France* 2003, *104,* 635.

[13] A. P. Hitchcock, aXis2000 is written in interactive data language (IDL) and available at http://unicorn.mcmaster.ca/aXis2000.html. 2010,.

[14] M. D. Abramoff, P. J. Magelhaes, S. J. Ram, Image processing with Image J. *Biophoton Int.* 2004, *11,* 36.

[15] G. N. George, I. J. Pickering, EXAFSPAK: A Suite of computer programs for analysis of X-ray absorption spectra available at http://ssrl.slac.stanford.edu/exafspak.html. 2001,.

[16] J. J. Dynes, T. Tyliszczak, T. Araki, J. R. Lawrence, G. D. W. Swerhone, G. G. Leppard, A. P. Hitchcock, Speciation and quantitative mapping of metal species in microbial biofilms using scanning transmission X-ray microscopy. *Environ.Sci.Technol.* 2006, *40,* 1556.

[17] I. N. Koprinarov, A. P. Hitchcock, C. T. McCrory, R. F. Childs, Quantitative mapping of structured polymeric systems using singular value decomposition analysis of soft X-ray images. *J Physical Chem B* 2002, *106,* 5358.

[18] C. Shi, S. C. Kendall, E. Grote, S. Kaminskyj, M. C. Loewen, N-terminal residues of the yeast pheromone receptor, Ste2p, mediate mating events independently of G1-arrest signaling. *J.Cell.Biochem.* 2009, *107,* 630.

[19] C. I. E. Wiramanaden, K. Liber, I. J. Pickering, Selenium Speciation in Whole Sediment using X-ray Absorption Spectroscopy and Micro X-ray Fluorescence Imaging. *Environ.Sci.Technol.* 2010, *44,* 5389.

[20] J. Kessi, M. Ramuz, E. Wehrli, M. Spycher, R. Bachofen, Reduction of selenite and detoxification of elemental selenium by the Phototrophic Bacterium *Rhodospirillum rubrum* . *Appl.Environ.Microbiol.* 1999, *65,* 4734.

[21] M. Ikram, M. Faisal, Comparative assessment of selenite (SeIV) detoxification to elemental selenium (Se^0) by *Bacillus* sp. *Biotechnol.Lett.* 2010, *32,* 1255.

[22] W. Hunter, L. Kuykendall, Reduction of selenite to elemental red selenium by *Rhizobium* sp. strain B1. *Curr. Microbiol.* 2007, *55,* 344.

[23] W. Hunter, D. Manter, Reduction of selenite to elemental red selenium by *Pseudomonas* sp. strain CA5. *Curr. Microbiol.* 2009, *58,* 493.

[24] J. Dobias, E. I. Suvorova, R. Bernier-Latmani, Role of proteins in controlling selenium nanoparticle size. *Nanotechnology* 2011, *22,* 195605.

[25] J. R. Lawrence, G. D. W. Swerhone, G. G. Leppard, T. Araki, X. Zhang, M. M. West, A. P. Hitchcock, Scanning transmission X-ray, laser scanning, and transmission electron microscopy mapping of the exopolymeric matrix of microbial biofilms. *Appl. Environ. Microbiol.* 2003, *69,* 5543.

[26] J. A. Brandes, C. Lee, S. Wakeham, M. Peterson, C. Jacobsen, S. Wirick, G. Cody, Examining marine particulate organic matter at sub-micron scales using scanning transmission X-ray microscopy and carbon X-ray absorption near edge structure spectroscopy. *Mar.Chem.* 2004, *92,* 107.

[27] J. Zhang, X. G. Gao, L. Zhang, Y. Bao, Biological effects of a nano red elemental selenium. *Biofactors* 2001, *15,* 27.

[28] Y. Ogasawara, G. Lacourciere, T. C. Stadtman, Formation of a selenium-substituted rhodanese by reaction with selenite and glutathione: Possible role of a protein perselenide in a selenium delivery system. *PNAS* 2001, *98,* 9494.

CHAPTER 5. *ARTHROBACTER sp*. SASK-Se22 BIOFILM DETOXIFIES SELENIM OXYANIONS: AN INVESTIGATION USING SYNCHROTRON-BASED TOOLS

This manuscript will be submitted for publication in *Geochimica et Cosmochimica Acta* with the following authors: Soo In Yang, Graham N. George, John R. Lawrence, Mercedes G. Gallegos, James J. Dynes, Barry Lai, Susan G. W. Kaminskyj, and Ingrid J. Pickering. In this research, I planned, designed and conducted experiments, and played a major role in preparing the manuscript. Other coauthors provided advice, help on experiment, and contributed to the preparation of the manuscript.

In this study, a selenium resistant isolate, *Arthrobacter* sp. SASK-22 pure-culture, was identified using 16S rRNA gene sequencing. Pure culture biofilms were formed and their detoxification of selenium oxyanions was investigated using XAS, XRF, and STXM imaging techniques. Compared to a multispecies biofilm, the isolated *Arthrobacter* sp. SASK-22 pure-culture biofilm was seen to have both a superior ability to biotransform selenium oxyanions and unique characteristics in terms of its biotransformation of selenium oxyanions to elemental selenium.

5.1. ABSTRACT

Elevated selenium in the environment has drawn attention for a long time due to its toxicity and tendency to bioaccumulate in higher trophic levels. Biofilms are known for their crucial role in the geochemical cycling of elements of concern such as selenium; however, there are important limits to the analyses of biotransformation due to issues with sample preparation and with a lack of suitable analytical tools. We used synchrotron-based spectroscopic and imaging techniques as well as conventional microscopic techniques to investigate biofilms formed from the newly discovered highly selenium resistant *Arthrobacter* sp. SASK-Se22. Selenium X-ray absorption K near-edge spectroscopy showed that the *Arthrobacter* sp. biofilm biotransformed selenium oxyanions into less toxic elemental selenium. Differential distribution patterns of selenium species in the biofilm were observed with X-ray fluorescence (XRF) imaging, suggesting that most of the generated elemental selenium is released into the environment. Scanning transmission X-ray microscopy (STXM) observations allow correlation of elemental selenium

with macromolecular biofilm structure. The distribution of selenite and selenate determined using XRF and correlated with elemental selenium and biofilm structure shown from STXM, demonstrated selenium biotransformation in *Arthrobacter* sp SASK-Se22 biofilm. The investigation using transmission electron microscopy showed that the biogenic elemental selenium comprises sub-micron particulates ranging from 100 to 300 nm in diameter.

5.2. INTRODUCTION

Increased levels of selenium in the environment released during anthropogenic activities, such as mining and processing, and natural exposure in certain areas are of rising concern [1-5]. In general, major aqueous environmental selenium species are selenite and selenate, which are biologically very reactive and can be toxic [6, 7]. As a result, the toxicity or impacts of selenium in the environment have drawn an attention for a long time [8-11], as has the need for remediation using environmentally friendly methods, such as bioremediation.

Biofilms, or microbial consortia, play important roles in the biogeochemical cycling process of elements of concern in the aquatic environment [12, 13]. Many have reported the contribution of biofilms to the geocycling of selenium and its application for bioremediation [14-17]. Nonetheless, our understanding of how biofilms regionally transform selenium oxyanions is limited and speciation of selenium using conventional microscopic techniques is not practically achievable. In addition, investigation using conventional microscopy involves extensive chemical or physical modification, which may introduce artifacts. Thus, determining chemical information with a minimum of sample preparation may lead to improved characterization of biofilms.

To investigate the fate of selenium oxyanions in biofilms, we grew biofilms using a selenium-resistant *Arthrobacter* sp. SASK-22 [18] pure culture, isolated from selenium-containing coal mine-affected water, and employed a suite of synchrotron-based hard and soft X-ray absorption spectroscopic imaging techniques. X-ray absorption spectroscopy (XAS) was used to determine selenium chemical speciation, and X-ray fluorescence imaging (XRF) and soft X-ray scanning transmission X-ray microscopy (STXM) were used to reveal selenium distributions in the context of the microorganisms. Laboratory-based confocal laser scanning microscopy (CLSM) and transmission electron microscopy (TEM) provided complementary information.

Examination of *Arthrobacter* sp. SASK-Se22 pure culture biofilms suggested biofilms are highly involved in the sequestration of selenium. In particular, very high selenite levels lead to the production of elemental selenium nanoparticles.

5.3. MATERIALS AND METHODS

5.3.1. Identification of isolate

Arthrobacter sp. SASK-Se22 was isolated from samples of water taken from Goddard Marsh, a selenium-affected location in British Columbia, Canada. The universal transverse mercator (UTM) of the marsh is zone 11, 0653165(Easting), and 5514141(Northing). One hundred microlitre aliquot of the marsh water was plated onto 10 % tryptic soy agar (TSA) containing 400 or 500 mM sodium selenate. Dark red colonies were selected after thirty days of incubation at room temperature (RT; 22 ± 3 °C). The genus identities of isolates were confirmed to be *Arthrobacter, Bacillus, Pseudomonas, and Rhodococcus* sp. as reported [18]. The partial 16S rRNA gene sequencing of the most selenium resistant isolate was performed at Macrogen Inc (Seoul, Republic of Korea) using a pair of bacterial universal primers; forward (CCAGCAGCCGCGGTAATACG) and reverse primers (TACCAGGGTATCTAATCC). The 16S rRNA gene sequence was deposited in the National Center for Biotechnology and Information (NCBI) gene data bank.

5.3.2. Biofilm formation

Biofilms were grown on the surface of polycarbonate strips (1 cm × 10 cm) immersed in 16 mL of 10 % tryptic soy broth (TSB) at room temperature (RT) on a gyratory shaker at 100 rpm. After growth for 3 weeks to allow thick biofilm formation, the biofilms were transferred into fresh 10 % TSB media, containing 0.63-63 mM selenate or selenite, and incubated under the same conditions for 1 or 2 months. Biofilm formation was examined using confocal laser scanning microscopy (CLSM) at Environment Canada, Saskatoon, SK, Canada as described elsewhere [18, 19].

5.3.3. X-ray absorption spectroscopy

We used X-ray absorption spectroscopy to investigate selenium chemical species changes averaged over the *Arthrobacter* sp. SASK-Se22 biofilm. Selenium-exposed biofilms were carefully rinsed using filtered 10 % TSB to remove loosely bound selenium. Biofilms were then recovered by scraping using sterile silicone tubing fragments and packed into XAS cuvettes followed by a flash freezing in iso-pentane containing liquid nitrogen (NL). The media including precipitate samples were centrifuged at 6,500 g for 5 mins after being transferred into micro-centrifuge tubes. The suspension (media) and precipitate samples were separately collected; then, the samples were prepared by the same method and preserved in NL containing Dewar for less than 3 weeks. Selenium X-ray absorption K near-edge spectra were collected at beamline 7-3 of Stanford Synchrotron Radiation Lightsource (SSRL), USA as previously described [18]. The spectra were least squares fitted with our selenium reference spectra (1 μM solution for soluble selenium compounds and powder mixed with BN for insoluble), collected in advance, and processed using EXAFSPAK [20]. Data were processed using EXAFSPAK software [20] as Pickering *et al* described [21].

5.3.4. Micro X-ray fluorescence imaging and μ-XAS

Selenium exposed biofilm samples were carefully harvested as described above and 1 μL aliquot of slurry was placed onto a silicon nitride window (0.5 mm × 0.5 mm, NX5050B, Norcada Inc) and air-dried. The biofilm samples were measured at beamline 2-3 of SSRL which is equipped with a Si(220) double crystal monochromator and a horizontally and vertically focused Kirkpatrick Baez (KB) mirror pair, focusing a beam down to a 2.5 μm × 2.5 μm area of the sample. Biofilm samples and the Vortex™ detector to measure fluorescence were mounted at 45° and 90° to the incident beam, respectively. Sub-micron sized scanning at using a step size of 200 nm × 200 nm was achieved by over-sampling with 1 second dwell time on each pixel. Data was processed using Microanalysis Toolkit [22]. Selenium K near-edge micro X-ray absorption spectra (μ-XAS) were collected in duplicate from selected pixels on the scanned image and were processed as described above for bulk XAS.

5.3.5. Nano X-ray fluorescence imaging

Biofilm samples were prepared as described above and brought to beamline 2-ID-D of the Advanced Photon Source (APS), USA. The biofilms prepared on silicon nitride windows were mounted on an aluminum frame in a flowing helium gas environment. The biofilm samples and Vortex silicon drift detector (SII Nano Technology USA Inc., CA, USA) were oriented at 15° and 90° to the incident beam, respectively. The regions of interest on the samples were raster scanned at 0.5 seconds on each pixel. Data were processed using MAPS [23].

5.3.6. Chemically specific imaging of selenium species in biofilm

The APS 2-ID-D beamline was carefully calibrated by adjusting the monochromator angle by measuring red elemental selenium (#18227, Millipore, MA, USA). The white line energies of the most abundant selenium species (selenate, selenite, and elemental selenium at 12,667.3, 12,663.9, and 12,659.5 eV, respectively) were measured from the selenium reference spectra previously collected from beamline 7-3 and 9-3 of SSRL. For selenate-treated biofilms, the incident energy was set to the energies of the highest spectral intensities of selenate, selenite, and elemental selenium and a raster scan of an area of the biofilm was repeated at each energy. Because selenite oxidation in the biofilms was not observed in bulk measurements, for selenite-treated biofilms were scanned at two energies, corresponding to selenite and elemental selenium white line energies. Each raster scanned image was aligned and processed using MAPS [24] and Axis2000 [25]. The upper 90 % of the fluorescence signal was considered (10 % threshold) unless otherwise stated.

5.3.7. Scanning transmission X-ray microscopy

Biofilm samples used for nano X-ray fluorescence imaging were carefully transported to the Spectromicroscopy (SM) beamline at the Canadian Light Source (CLS), Canada for scanning transmission X-ray microscopy (STXM) measurement. Data were collected using point, line, and whole scanning modes at a sequence of energies at the carbon K-edge and at the selenium L-edges and were processed using aXis2000 [25] as reported[26]. The macromolecular (protein, lipid, and polysaccharide) structure of biofilms together with selenium species were identified using singular value decomposition (SVD). Previously collected carbon and selenium model spectra

were used for SVD analysis [27]. Extracted spectra from energy calibrated optical density images were background subtracted and normalized using EXAFSPAK [20].

5.3.8. Size determination for selenium sub-micron particulates

Biofilm samples for transmission electron microscopy (TEM) were prepared as described by Shi *et al* [28]. Thin-sectioned biofilms (70 nm) were prepared using Reichert-Jung Ultracut microtome (Reichert Microscope Services, Depew, NY, USA).

5.4. RESULTS AND DISCUSSION

5.4.1. Identification of selenium resistant bacterium

The partial 16S rRNA gene sequencing result for the selenium resistant isolate was analyzed using a Basic Local Alignment Search Tool (BLAST) search [29]. The result indicated that the isolate is an unknown strain of *Arthrobacter* sp. We named it *Arthrobacter* sp. SASK-Se22 and the sequence was deposited in GenBank (accession code JN035620; also shown in Appendix). No further microbiological characterization studies were carried out.

5.4.2. Arthrobacter sp. *biofilms biotransform selenium oxyanions*

X-ray absorption K near-edge spectra of selenate or selenite amended biofilms, media, and precipitates after 1 or 2 month incubations are shown in Figure 5.1 and 5.2. The results of least square fitting of the observed selenium spectra are shown in Table 5.1. *Arthrobacter* sp. SASK-Se22 biofilm showed a greater degree of biotransformation of selenite compared to selenate. Under all conditions examined, the amended selenate and selenite were at least partially biotransformed by the pure culture biofilm, leading to the presence of reduced selenium species in all biofilms, precipitate, and media. The selenium species observed are mainly selenate, selenite, and elemental selenium. We cannot rule out the possibility of volatile selenium species such as dimethyl diselenide or dimethyl selenide. However, we did not include analysis of the gaseous phase in our evaluation. Further selenium quantification measurements may show the presence and quantity of gaseous selenium. We did not observe changes in selenium chemical

species in control samples (no biofilms) examined under the same condition (data not shown), supporting the observation that selenium reduction is driven by biofilms.

Under selenate-amendment, reduction of the selenate in biofilm was observed, with a greater proportion of the observed selenium being reduced when the incubation was extended to 2 months. Measurements of the media and precipitate revealed that elemental selenium was additionally present in both of these components of the system. With extremely low solubility, elemental selenium was not expected to be present in media samples; however, its observation (Table 5.1) may suggest the presence of a colloid of elemental selenium. Due to the higher reactivity of selenite, the proportion of biotransformed selenium in selenite-amended biofilm was greater than in the selenate treated biofilms. As a result, the proportion of elemental selenium observed in selenite-amended biofilm was high in all the conditions examined. In 0.63 mM selenite-amended condition, elemental selenium was the only selenium species observed in biofilm, media, and precipitate samples. The prolonged presence and increased ratio of elemental selenium in media may imply its high stability, perhaps due to biologically generated organic materials chemically bound to the elemental selenium particles or used for nucleation of selenium particles.

The dependency of selenium toxicity on its chemical species has been a controversial topic for a long time [10, 30-33]. A recent report investigating the toxicity of elemental selenium nano-particles to Japanese Medaka fish indicated that selenium nano-particles could be 5 times more toxic to aquatic animals compared to selenite by causing bioaccumulation of selenium in the liver [34]. In contrast to this, Zhang *et al* [35] suggested that elemental selenium nanoparticles are 7 times less toxic than selenite in mice. In this regard, our observation of elemental selenium in the biofilm media may suggest a controversial toxicity issue. However, the lower solubility compared to selenium oxyanions implies easier recovery of selenium from the aquatic system by simple physical and chemical methods, such as centrifugation or coagulation, suggesting a possible application of this biofilm system to the bioremediation of selenium-affected wastewater treatment.

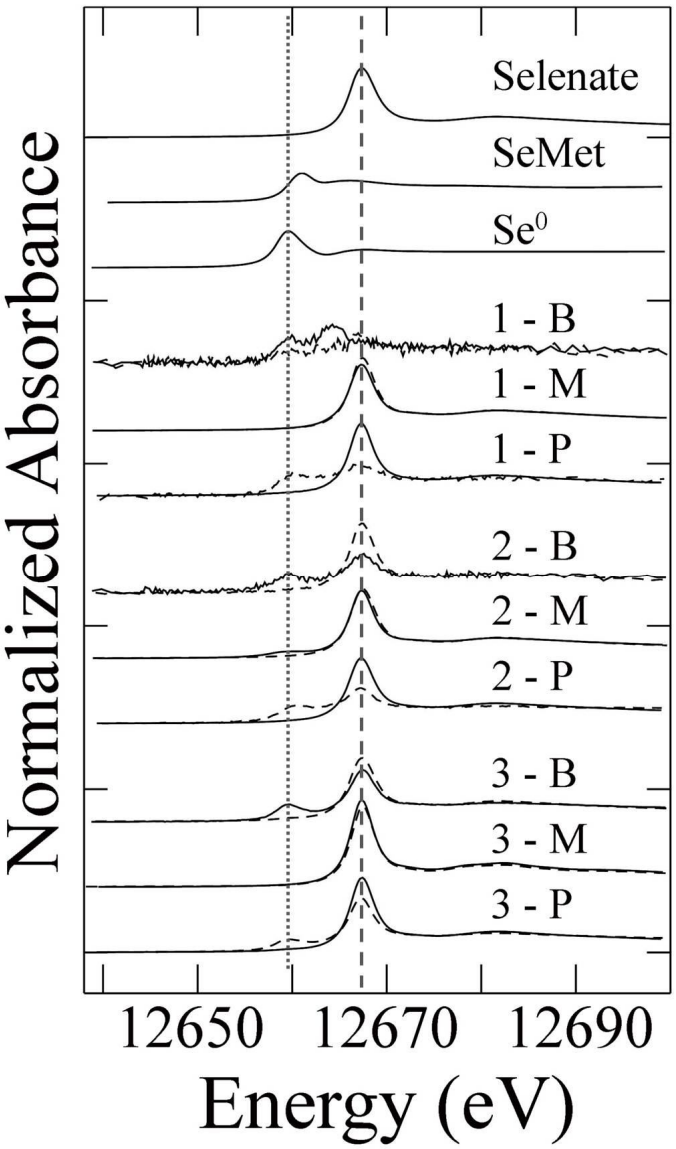

Figure 5.1. Selenium K near-edge spectra of selenate-amended biofilms of *Arthrobacter* sp. SASK-Se22. The spectra of observed selenium species are shown at the top together with the white line positions of elemental selenium (Se^0; dotted line) and selenate (broken line). Label 1, 2, and 3 represents 0.63, 6.3, and 63mM of selenite, respectively, along with the initials of biofilm (B), medium (M), and precipitate (P). Spectra following incubation periods of 1 month (broken line) and 2 months (solid line) are superimposed.

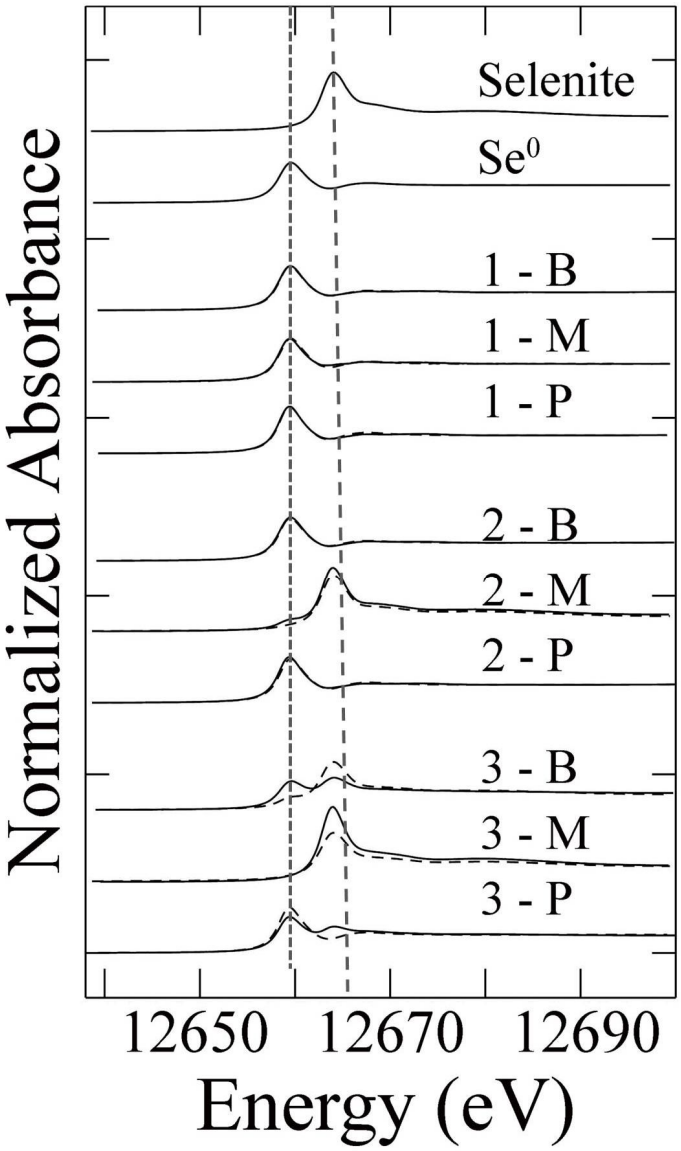

Figure 5.2. Selenium K near-edge spectra of selenite-amended biofilms of *Arthrobacter* sp. SASK-Se22. The spectra of observed selenium species are shown at the top together with the white line positions of elemental selenium (Se^0; dotted line) and selenite (broken line). Label 1, 2, and 3 represents 0.63, 6.3, and 63mM of selenite, respectively, along with the initials of biofilm (B), medium (M), and precipitate (P). Spectra following incubation periods of 1 month (broken line) and 2 months (solid line) are superimposed.

Table 5.1. Observed percentages of selenium species observed in *Arthrobacter* sp. SASK-Se22

Amendment conditions			Observed species in biofilm			Observed species in media			Observed species in precipitate		
Species	Se [mM]	Time [days]	Selenate	Selenite	Elemental Selenium	Selenate	Selenite	Elemental Selenium	Selenate	Selenite	Elemental Selenium
Selenate	0.63	30	27[B]	22[B]	51[B]	100			20	22	58
Selenate	6.33	30	100			100			30	10	28[C]
Selenate	63.3	30	94		6	100			65	4	31
Selenate	0.63	60		47[D]	53[D]	95	5[D]		100		
Selenate	6.33	60	40		60	89		11	95		5
Selenate	63.3	60	61		39	100			100		
Selenite	0.63	30			100			100			100
Selenite	6.33	30			100		95	5			100
Selenite	63.3	30		77	23		100				100
Selenite	0.63	60			100			100			100
Selenite	6.33	60			100		90	10			100
Selenite	63.3	60		36	63		100			21	79

[A] Least square fitting results gave three times the estimated standard deviation (esd) in the fit of less than 3 % unless otherwise stated.
[B] 3 x esd of 8 %
[C] also fits 32 % of selenomethionine
[D] 3 x esd of 6 %.

5.4.3. Localization of selenium (X-ray fluorescence imaging)

The distribution of selenium in the *Arthrobacter* sp. SASK-Se22 pure-culture biofilm is shown in Figure 5.3. Micro X-ray absorption spectra collected from low, middle, and high selenium areas suggested the presence of elemental selenium as the dominant selenium species in the biofilm. This observation also agrees with the selenium K near-edge spectra averaged over the whole biofilm shown in Figure 5.2 and Table 5.1.

An elemental distribution map observed in selenite-amended *Arthrobacter* sp. SASK-Se22 biofilm are shown in Figure 5.4 together with a multichannel analyzer (MCA) spectrum from the fluorescence detector. In the MCA spectrum, 2 prominent fluorescence emission lines can be seen: silicon $K_{\alpha\beta}$ and selenium K_{α}. The silicon fluorescence signal was expected because the biofilms were supported on silicon nitride windows. The intense selenium signal is derived from the abundant presence of elemental selenium in the biofilm; due to its prominent contribution, the Compton and elastic scatter peaks are superimposed with the selenium K_{β} fluorescence spectrum. Thus, the relative intensity scales of elements shown in the elemental maps in Figure 5.4 are not comparable. In Table 5.2, the observed selenium concentration was in fact several orders of magnitude higher than any other elements measured in the biofilms and than selenium observed in the selenate-amended biofilm (Table 5.2). This result suggests that *Arthrobacter* sp SASK-Se22 biofilms actively biotransform selenite into elemental selenium and that its selenium particles dissociate from the cells. The presence of extracellular selenium particulates may suggest the existence of extracellular selenite-reducing enzymes, or excretion of reducing molecules, such as glutathione, or extracellular nucleation of selenium after reduction inside of the cells. Even though further examination is required to identify this fate of selenite biotransformation, this observation suggests the possible application of this biofilm in bioremediation of selenium oxyanions or production of elemental selenium particles.

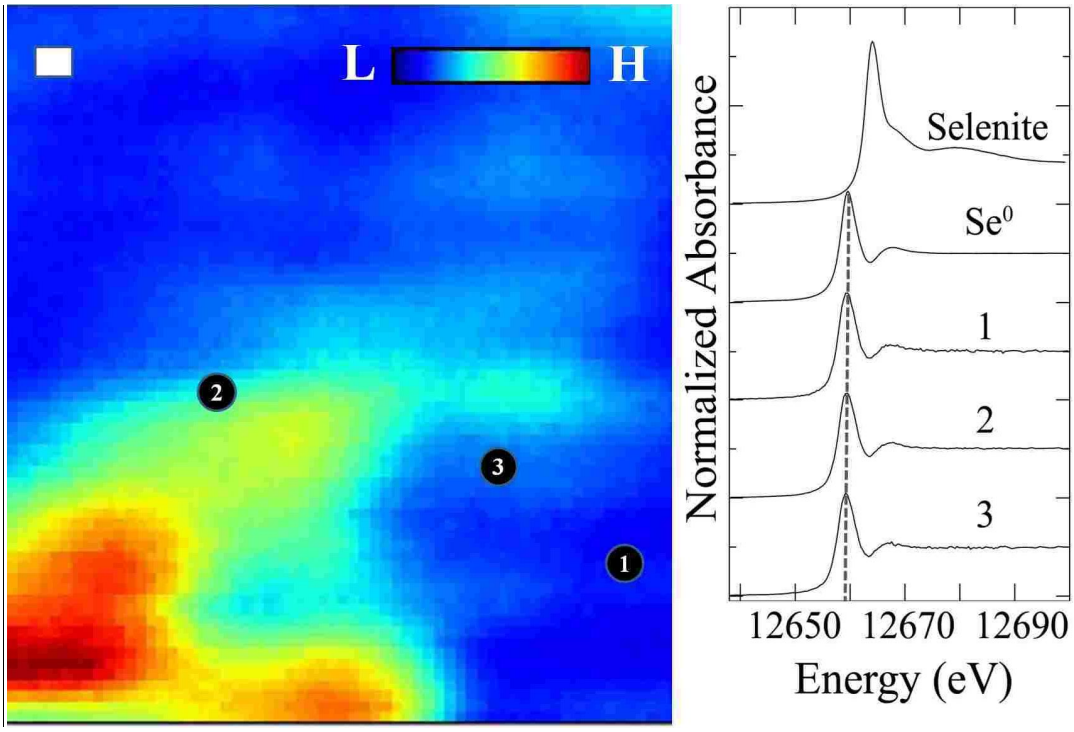

Figure 5.3. Micro X-ray fluorescence map of selenium in *Arthrobacter* sp. SASK-Se22 biofilm (left), incubated for 1 month in 6.3 mM of selenite. Intensity bar indicates low (L) to high (H) in selenium concentration. The white scale bar equals 1 μm. μ-XAS spectra (right) collected on areas 1-3 in the XRF selenium map, together with spectra of selenite and elemental selenium (Se^0). The broken line indicates the peak position of the elemental selenium.

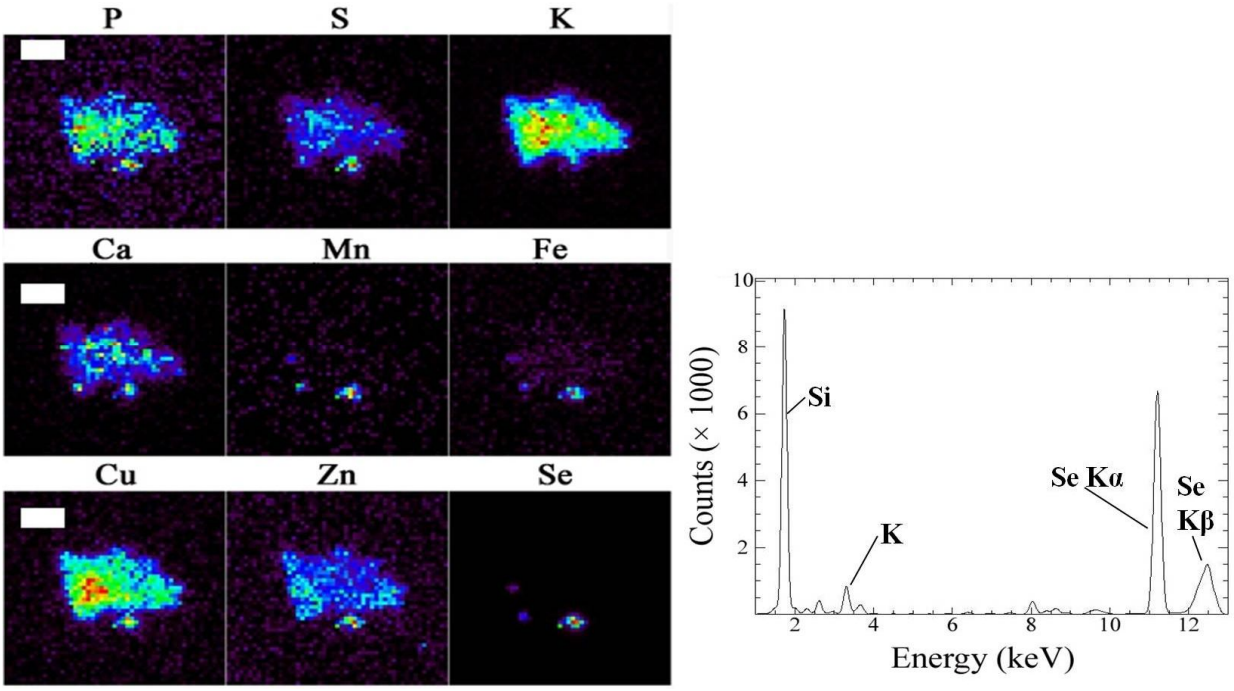

Figure 5.4. Nano X-ray fluorescence images (n-XRF, left) and multichannel analyzer spectrum (MCA, right) of biofilms of *Arthrobacter* sp. SASK-Se22 incubated in 6.3 mM selenite for 2 months. In the n-XRF image, the relative intensity is displayed independently for each elemental map and the scale bars show 2 µm. The scale bars are shown in P, Ca, and Cu maps and the sizes of each map are identical. In the MCA, prominent fluorescent emission spectra are indicated. The monochromator energy was set to 12,659.5 eV.

Table 5.2. Maximum elemental concentrations observed in *Arthrobacter* sp. SASK-Se22.

	Elemental concentration (µg/cm^2) *										
	P	S	K	Ca	Mn	Fe	Ni	Cu	Zn	Se	Se (avg)
Control (no Se)	3.38	9.75	10.0	6.16	0.01	0.01	0.01	0.11	0.10	0.00	0.00
Selenate	1.51	5.89	1.82	6.16	0.02	0.18	0.12	0.23	0.08	0.09	0.04 ± 0.02
Selenite	2.31	2.55	2.14	0.84	0.09	0.16	0.05	0.11	0.07	80.4	32.7 ± 25

*Average concentration was calculated by applying 10 % threshold. All biofilm samples were measured at the white line energy of elemental selenium (12659.5 eV) in order to maximize the signal from selenium. Elemental concentration from selenite-amended biofilm was derived from Figure 5.4. Control (no selenium) and selenate-amended biofilms (2 months) are not shown.

5.4.4. Regional distribution of selenium species in selenate-amended biofilm

We investigated the distribution of selenium chemical species in the *Arthrobacter* sp. SASK-Se22 biofilms using XRF. Spatial distributions of amended-selenate and biotransformed elemental selenium species found in the biofilm are shown in Figure 5.5. In addition, biological structures in the biofilm shown as protein, lipid, and polysaccharide were investigated using scanning transmission X-ray microscopy (STXM) at the carbon K-edge. Both XRF and STXM indicated that both elemental selenium and selenate were distributed over the whole area of the biofilm. In addition, *Arthrobacter* sp SASK-Se22 cells, indicated with arrows in STXM image, appear to be highly associated with selenate rather than elemental selenium (Figure 5.5). However, the concentration of selenium observed in Figure 5.5 showed 4 times higher selenate intensity than elemental selenium, which may suggest the presence of small particulate elemental selenium over the biofilm.

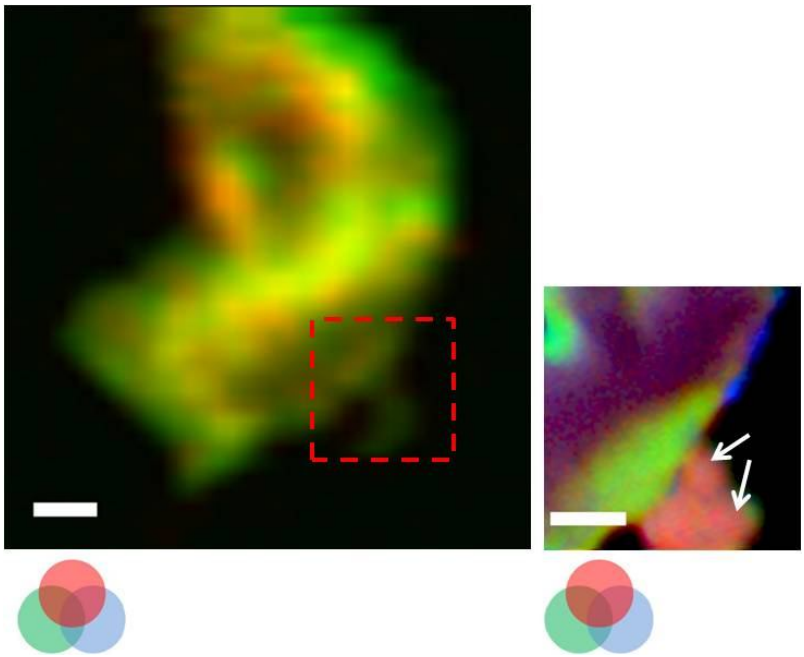

Figure 5.5. Chemically specific XRF (left) and STXM (right) images on the same area of 6.3 mM selenate-amended biofilms for 2 months. The red box indicates the area which was investigated using STXM. The XRF image shows elemental selenium (red) and selenate (green). The STXM image shows protein, polysaccharide, and lipid in red, green, and blue, respectively. Scale bar indicates 1 μm.

5.4.5. Particulate selenium and its association with cells and biofilm

An investigation using STXM scanned in both carbon K and selenium L edges allowed us to visualize the biofilm structure associated with elemental selenium in *Arthrobacter* sp. SASK-Se22 biofilms under selenite-amended conditions (Figure 5.6). From our observations of the whole biofilm (Table 5.1 and Figure 5.1, 5.2), the proportions of selenium oxyanions are very low in the biofilm. These results with Table 5.2 clearly indicate that *Arthrobacter* sp. SASK-Se22 biofilm transforms more selenite than selenate. In addition, the formation of larger elemental selenium particles and their association with bacterial cells implies how this bacterium transforms selenium oxyanions differently (Figures 5.5 and 5.6). We cannot confirm how *Arthrobacter* sp. SASK-Se22 biofilm regionally biotransformed selenium oxyanions since we only examined end-point products by measuring them after long-term exposure (1 and 2 months). However, clear dissociation of elemental selenium from *Arthrobacter* sp SASK-Se22 cells was observed in the STXM and transmission electron microscope (TEM) images of Figure 5.6. This may imply a possible application of *Arthrobacter* sp. SASK-Se22 biofilm in production of elemental selenium nanoparticles because it may be easier to recover elemental selenium from this type of biofilm compared to other biofilms of selenium-reducing microorganisms, which showed close association of the elemental selenium with the cells [36, 37].

The identity of the selenium particulate were investigated by extracting the selenium L-edge spectrum from the intense selenium spot, followed by least square fitting (Figure 5.6). The result confirmed the identity of elemental selenium. The different selenium species observed using XAS (Figure 5.1 and 5.2, Table 5.1) and variation in selenium distribution (Figure 5.5, 5.6) suggested that the overall intensity difference (Table 5.2) is due to the presence and amount of elemental selenium in the biofilms. The observed selenium particles were less than 0.3 μm in diameter.

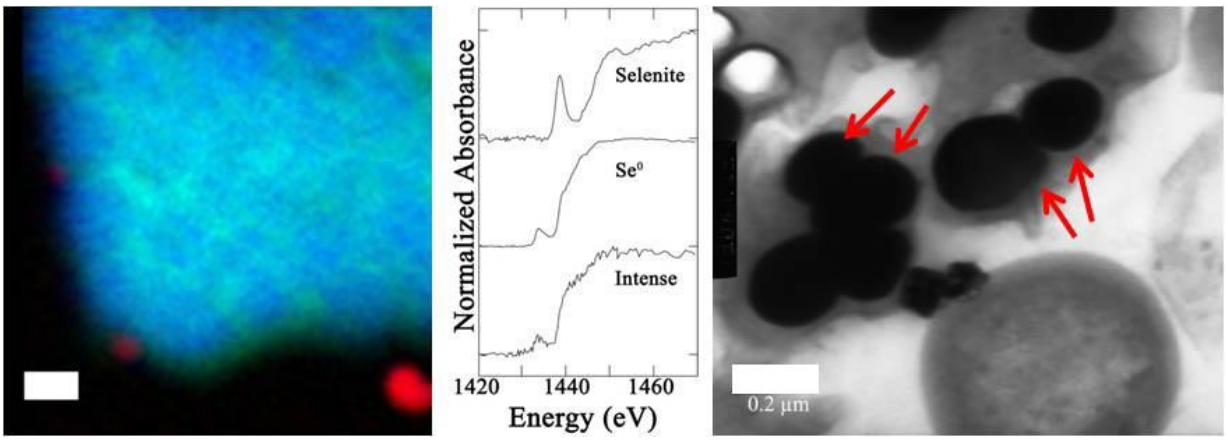

Figure 5.6. Scanning transmission X-ray microscopy image (STXM, left) shown in Figure 5.4 (6.3 mM selenite-amended biofilm for 2 months), selenium L_3 near-edge spectra extracted from the STXM data (middle), and transmission electron microscopy (TEM) (right) on a different area are shown. In the STXM image, protein (*Arthrobacter* sp. SASK-22), extracellular polymeric substance (EPS), and selenium are shown in blue, green, and red, respectively. In the spectra, 'Intense' shows the extracted Se L_3 near-edge spectrum from the intense red spots shown in the STXM image, together with spectra of selenite and Se^0 (elemental selenium) collected under the same conditions. In the TEM micrograph, arrows indicate elemental selenium particles. Scale bars in STXM and TEM show 1 and 0.2 µm, respectively.

5.5. CONCLUSIONS

Our observation of elemental selenium and the distribution of selenite and selenate, acquired from XRF correlated with STXM, demonstrated selenium biotransformation in *Arthrobacter* sp. SASK-Se22 biofilm. Transmission electron microscopy indicated that the biogenic elemental selenium were present as sub-micron particulates ranging from 100 to 300 nm in diameter. All of these observations suggested that the *Arthrobacter* sp. SASK-Se22 biofilm is highly selenium resistant, generates selenium particles outside of the cells, and actively utilizes selenite. These characteristics may suggest its possible applications in bioremediation of selenium or industries where small sizes (nm to µm) of elemental selenium particles are required, such as the semi-conductor industry.

5.6. ACKNOWLEDGEMENTS

The authors thank to all the Pickering/George group members at University of Saskatchewan and George Swerhone at Environment Canada. This research is supported by an NSERC Discovery Grant (to Pickering) and by Environment Canada. Pickering is a Canada Research Chair and Yang is a CIHR-THRUST Fellow. STXM was carried out at the Canadian Light Source (CLS), XRF at the Advanced Photon Source (APS) and XAS at the Stanford Synchrotron Radiation Lightsource (SSRL). The CLS is supported by the Natural Sciences and Engineering Research Council of Canada, the National Research Council Canada, the Canadian Institutes of Health Research, the Province of Saskatchewan, Western Economic Diversification Canada, and the University of Saskatchewan. Use of the APS, an Office of Science User Facility operated for the U.S. Department of Energy (DOE) Office of Science by Argonne National Laboratory, was supported by the U.S. DOE under Contract No. DE-AC02-06CH11357. SSRL is a national user facility operated by Stanford University on behalf of the U.S. Department of Energy, Office of Basic Energy Sciences. The SSRL Structural Molecular Biology Program is supported by the Department of Energy, Office of Biological and Environmental Research, and by the National Institutes of Health, National Center for Research Resources, Biomedical Technology Program.

5.7. REFERENCES

[1] Y. E. Yudovich, M. P. Ketris, Selenium in coal: a review. *Int. J. Coal Geol.* **2006,** *67,* 112.

[2] R. B. Finkelman, H. E. Belkin, B. Zheng, Health impacts of domestic coal use in China. *PNAS* **1999,** *96,* 3427.

[3] P. L. Orr, K. R. Guiguer, C. K. Russel, Food chain transfer of selenium in lentic and lotic habitats of a western Canadian watershed. *Ecotoxicol. Environ. Saf.* **2006,** *63,* 175.

[4] W. Maher, A. Roach, M. Doblin, T. Fan, S. Foster, R. Garret, G. Moller, L. Oram, D. Wallschlager, *in Ecological Assessment of Selenium in the Aquatic Environment* **2010**, pp. 47-92 (CRC Press: New York).

[5] S. N. Luoma, T. S. Presser, Emerging opportunities in management of selenium contamination. *Environ.Sci.Technol.* **2009,** *43,* 8483.

[6] V. Van Fleet-Stalder, T. G. Chasteen, I. J. Pickering, G. N. George, R. C. Prince, Fate of selenate and selenite metabolized by *Rhodobacter sphaeroides*. *Appl. Environ. Microbiol.* **2000,** *66,* 4849.

[7] D. Tanzer, K. G. Heumann, Determination of dissolved selenium species in environmental water samples using isotope dilution mass spectrometry. *Anal.Chem.* **1991,** *63,* 1984.

[8] A. D. Lemly, Symptoms and implications of selenium toxicity in fish: the Belews Lake case example. *Aquatic Toxicology* **2002,** *57,* 39.

[9] D. Janz, D. DeForest, M. Brooks, P. Chapman, G. Gilron, D. Hoff, W. Hopkins, D. McIntyre, C. Mebane, V. Palace, J. Skorupa, M. Wayland, *in Ecological Assessment of Selenium in the Aquatic Environment* **2010**, pp. 141-231 (CRC Press:.

[10] V. Valdiglesias, E. Pásaro, J. Méndez, B. Laffon, In vitro evaluation of selenium genotoxic, cytotoxic, and protective effects: a review. *Arch.Toxicol.* **2010,** *84,* 337.

[11] A. Fernandez-Martinez, L. Charlet, Selenium environmental cycling and bioavailability: a structural chemist point of view. *Reviews in Environmental Science and Biotechnology* **2009,** *8,* 81.

[12] D. H. Nies, Microbial heavy-metal resistance. *Appl.Microbiol.Biotechnol.* **1999,** *51,* 730.

[13] E. van Hullebusch, M. Zandvoort, P. Lens, Metal immobilisation by biofilms: mechanisms and analytical tools. *Rev. Environ. Sci. Biotechnol.* **2003,** *2,* 9.

[14] S. L. Hockin, G. M. Gadd, Linked Redox Precipitation of Sulfur and Selenium under Anaerobic Conditions by Sulfate-Reducing Bacterial Biofilms. *Appl.Environ.Microbiol.* **2003,** *69,* 7063.

[15] J. Chung, B. Rittmann, N. Her, S. Lee, Y. Yoon, Integration of H_2-Based Membrane Biofilm Reactor with RO and NF Membranes for Removal of Chromate and Selenate. *Water, Air, & Soil Pollution* **2010,** *207,* 29.

[16] S. Hockin, G. M. Gadd, Removal of selenate from sulfate-containing media by sulfate-reducing bacterial biofilms. *Environ.Microbiol.* **2006,** *8,* 816.

[17] W. Hunter, L. Kuykendall, Removing Selenite from Groundwater with an In Situ Biobarrier: Laboratory Studies. *Curr.Microbiol.* **2005,** *50,* 145.

[18] S. I. Yang, J. R. Lawrence, D. W. G. Swerhone, I. J. Pickering, Biotransformation of selenium and arsenic in multi-species biofilm. *Environ. Chem.* Accepted on September, 2011.

[19] J. R. Lawrence, G. D. W. Swerhone, G. G. Leppard, T. Araki, X. Zhang, M. M. West, A. P. Hitchcock, Scanning transmission X-ray, laser scanning, and transmission electron microscopy mapping of the exopolymeric matrix of microbial biofilms. *Appl. Environ. Microbiol.* **2003,** *69,* 5543.

[20] G. N. George, I. J. Pickering, EXAFSPAK: A Suite of computer programs for analysis of X-ray absorption spectra available at http://ssrl.slac.stanford.edu/exafspak.html. **2001,**.

[21] I. J. Pickering, R. C. Prince, M. J. George, R. D. Smith, G. N. George, D. E. Salt, Reduction and coordination of arsenic in Indian mustard. *Plant Physiol.* **2000,** *122,* 1171.

[22] S. Webb, MicroAnalysis Toolkit. *2010,*http://home.comcast.net/~sam_webb/smak.html.

[23] VOGT S., MASER J., JACOBSEN C., Data analysis for X-ray fluorescence imaging. **2003,** 6; 695.

[24] S. Vogt, MAPS: A set of software tools for analysis and visualization of 3D X-ray fluorescence data sets. *J Phys IV France* **2003,** *104,* 635.

[25] A. P. Hitchcock, aXis2000 is written in interactive data language (IDL) and available at http://unicorn.mcmaster.ca/aXis2000.html. **2010,**.

[26] J. J. Dynes, T. Tyliszczak, T. Araki, J. R. Lawrence, G. D. W. Swerhone, G. G. Leppard, A. P. Hitchcock, Speciation and quantitative mapping of metal species in microbial biofilms using scanning transmission X-ray microscopy. *Environ.Sci.Technol.* **2006,** *40,* 1556.

[27] I. N. Koprinarov, A. P. Hitchcock, C. T. McCrory, R. F. Childs, Quantitative mapping of structured polymeric systems using singular value decomposition analysis of soft X-ray images. *J Physical Chem B* **2002,** *106,* 5358.

[28] C. Shi, S. C. Kendall, E. Grote, S. Kaminskyj, M. C. Loewen, N-terminal residues of the yeast pheromone receptor, Ste2p, mediate mating events independently of G1-arrest signaling. *J.Cell.Biochem.* **2009,** *107,* 630.

[29] S. F. Altschul, W. Gish, W. Miller, E. W. Myers, D. J. Lipman, Basic local alignment search tool. *J.Mol.Biol.* **1990,** *215,* 403.

[30] D. Janz, D. DeForest, M. Brooks, P. Chapman, G. Gilron, D. Hoff, W. Hopkins, D. McIntyre, C. Mebane, V. Palace, J. Skorupa, M. Wayland, *in Ecological Assessment of Selenium in the Aquatic Environment* **2010**, pp. 141-231 (CRC Press:.

[31] M. Ikram, M. Faisal, Comparative assessment of selenite (SeIV) detoxification to elemental selenium (Se^0) by *Bacillus* sp. *Biotechnol.Lett.* **2010,** *32,* 1255.

[32] K. B. Miklós Mézes, Prooxidant mechanisms of selenium toxicity – a review. *Acta Biologica Szegediensis* **2009,** *53,* 15.

[33] R. Abdulah, K. Miyazaki, M. Nakazawa, H. Koyama, Chemical forms of selenium for cancer prevention. *J Trace Elem Med Biol* **2005,** *19,* 141.

[34] H. Li, J. Zhang, T. Wang, W. Luo, Q. Zhou, G. Jiang, Elemental selenium particles at nano-size (Nano-Se) are more toxic to Medaka (*Oryzias latipes*) as a consequence of hyper-accumulation of selenium: A comparison with sodium selenite. *Aquatic Toxicology* **2008,** *89,* 251.

[35] J. Zhang, X. G. Gao, L. Zhang, Y. Bao, Biological effects of a nano red elemental selenium. *Biofactors* **2001,** *15,* 27.

[36] R. R. Mishra, S. Prajapati, J. Das, T. K. Dangar, N. Das, H. Thatoi, Reduction of selenite to red elemental selenium by moderately halotolerant *Bacillus megaterium* strains isolated from Bhitarkanika mangrove soil and characterization of reduced product. *Chemosphere In Press, Corrected Proof,*.

[37] J. Kessi, M. Ramuz, E. Wehrli, M. Spycher, R. Bachofen, Reduction of selenite and detoxification of elemental selenium by the Phototrophic Bacterium *Rhodospirillum rubrum* . *Appl.Environ.Microbiol.* **1999,** *65,* 4734.

CHAPTER 6. SUMMARY, DISCUSSION, AND FUTURE WORK

Selenium is an essential micronutrient, yet can be toxic at elevated levels. Selenium toxicity greatly depends on its chemical forms. Biofilm has been known for its increased resistance to toxic metals and its role in the biogeochemical cycling of elements. With this in mind, natural and laboratory-grown biofilms exposed to elevated concentrations of selenium were investigated to examine the biotransformation of selenium oxyanions using less destructive synchrotron-based spectroscopic and imaging techniques. In this research, the following objectives were addressed: 1. Characterize the selenium species in natural biofilm collected from the coal mine-affected area. 2. Study selenium and arsenic biotransformation in multispecies biofilm under elevated levels. 3. Investigate selenium biotransformation in multispecies biofilm using a novel combination of synchrotron-based imaging techniques. 4. Examine selenium biotransformation in a pure-culture biofilm of *Arthrobacter* sp. SASK-22.

In harvested natural biofilm, the speciation of selenium was investigated using X-ray absorption K near-edge spectroscopy. Least squares fitting of the biofilm spectrum with model compounds showed that 80% of the selenium in biofilm consisted of methylated selenium species (modeled as selenomethionine and the trimethylselenonium ion) as well as elemental selenium. Considering the dominant presence of selenate and selenite in natural waters, the observation of methylated and zero oxidation state selenium suggested either biotransformation of selenium oxyanions or sorption onto the biofilm of reduced selenium species already present in the water. In addition, such a high proportion of reduced selenium species in the natural biofilm implied the presence of selenium reducing communities in the biofilms and necessitated further controlled studies to examine how these naturally forming multi-species microbial communities transform selenium.

Multispecies biofilms incubated at high concentrations of selenium and arsenic showed that selenium and arsenic oxyanions significantly affected both microbial diversity and structure. Investigations using confocal laser scanning microscopy (CLSM) showed that populations in the multispecies biofilms were morphologically simplified in the presence of selenium or arsenic species. Biotransformation of selenium and arsenic oxyanions to chemically more stable or less toxic species were demonstrated using synchrotron-based X-ray absorption spectroscopy (XAS).

Imaging using micro X-ray fluorescence (μ-XRF) indicated that selenium was highly localized in the biofilm in the form of reduced chemical species. In addition, results from CLSM and μ-XRF techniques were combined in a unique correlative microscopy approach. The combined observations demonstrated that biotransformation and bioaccumulation of selenium occur regionally in the biofilms, showing highly localized reduced-selenium species in the multicellular structure. This may be due to localized selenium-reducing communities within the multispecies biofilm structure. In addition, this combined methodology will be useful in future investigations of metal or metalloid distributions in biological samples.

The subsequent study of multispecies biofilms was driven by the need for higher resolution imaging of the biofilms to obtain more detailed information regarding the distribution and speciation of selenium with respect to the bacterial population. Biotransformation of selenium oxyanions to elemental selenium and subsequent sequestration in biofilms were observed using scanning transmission X-ray microscopy (STXM) and XRF imaging techniques at the selenium L and K near-edges. STXM at the carbon K-edge additionally showed a close association of selenium particles with lipid. The distributions of selenate and selenite as well as elemental selenium within a complex multispecies biofilm structure were investigated using novel applications of STXM and XRF on identical areas of biofilms. This observation showed how multispecies biofilms biotransform selenium. This unique approach also provided an example of the successful application of synchrotron-based imaging techniques in biofilm research. Further research using conventional imaging techniques may employ rRNA-based fluorescence *in-situ* hybridization (FISH) to identify the microbial communities responsible for selenium utilization in the mixed system. The result will provide an important piece of puzzle.

A highly selenium resistant isolate, *Arthrobacter* sp. SASK-Se22, cultured as a biofilm was examined using selenium X-ray absorption K near-edge spectroscopy. Selenium oxyanions were biotransformed by the biofilm into less toxic elemental selenium. The presence of elemental selenium which had dissociated from cells and a broad distribution of selenium oxyanions were observed using XRF imaging, suggesting that most of generated elemental selenium is excreted out into the environment. However, correlation of elemental selenium with macromolecular biofilm structure was observed using STXM, showing a strong relationship of elemental selenium with lipid. Investigations using transmission electron microscopy showed that the

biogenic elemental selenium is present as sub-micron particulates ranging from 100 – 300 nm in diameter.

Overall, the initial observation of selenium biotransformation in natural biofilm was proven under the controlled conditions. Furthermore, the selenium species observed in the natural biofilm were in general agreement with those measured in biofilms cultured in the laboratory, suggesting that biofilm plays a major role in the reduction process of selenium oxyanions. In terms of techniques, the combination of synchrotron-based imaging techniques used in this research is an excellent vector for investigating biochemistry in biofilms, such as a change in biofilm elemental composition in response to toxins or stress.

We still do not know much about how biofilm modifies its metabolism as a response to stress by selenium oxyanions and how it responds at a molecular level, such as gene transcription/translation of relevant enzymes. These physiological responses of biofilms may be led by several selenium-reducing microorganisms in mixed culture. Thus, under high concentration of selenium, the response of the biofilm may be carried out among selenium resistant and utilizing microorganisms acting as a group. This can be examined as suggested in the following paragraphs.

Microbial diversity present in the mixed biofilms can be investigated using denaturing gradient gel electrophoresis; as a result, the majority of microbial species in biofilm can be identified. Microbe-specific mRNA/rRNA-based fluorescence *in-situ* hybridization will provide information on the distribution and proliferation of microorganisms in biofilm structure with minimal disturbance to the physical structure. Furthermore, n-XRF combined with this microscopic technique can show which microorganisms are actually involved in the selenium reduction in biofilms.

A future microbial characterization study of *Arthrobacter* sp SASK-Se22 is important in order to better understand this bacterial species. Conventional microbiological characterization methodology, including optimal growth temperature, pH, nutritional requirement, and microbial activity tests using selenium species, could be carried out. In parallel, a growth optimization study for the production of selenium particles will be important to understand the correlation

between selenium particle size and the growth conditions. Conventional microbiological techniques could be used for these studies.

In addition, laboratory and pilot scale *Arthrobacter* sp SASK-Se22 based-bioreactors can be studied in order to optimize their utilization in selenium bioremediation. The recovery efficiency of dissolved selenium can be monitored under diverse physical and chemical conditions to optimize the bioreactor system. Additionally, a co-culture system can be examined to increase stability and efficiency of the biofilm.

Future work may also include investigation of selenium-reducing enzyme(s) in the *Arthrobacter* sp SASK-Se22. If characterization studies show that the bacterium has extreme selenite-utilizing capability, then the enzyme(s) related to this biochemical pathway may be structurally unique. If so, isolation followed by structural characterization using protein crystallography as well as x-ray absorption spectroscopy will provide important information on the nature of this enzyme.

CHAPTER 7. APPENDIX

Arthrobacter sp. SASK-Se22 16S rRNA sequence reported in GenBank.

```
LOCUS       JN035620               1452 bp    DNA     linear   BCT 05-JUL-2011
DEFINITION  Arthrobacter sp. SASK-Se22 16S ribosomal RNA gene, partial
            sequence.
ACCESSION   JN035620
VERSION     JN035620.1  GI:338858997
KEYWORDS    .
SOURCE      Arthrobacter sp. SASK-Se22
  ORGANISM  Arthrobacter sp. SASK-Se22
            Bacteria; Actinobacteria; Actinobacteridae; Actinomycetales;
            Micrococcineae; Micrococcaceae; Arthrobacter.
REFERENCE   1  (bases 1 to 1452)
  AUTHORS   Yang,S.I., George,G.N., Lawrence,J.R. and Pickering,I.J.
  TITLE     Arthrobacter sp. SASK-Se22 biofilm detoxify selenium oxyanions
  JOURNAL   Unpublished
REFERENCE   2  (bases 1 to 1452)
  AUTHORS   Yang,S.I., George,G.N., Lawrence,J.R. and Pickering,I.J.
  TITLE     Direct Submission
  JOURNAL   Submitted (26-MAY-2011) Geological Sciences, University of
            Saskatchewan, 114 Science Places, Saskatoon, SK S7N 5E2, Canada
FEATURES             Location/Qualifiers
     source          1..1452
                     /organism="Arthrobacter sp. SASK-Se22"
                     /mol_type="genomic DNA"
                     /strain="SASK-Se22"
                     /isolation_source="coal mining effluent"
                     /db_xref="taxon:1051532"
                     /country="Canada: British Columbia"
     rRNA            <1..>1452
                     /product="16S ribosomal RNA"
ORIGIN
        1 tactgctcag gatgaacgct ggcggcgtgc ttaacacatg caagtcgaac gatgatccca
       61 gcttgctggg ggattagtgg cgaacgggtg agtaacacgt gagtaacctg cccttaactc
      121 tgggataagc ctgggaaact gggtctaata ccggatatga ctcctcatcg catggtgggg
      181 ggtggaaagc tttattgtgg ttttggatgg actcgcggcc tatcagcttg ttggtgaggt
      241 aatggctcac caaggcgacg acgggtagcc ggcctgagag ggtgaccggc cacactggga
      301 ctgagacacg gcccagactc ctacgggagg cagcagtggg gaatattgca caatgggcga
      361 aagcctgatg cagcgacgcc gcgtgaggga tgacggcctt cgggttgtaa acctctttca
      421 gtagggaaga agcgaaagtg acggtacctg cagaagaagc gccggctaac tacgtgccag
      481 cagccgcggt aatacgtagg gcgcaagcgt tatccggaat tattgggcgt aaagagctcg
      541 taggcggttt gtcgcgtctg ccgtgaaagt ccggggctca actccggatc tgcggtgggt
      601 acgggcagac tagagtgatg taggggagac tggaattcct ggtgtagcgg tgaaatgcgc
      661 agatatcagg aggaacaccg atggcgaagg caggtctctg ggcattaact gacgctgagg
      721 agcgaaagca tggggagcga acaggattag ataccctggt agtccatgcc gtaaacgttg
      781 ggcactaggt gtgggggaca ttccacgttt tccgcgccgt agctaacgca ttaagtgccc
      841 cgcctgggga gtacggccgc aaggctaaaa ctcaaaggaa ttgacggggg cccgcacaag
      901 cggcggagca tgcggattaa ttcgatgcaa cgcgaagaac cttaccaagg cttgacatga
      961 accggaaata cctggaaaca ggtgccccgc ttgcggtcgg tttacaggtg gtgcatggtt
     1021 gtcgtcagct cgtgtcgtga gatgttgggt taagtcccgc aacgagcgca accctcgttc
     1081 tatgttgcca gcgcgtgatg gcggggactc ataggagact gccggggtca actcggagga
     1141 aggtggggac gacgtcaaat catcatgccc cttatgtctt gggcttcacg catgctacaa
     1201 tggccggtac aaagggttgc gatactgtga ggtggagcta atcccaaaaa gccggtctca
     1261 gttcggattg gggtctgcaa ctcgacccca tgaagtcgga gtcgctagta atcgcagatc
     1321 agcaacgctg cggtgaatac gttcccgggc cttgtacaca ccgcccgtca agtcacgaaa
     1381 gttggtaaca cccgaagccg gtggcctaac cccttgtggg agggagctgt cgaagtggga
     1441 ctggcgatgg ac
```